Prog. Energy Combust. Sci. 1986. Vol. 12. pp. 257–303.
Printed in Great Britain.

0360–1285/86 $0.00+.50

NONREACTING TURBULENT MIXING FLOWS[1]

F. C. GOULDIN,* R. W. SCHEFER,† S. C. JOHNSON† AND W. KOLLMANN‡
*Cornell University, Ithaca, NY 14853, U.S.A.
†Combustion Research Facility, Sandia National Laboratories, Livermore, CA, U.S.A.
‡University of California, Davis, CA 95616, U.S.A.

Abstract—This paper provides a comprehensive review of available data on turbulent nonreacting flows which could be of use in the evaluation of turbulence modeling schemes. The review is limited to parabolic, stationary shear flows with well-defined boundary conditions; these flows have many of the characteristics of flows found in combustion devices and are typical of laboratory flames for which model evaluation data are most likely to be available. This report is an outgrowth of a study conducted under the direction of the Air Force Office of Scientific Research. A bound volume containing, in detail, the results of that study will be available in the near future.

CONTENTS

NOMENCLATURE

C_u, C_θ, C_L flow constants in similarity forms
D, h initial round-jet diameter, plane-jet thickness
f mixture fraction (mass basis)
f, f_α velocity function in similarity form, spectra of α
g_{ij} functions for turbulence quantities in similarity form
K_u, K_θ kurtosis of velocity and scalar distributions
k scalar function in similarity form
L_u, L_θ half radii for velocity and scalar
P probability density function

[1]Research Supported by U.S. Department of Energy, Office of Basic Energy Sciences, and Air Force Office of Scientific Research under Grant No. 83-0356

Pr_t turbulent Prandtl number
q^2 twice the turbulence kinetic energy
R density ratio ρ_1/ρ_j
$R_u(x, \tau)$ velocity space–time correlation
$R_{\theta\theta}(\tau)$ scalar autocorrelation
S_u, S_θ skewness of velocity and scalar distributions
T temperature
U, V, W, u, v, w instantaneous and fluctuating velocity components
u_0 mean centerline velocity
y_u, y_θ half width for velocity and scalar
x, x_0 axial, streamwise coordinate, virtual origin
$x_{0,1}, x_{0,2}$ virtual origin for mixture fraction and half radius, respectively
y, z, r lateral coordinates
Θ, θ instantenous and fluctuating scalar quantity
θ_0 mean scalar on the centerline
γ_u, γ_θ intermittency based on velocity and scalar quantities
ρ, ρ_0 density, mean centerline density

Subscripts and superscripts

0, *cl* value at centerline
a, 1 mean value in the ambient fluid
j mean value in initial jet flow or other initial value
(1) conditional average, averaged in the turbulent fluid
air conditional average on fluid originating from air
jet conditional average on fluid originating from jet
∂_β denotes differentiation with respect to β

I. INTRODUCTION

The literature on turbulent mixing flows is quite extensive, and there are several reviews available on the subject (see for example Townsend,[80] Hinze,[52] Rajaratnam,[67] Abramovich,[1] Fischer *et al.*[44] and List[61]). Not all of the literature on free-shear flows is entirely relevant to combustion problems. Time and space contraints place a practical limit on the types of flows that can be considered in this review. Hence at the outset several conditions and restrictions are made to help define and limit the type of flows reviewed. As noted the overall objective of this work is to review data available on various classes of turbulent flows for their suitability as test flows for the evaluation of turbulence models applicable to reacting flow problems. For this purpose the study is limited to flows that are stationary and parabolic and have well-defined boundary conditions. Furthermore it is appropriate to restrict attention to free-shear flows since these flows (as opposed to boundary layer flows) are found in most combustion devices and are typical of the laboratory flames for which model validation data are most likely to be available. In this review attention is limited primarily to studies where both scalar and velocity data are obtained. This focus is quite restrictive but is justified on the grounds that both types of data are necessary for satisfactory evaluation of model performance.

Wake flows will not be considered for several reasons. One, emphasis in the constant-density mixing-flows part of this review is placed on taking advantage of similarity, and many wake flows are not similar (see below). Two, since the flow immediately behind a bluff body is elliptic, parabolic flow calculations must be initiated downstream of this elliptic flow region where the specification of necessary initial conditions is difficult. Three, since little reactive flow data are available for wake flows, it seems appropriate to concentrate effort on jets and mixing layers, flows for which reacting flow data are available.

Scalar mixing measurements require the introduction of a scalar nonuniformity either in temperature or composition, which may cause a density nonuniformity. It is therefore necessary to establish a criterion to distinguish those experiments where the density variations are significant from those where they are not. With the exception of two-dimensional mixing layers, very large initial density differences are required for density fluctuations to be significant beyond the initial mixing region. Consequently, surprisingly large initial density differences are acceptable in constant-density mixing studies. Exactly how large these differences may be is not clear. For present purposes we arbitrarily classify those flows with an initial density ratio of high over low density ≥ 1.5 as variable-density flows. Flows having a value for this ratio < 1.5 are considered constant-density mixing flows.

1.1. *Data Needs For Model Evaluation*

The capability of modern experimental techniques is such that copious amounts of very detailed data can now be collected (especially for room temperature, constant density flows). Experiments are undertaken for various reasons and no two experiments are likely to generate the same data. Thus a brief discussion of the type of data required for model evaluation is appropriate.

First and foremost, first moments of axial velocity and scalar quantities are needed at sufficient axial and lateral locations to fully characterize the evolution of the mean velocity and scalar fields. Of equal importance is the specification of necessary inlet and boundary conditions. Of nearly equal importance are

data for second-order correlations, e.g. Reynolds stresses, since these correlations are predicted by most turbulence models. Many studies report data for other quantities such as spectra, intermittency, dissipation, higher moments, etc. Of this type of information, intermittency and data which allow for a comparison with the important terms in equations for turbulence quantities, such as a turbulence kinetic energy budget, seem exceptionally useful. Also pdf data are extremely valuable to researchers developing model evolution equations for pdf's and to those using pdf's in the modeling of nonpremixed flames.

For flows exhibiting similarity, the specification of the mean velocity and mean scalar fields is straight forward and requires relatively few data. (However many measurements are usually necessary to establish the existence of similarity.) In similar jet and wake flows,[80] the following relationships are true:

$$U = U_1 + u_0 f\left(\frac{z}{l_0}\right) \tag{1}$$

$$\overline{u_i u_j} = q_0^2 g_{ij}\left(\frac{z}{l_0}\right)$$

$$\overline{q^2} = q_0^2 g\left(\frac{z}{l_0}\right)$$

$$\overline{u_i^2} = q_0^2 g_i\left(\frac{z}{l_0}\right), \text{ etc.}$$

where z is the lateral or transverse coordinate. The parameters u_0, q_0 and l_0, which are functions of the streamwise coordinate x alone, describe the spreading rate of the mean velocity and turbulence fields, while the functions f, g_{ij}, g_i and g describe the lateral variation of flow field properties. When similarity does not exist, a large number of measurements at different axial and lateral stations are required to determine the mean field properties. The exact amount of data required depends on the character of the flow and, hence, cannot be predetermined.

For boundary conditions, the axial pressure gradient and conditions at large lateral distance should be investigated. It is easy to underestimate the significance of the boundary conditions. For example, flow entrainment can induce large-scale recirculating flows in free jet experiments performed in rooms.[19] (This flow is induced apparently by jet entrainment.) It is clear that the investigator must exercise great care in avoiding outside interferences. In confined flows it is essential that axial pressure gradients and coflowing stream velocity be carefully measured. Finally, the assumption is frequently made that the flow is nonturbulent away from the jet. This assumption should also be verified.

The determination of appropriate initial conditions is a tricky business with several unresolved problems. First, different modeling approaches, e.g. k–ε vs a pdf approach, may have widely different requirements for initial conditions, while similar approaches may still have different needs. Second, since most turbulence models do not attempt to model the transition from laminar to turbulent flow, it would seem desirable for the inlet flow to be turbulent or have turbulent regions, e.g. a turbulent boundary layer. Third, new turbulence models, not yet developed, are likely to require information on the inlet flow not considered at present to be important. Fourth, and most significantly, there is confusion regarding the influence of initial conditions on the developed, self-preserving, turbulent flow far downstream of the nozzle-forming the jet.

Experimental data on jets exhibit variation in spreading rate and in the centerline variation of mean velocity and of its variance (see Table 1). These variations may be manifestations of sensitivity to inlet conditions. There is some experimental evidence[50] for free round and plane jets that, when the flow is initially laminar, jet spreading rates, centerline mean velocity decay and centerline turbulence characteristics are functions of the initial velocity and the experimental system. Hill *et al.*[50] attributed the observed sensitivity to large-scale structures seen by spark schlieren in the laminar- but not in the turbulent-flow cases. It should be noted that the measurements of Hill *et al.* as reported were not carried to large axial distance where one might reasonably expect initial conditions to have little influence on jet properties. According to Wygnanski and Fielder's data,[85] the round jet does not become self-preserving in turbulence quantities until $x/D > 60$, while for a plane jet an $x/D > 40$ is required according to the data of Gutmark and Wygnanski.[47] In view of the large axial distance required to obtain good flow similarity, it is reasonable to suspect that the sensitivity to initial conditions reported by Hill *et al.*[50] is the result of not obtaining self-preserving flow. On the other hand Bradshaw[19, 20] attributes variations in jet spreading and centerline evolution to different initial conditions and to conditions in the fluid into which the jet is flowing. Clearly there is a significant uncertainty associated with the establishment of appropriate inlet conditions.

One appropriate response, for now, to the problem of choosing and measuring inlet conditions is to design an experiment with well-defined and easily-determined inlet conditions. Laminar flow with thin laminar boundary layers for which displacement and momentum thickness are measured is one example. In this case the inlet flow is well known, but transition to turbulence occurs in the calculation domain. Such transitional flows are difficult to calculate using current turbulence models.

TABLE 1a. Plane jet data

Reference	Initial conditions AR	RE ×10⁻³	R	Velocity C_u	x_0/h	C_{L_u}	x_0/h
Robins (Everitt and Robins[42])	128	16	1	0.18–0.21	—	0.10	—
	64	30	1	0.17–0.19	—	0.10–0.11	—
	32	30	1	0.14–0.18	—	0.11	—
	21	75	1	0.19–0.22	—	0.09	—
Heskestad[49]	120	34	1	0.16	6	0.11	6
Gutmark and Wygnanski[47]	38	30	1	0.17	2	0.10	2
Antonia *et al.* (Table 4)	19.7	7.62	1.087	0.143	9	0.104	5
Davies *et al.*[30]	6.0	51.8	1.049	0.146	1.17	0.109	1.17
Jenkins and Goldschmidt[53]	23.9	14.3	1.037	0.160	4.0	0.088	−4.5
			1.070	0.160	4.0	0.091	−3.0
			1.117	0.160	4.0	0.096	−2.5
Bashir and Uberoi[12]	40	2.77	1.201	0.22	2.42	0.088	2.42
	20	—	1.2	0.206	1.94	—	—
	144	—	1.2	0.240	4.6	0.104	4.5
Fischer *et al.*[44]	—	—	—	0.172	—	0.096	—
van der Hegge Zijnen[86, 87] **	20	—	1	0.161	−0.6	—	—
	25	—	1	0.206	−1.2	—	—
Albertson *et al.*[3]	—	—	—	0.190	—	—	—
Abramovich[1] **	—	—	—	0.140	—	0.096	—

TABLE 1b. Round jet data

Reference	Initial conditions RE ×10⁻³	R	Velocity C_u	x_0/D	C_{L_u}	x_0/D
Corrsin[29]	19.1	1.05	0.18		0.17	
Wygnanski and Fiedler[85]	~100	1	0.179–0.203	3–7	0.168	—
van der Hegge Zijnen[51]	—	1	0.17	0.5	0.16	0.5
Corrsin and Uberoi[28]	~55	1.05	0.193	2.6	0.139	5
	~55	2.00	0.225	2.3	0.231	3
	~55	1.57	0.175	1.01	—	—
Kiser[56]	~30	1	0.164	1.2	0.163	1.2
Keagy and Weller[54]	54.7	0.63	0.096	0.8	0.166	—
	27.7	1.04	0.120	1.1	0.178	—
	3.6	7.25	0.281	8.5	0.221	—
Wilson and Danckwerts[84]	20–40	1.07–1.67	$0.155\sqrt{R}$	—	0.2	—
Fischer *et al.*[44] **	—	—	0.161	—	0.178	—
Lockwood and Moneib[62]	50.4	1.86				
Dyer[40]	9.79	0.58				
Pitts and Kashiwagi[66]	3.76	1.61				
Birch *et al.*[18]		1.61				
Becker *et al.*[14]		1				
van der Hegge Zijnen[86, 87]		1	0.156	−0.6	0.188	—
Albertson *et al.*[3]		1	0.161	—	0.193	—

An alternate strategy for handling initial conditions is to start with a turbulent flow or turbulent boundary layer and thus avoid having transition in the calculation domain and perhaps avoid large-scale structures. The problem with an initially turbulent flow is that extensive measurements are required to specify the turbulent flow and it is likely, given our current imperfect understanding of turbulent flows, that not all quantities needed for future tests would be recognized as important and therefore measured. To guard against this possibility careful and thorough experimentation is recommened, and the raw data should be stored on magnetic tape for future needs to analyse the data for additional turbulence properties.

More research on the sensitivity of turbulent flows to inlet conditions and to conditions in the ambient fluid is needed. At the present time the authors believe that for model evaluation purposes it is best to have the intial flow turbulent, whether or not large structures are avoided thereby, since with this initial state, transition does not occur in the calculation

		Scalar					
$\frac{\langle u^2\rangle^{1/2}}{U_o}$	C_u/C_{L_u}	C_θ	x_o/h	$C_{L\Theta}$	x_o/h	$\frac{\langle\theta^2\rangle^{1/2}}{\theta_o}$	Comments
0.23	1.8–2.1						
0.22							
0.22							
0.25							
0.26	1.45						measures to 160 x/h
0.27	1.7						
0.192	1.38	0.18	8	0.128	5	0.170	
0.19	1.34	0.252	1.17	0.125	1.17	1.165	*
—	1.82	0.0132*	−7.5*	0.123	−4.8	—	$(\theta_o/\theta_j)^{-1/2}=C_\theta(x/h-x_o/h)$
—		0.0132*	−7.5*	0.128	−3.6	—	
—		0.0132*	−7.5*	0.137	−3.2	—	
0.25		0.29	2.42	0.183	2.42	0.22	
0.26		0.276	1.94	—	—	0.273	
0.247	2.31	0.258	4.6	—	—	0.256	
—	1.79	0.176	—	0.261	—	—	recommended values
—	—	—	—	—	—	—	**reported by Rajaratnam[67] and by Samaraweera[71]
—	—	—	—	—	—	—	
—	—	—	—	—	—	—	
1.46	—	—	—	—	—	—	

		Scalar					
$\frac{\langle u^2\rangle^{1/2}}{U_o}$	C_u/C_{L_u}	C_θ	x_o/D	C_{L_θ}	x_o/D	$\frac{\langle\theta^2\rangle^{1/2}}{\theta_o}$	Comments
0.25	1.06	0.22		0.22			$\Theta_j/\theta_o=C_u(X/D)^{1.1}$, $\Theta_j/\theta_o=C_\theta(X/D)^{0.92}$
0.29	1.07–1.21						
—	1.06	0.228	2.6	0.172	0		reported in Hinze[52]
0.23	1.39	0.28	2.9	0.165	5	—	
—		0.32	2.16	0.286	3	—	
0.225		0.238	0.87			0.145	
—	1.01	0.2	1.2	0.208	1.2	—	concentration
—		0.173	5.7	0.181			concentration
—	0.67	0.108	3.2	0.209			
—		0.050	16.7	0.312			
—	0.78	$0.175\sqrt{R}$	—	0.26	3.0	0.18	**recommended values
—	0.90	0.202	—	0.211	—	—	$U_e/U_j=0.033$
		0.278	3.7	0.264	2	0.21	
		0.228	2.6	0.172	0	0.15	$U_e/U_j=0.026$
		0.166	−3.8	0.216	0	0.29	
		0.180	1.8	0.194†	0	0.222	†mass fraction
		0.186	2.4	0.212	2.4	0.29	
—	0.83						marker nephlometry
—	0.83						reported by Rajaratnam[67]

domain. For the round jet, fully-developed turbulent pipe flow seems to be a good choice, while in other cases, a turbulent boundary layer can be induced by tripping. (For plane jets the turbulent boundary layer approach is debatable because of the growth of side-wall boundary layers in the jet nozzle and possible secondary flows.) For initially turbulent flow, means, variance and important correlation terms should be measured at the nozzle exit, as well as the turbulence dissipation rate if at all possible. The measurement of other properties as appropriate should be considered. It should be the obligation of the researcher to know his flow and what should be measured for inlet specification.

2. CONSTANT-DENSITY MIXING FLOWS

In this section, data for constant-density, turbulent, free-shear flows are reviewed and discussed. The extensive data of Antonia and co-workers on a plane, free jet are emphasized. Additional data needs for this type of flow are discussed in Section 5.

2.1. *Similarity*

As noted above, the development of a similar flow can be described by relatively few functions and parameters, and this simplification should be utilized whenever possible. Unfortunately, the conditions for similarity are quite restrictive, and even when similarity is allowed theoretically, it may not develop or be very late (far downstream) in developing practically. For example, the free jet data of Wygnanski and Fiedler[85] show that while first moments appear to have similar profiles after $x/D=20$, the second moments do not achieve similarity until over $x/D=60$ at which point the axial decay rate of the centerline mean axial velocity changes.

Townsend[80] discusses the conditions necessary for similarity in two-dimensional free shear flows. As noted above the conditions are very restrictive and as a consequence only a limited subset of free-shear flows are truly similar or self-preserving. The similarity constraints are determined by substituting the functional forms presented in Eq. (1) into the appropriate conservation equations and multiplying terms in order to gather the scales, U_1, u_0, etc. into groups. For similarity these groups must be either zero or independent of x, a condition which in turn determines how the scales vary with x. In general the constraint conditions cannot be met. Examples of flows satisfying similarity include the two-dimensional (plane) shear layer, the two-dimensional and axisymmetric jet with no coflow and the axisymmetric jet in a coflowing stream where $u_0 \propto U_1(x-x_0)^a$ and a is a constant. The two-dimensional wake does not satisfy similarity except in the limit $u_0/U_1 \ll 1$, i.e. the far wake.

Townsend also considers the case of passive scalar mixing in free shear flows.

$$\overline{\Theta} = \theta_0 f_\theta\left(\frac{z}{l_0}\right) \tag{2}$$

$$\overline{\theta^2} = \theta_0^2 g_\theta\left(\frac{z}{l_0}\right)$$

$$\overline{\theta u_i} = \theta_0 u_0 g_{\theta i}\left(\frac{z}{l_0}\right), \text{ etc.}$$

In Eq. (2) the scale for scalar fluctuations has been set equal to θ_0 as required for similarity, which means that at large x/D, $\overline{\theta^2}/\theta_0^2$ approaches a constant on the centerline or plane of symmetry of the flow. It can then be shown that similarity requires for the scalar field that $U_1 dT_1/dx = 0$ (or $U_1 dC_1/dx$) and, for u_0/U_1 constant or $u_0/U_1 \ll 1$, $\theta_0 \propto u_0$. For example, the plane jet data of Browne *et al.*[24] show $(U_j/u_0)^2 = 0.143$ $(x/D+5)$ and $(\Theta_j/\theta_0)^2 = 0.18$ $(x/D+8)$ in good agreement with the foregoing.

For variable density flows a similarity analysis might also be carried out. The Favre-averaged equations, which have the same general form as the Reynolds-averaged equations in constant density flows, could be considered. Then let

$$\bar{\rho} = \rho_1 + \rho_0 k\left(\frac{z}{l_0}\right) \tag{3}$$

and two new scales enter the problem, ρ_1 and ρ_0, as well as the function k. The axial variations of these scales for similarity are related to the variation of the other scales entering the problem, thus greatly restricting the variable-density flows which satisfy similarity. For example, if one considers a plane jet flow into still air it is found that similarity cannot be achieved. In early work, both Keagy and Weller[54] and Corrsin and Uberoi,[28] for variable-density flows, performed similarity analyses. Both analyses are based on unjustified assumptions regarding either the axial variations of the important scales in the problem or the functional forms describing radial variations of the jet properties.

In summary, similarity is found to hold for a limited class of constant-density free-shear flows. For this class of flows it is an extremely useful concept and should be used to check the quality of experimental data and to help report data in a compact form. Unfortunately similarity does not hold for variable density flows.

2.2. *Review of Data*

There are many reports of data where velocity and scalar quantities were not measured simultaneously. These measurements are not reviewed in any detail here for reasons stated above. The data are, however, useful for model validation since they can be used to find the parameters and functions appearing in the similarity expressions. These data are summarized in Table 1 by presenting in similarity form, results for the mean and variance.

The data are fit to similarity forms as noted below (see Townsend[80]).

Mixing layer:

$$u_0 = U_1 = \theta_0 = \text{constant} \tag{4}$$

$$l_0 = C_{L_u}(x-x_0)$$

$$l_0 = C_{L_\theta}(x-x_0).$$

Free plane jet:

$$U_1 = 0 \tag{5}$$

$$\left(\frac{U_j}{u_0}\right)^2 = C_u\left(\frac{x}{h}-\frac{x_0}{h}\right)$$

$$\frac{\overline{(u^2)}^{1/2}}{u_0} = \text{constant}$$

$$\frac{y_u}{h}=C_{L_u}\left(\frac{x}{h}-\frac{x_0}{h}\right)$$

$$\left(\frac{\Theta_j}{\theta_0}\right)^2=C_\theta\left(\frac{x}{h}-\frac{x_0}{h}\right)$$

$$\frac{\overline{(\theta^2)}^{1/2}}{\theta_0}=\text{constant}$$

$$\frac{y_\theta}{h}=C_{L_\theta}\left(\frac{x}{h}-\frac{x_0}{h}\right).$$

Free round jet:

$$U_1=0 \tag{6}$$

$$\left(\frac{U_j}{u_0}\right)=C_u\left(\frac{x}{D}-\frac{x_0}{D}\right)$$

$$\frac{\overline{(u^2)}^{1/2}}{u_0}=\text{constant}$$

$$\frac{L_u}{D}=\frac{C_{L_u}}{2}\left(\frac{x}{D}-\frac{x_0}{D}\right)$$

$$\left(\frac{\Theta_j}{\theta_0}\right)=C_\theta\left(\frac{x}{D}-\frac{x_0}{D}\right).$$

$$\frac{\overline{(\theta^2)}^{1/2}}{\theta_0}=\text{constant}$$

$$\frac{L_\theta}{D}=\frac{C_{L_\theta}}{2}\left(\frac{x}{D}-\frac{x_0}{D}\right).$$

where C_u, C_θ, C_{L_u}, and C_{L_θ} are flow constants in similarity form. Here θ refers to any scalar quantity and u refers to velocity. L_u and L_θ are measures of the round-jet diameter defined as the radial point where U/u_0 and $\overline{\Theta}/\theta_0$ are 0.5. Terms y_u and y_θ are corresponding values for the plane jet.

From the review of the literature values for the parameters in Eqs (5) and (6) were estimated and the results are presented in Table 1 for plane and round jets. Space limitations precluded a similar review for mixing layers.

With regard to Table 1 several comments can be made. Considerable data are available describing the axial and lateral variations in mean quantities. But there is relatively little data on turbulence quantities in part because of the difficulty in obtaining such data. The power law dependency on x predicted from similarity is observed to good accuracy for both spreading rate and velocity and scalar quantities. There is however some scatter in the measured constants of proportionality. While the scatter is not so large as to preclude the use of the data for model development and validation, it is certainly a source of concern. Some of the scatter is most likely the result of experimental problems. For example, Wilson and Danckwerts[84] cite specific experimental problems in Corrsin and Uberoi[28] (problems relating to the sensor performance). The Keagy and Weller[54] concentration data also appear questionable perhaps due to bias in sampling from variable density flows. Some departure from similarity in the Keagy and Weller data is also expected since measurements were made only to $x/D=24$. This distance corresponds to the near-field region of the jet where similarity would not be expected to hold. The scalar data of Jenkins and Goldschmidt[53] are suspect since they are reported in an inappropriate similarity form

$$\left(\frac{\Theta_j}{\theta_0}\right)^{1/2}=C_\theta\left(\frac{x}{h}-\frac{x_0}{h}\right).$$

Random error may also be a contributory factor to the scatter in the parameters presented in Table 1. However, axial and lateral profile data do not exhibit sufficient scatter to support this possibility.

Another likely source of problems is that in the region of most measurements, the flow is not fully developed in that the turbulence properties are not fully developed. As noted by Wygnanski and Fielder,[85] the second moments and correlations did not reach similarity until $x/D>60$ and C_u varied from 0.179 to 0.203 when far downstream data were considered in finding its value. Given such a large change in C_u this explanation for scatter in the data seems quite reasonable.

Some of the scatter in the C_u data is attributable to variations from one flow apparatus to another in the initial, mean, axial velocity profile. By definition, U_j is a momentum flux-weighted velocity:

$$\rho_j U_j^2 D^2\frac{\pi}{4}=2\pi\int_0^\infty \rho_j U^2 r\,dr.$$

However, jet velocities are frequently obtained from volume flow rate measurements, and in such cases, the ratio between U_j and the measured volume flow-rate based U depends on the initial velocity profile. Thus, when a volume-flow-rate weighted velocity is used for U_j, the resulting value for C_u will depend on the initial velocity profile thereby introducing apparent scatter into the data for C_u obtained from different experiments with differing initial velocity profiles.

For plane jets the question of attainment of similarity is confused by the ultimate transition of the flow from two-dimensional to axisymmetric far downstream of the jet nozzle. The region of this transition depends on the aspect ratio of the jet nozzle. The greater the aspect ratio the further downstream the transition occurs, and therefore the greater is the region in which the plane jet can

become fully developed. If the jet nozzle aspect ratio is too small, the plane jet will never attain similarity. For higher aspect ratio jets, care must be taken to distinguish the plane jet region with similarity from the transition region further downstream. The problems of attaining similarity and differentiating the similar region from the transition region may be the explanation of some of the observed scatter in Table 1b (e.g. the data of Heskestad are obtained quite far downstream) and of the variations in C_u and C_{L_u} with aspect ratio. Other explanations such as dependency on initial conditions and on conditions in the surrounding fluid can be offered as above. Such sensitivity to these conditions may imply that the flow is not fully developed.

Further jet experiments at large x/D are recommended to help determine the cause of the observed variations and to obtain good values for the constants appearing in the similarity relations. These measurements will be quite difficult since the quantities to be measured will be far below their initial values, and there may be subtle room-interference effects which will be difficult to detect. Similarity is an important and useful concept, and additional research is needed to determine under what conditions similarity is valid. In the present context for constant-density mixing flows, similarity allows data for velocity and for scalar quantities obtained in different experiments or at different times in the same apparatus to be used together for model evaluation purposes.

There is considerable scatter in the data for the virtual origin x_0. Since x_0 depends on the initial conditions and on the development of the initial mixing layers in the potential core region of the jet, this scatter is not surprising. As most turbulence models are not intended to model both the initial region of mixing and the downstream region, comparison of x_0 from model predictions with experimental data does not seem worthwhile. On the other hand, it should be noted that strict similarity requires that x_0 for velocity and scalar fields be the same, and variations in x_0 between velocity and scalar may be an indication of lack of similarity and/or of experimental problems.

With assumptions, the most significant being the introduction of a constant eddy viscosity, expressions for the lateral variation of $\bar{U}/u_0$ can be obtained (see Eq. (1)). For free jets these expressions are[80]:

Plane jet:

$$f(\xi)=\operatorname{sech}^2(0.88\xi) \tag{7}$$

Round jet:

$$f(\xi)=(1+0.414\xi)^{-2} \tag{8}$$

where ξ equals y/y_u or r/L_u as appropriate.

Experience has shown that for free jets, initial density differences between the jet fluid and surrounding fluid are quickly reduced to relatively low levels. Therefore in regions where similarity is valid the flow may, in many cases, also be considered a constant density flow even when there is an initial density difference. For these flow cases, Thring and Newby[79] using momentum conservation have shown that the influence of the initial density difference on the flow in the similar region may be accounted for replacing D (or R) by

$$D_e=D\left(\frac{\rho_j}{\rho_1}\right)^{\frac{1}{2}} \tag{9}$$

in the constant-density scaling expressions given above.

To show this result, consider a free round jet. After neglecting contributions to the total momentum flux from normal turbulent stresses and assuming a uniform pressure, one can show for the total momentum flux that

$$2\pi\int_0^\infty r\mathrm{d}r\rho_1\bar{U}^2=\frac{\pi}{4}D^2\rho_j U_j^2=\frac{\pi}{4}D_e^2\rho_1 U_j^2. \tag{10}$$

It is assumed that $\rho=\rho_1$ at the point of interest. Clearly for this to be true D_e must be defined as above and thence U will scale as in the constant density case.

Several investigators (e.g. Wilson and Danckwerts[84]) have tested this scaling and found it to be satisfactory. However, the alternate length scale, D_e, is used only in the expression for U_j/u_0 and not in the other expressions in Eq. (6) which is not logical. Instead it would be more logical to introduce an alternate velocity scale, U_e, to reflect variations in momentum flux with variations in ρ_j:

$$U_e=U_j\left(\frac{\rho_j}{\rho_1}\right)^{\frac{1}{2}} \tag{11a}$$

and thus

$$C_u=C_u^e/\left(\frac{\rho_j}{\rho_1}\right)^{\frac{1}{2}}.$$

Here C_u is the measured C_u using U_j as the velocity scale, while C_u^e is a constant velocity-scale parameter (independent of ρ_1/ρ_j) which one would obtain using U_e as the scale. Similar reasoning for the scalar quantities temperature and mass fraction leads to

$$\Theta_e=\Theta_j\left(\frac{\rho_j}{\rho_1}\right)^{\frac{1}{2}} \tag{11b}$$

and

$$C_\theta = C_\theta^* \Big/ \left(\frac{\rho_j}{\rho_1}\right)^{\frac{1}{2}} .$$

In mole fraction units the appropriate scaling to account for an initial density difference is

$$\Theta_e = \Theta_j \Big/ \left(\frac{\rho_j}{\rho_1}\right)^{\frac{1}{2}} \tag{11c}$$

and

$$C_\theta = C_\theta^* \left(\frac{\rho_j}{\rho_1}\right)^{\frac{1}{2}} .$$

Finally it is noted that for a free-plane jet the same correction factors apply.

The data in Tables 1a and 1b are analysed according to the corrections given in Eqs (11a) and (11b) with the results presented in Table 2. It is seen that in general the correction gives the right trend, but the quantitative results are not as good as those reported by Wilson and Danckwerts,[84] Table 1a.

By substitution of the similarity relations into the momentum–flux relationship, Eq. (10), an expression relating the constants in the centerline velocity scaling and the scaling for $l_0(y_u$ or $L_u)$ is obtained in terms of f. For a free round jet one obtains

$$\frac{C_u}{C_{L_u}} = (2\int f^2 \xi \mathrm{d}\xi)^{1/2} = 0.897 \tag{12}$$

and for a free plane jet

$$\frac{C_u}{C_{L_u}} = 2\int f^2 \xi \mathrm{d}\xi = 1.515 \tag{13}$$

where f is given by Eq. (7) or (8), respectively. Comparison with experimental results, Table 1, shows satisfactory agreement. But the agreement is not good enough to use either Eq. (12) or (13) to find one constant from the other. The observed differences may be attributed to at least three causes, other than experimental error: (1) the neglect of normal stresses in Eq. (10), (2) an unsatisfactory expression for f, and (3) the velocity scale reported as U_j may be a volume-flux-, not a momentum-flux-weighted quantity. If the velocity function f is wrong, and it is likely that it is not absolutely correct, doubt is easily cast on the assumption of constant eddy viscosity.

The data presented in Table 1 are useful in the evaluation of turbulence models, but the results of comparison should be interpreted with discretion. There are enough oustanding questions regarding these data as noted above to make it inappropriate to recommend at this time a particular set of values. This task is for the time being left to the modeler.

Data for free shear flows obtained from experiments where both velocity and scalar were measured are summarized in Table 3; diagrams of the flow configurations are shown in the table. A review of this table shows that there are several problems in using the data for model evaluation. In some cases data were obtained at only one or a few axial stations, usually at small x/D—e.g. Keagy and Weller,[54] Chevray and Tutu,[26] Catalano *et al.*,[25] Vankataramani *et al.*[82] Also there are cases where only a few or no turbulence properties were measured—e.g. Fielder[45] does not measure $u\theta$ or uv, the only turbulence property measured by Wilson and Danckwerts[84] is θ^2, and Sreenivasan *et al.*[78] do not give data for uv.

With regard to the plane jet data it is noted that Bashir and Uberoi[12] report data on y_u and U_j/u_0 for these different apect ratio jets (20, 40 and 144). They

TABLE 2.

Reference	R	C_u	C_u^e	C_θ	C_θ^e
Plane jets:					
Antonia *et al.*[7,8,9,11]	1.087	0.143	0.137	0.18	0.173
Davies *et al.*[30]	1.049	0.146	0.142	0.252	0.246
Jenkins and Goldschmidt[53]	1.037	0.160	0.157		
	1.07	0.160	0.155		
	1.117	0.160	0.151		
Bashir and Uberoi[12]	1.2	0.22	0.201	0.29	0.265
	1.2	0.206	0.188	0.276	0.252
	1.2	0.24	0.219	0.258	0.235
Round jets:					
Corrsin and Uberoi[28]	1.05	0.193	0.188	0.28	0.273
	2.00	0.225	0.159	0.32	0.226
	1.57	0.175	0.140	0.238	0.190
Keagy and Weller[54]	0.63	0.096	0.121	0.173	
	1.04	0.120	0.118	0.108	
	7.25	0.281	0.1044	0.050	
Lockwood and Moneib[62]	1.86		0.278	0.278	0.204
Wilson and Danckwerts[84]	range		0.155		0.175

TABLE 3. Free shear flows

Reference	Flow	Measurements reported: Velocity	Measurements reported: Temperature
Antonia and Bilger[6]	Round jet in wind tunnel. $D=15.9$ mm; 305×305 mm; $\Theta_i=170$°C; $U_j=45.7$ m/sec; $U_j/U_e=16.8$, 5.6 and 3.0; $R=1.571$; $Re=26100$, 22800, 18500.	Radial profiles of $\langle U\rangle$, $\langle u^2\rangle^{1/2}$, $\langle u\Theta\rangle$ at several x/d. Axial profiles of $\langle u^2\rangle^{1/2}$ to $x/D\simeq70$.	$\langle\Theta\rangle$, $\langle\theta^2\rangle^{1/2}$ radial profiles at several x/d and along centerline to $x/D\simeq80$.
Antonia *et al.*[10]	Round jet in wind tunnel. $D=20.3$ mm; 305×305 mm. $\Theta_j=34$°C; $U_j=32$ m/sec; $T_1=15$°C; $U_j/U_e=6.6$, 2.9 and 1.9; $Re=41500$, 32000, 23200.	$\langle U\rangle$, $\langle U\rangle^{(1)}$ $\langle u^2\rangle^{(1)}$ $\langle v^2\rangle^{(1)}$ $\langle uv\rangle^{(1)}$ $\langle uv\rangle$, $\langle v^2\rangle$, S_u, K_u, $S_u^{(1)}$, $K_u^{(1)}$, and S_v, K_v, $S_v^{(1)}$, $K_v^{(1)}$.	γ_θ, f_γ, $\langle\Theta\rangle$, $\langle\Theta\rangle^{(1)}$ $\langle\theta^2\rangle$, $\langle\theta^2\rangle^{(1)}$ $\langle u\theta\rangle$, $\langle u\theta\rangle^{(1)}$ $\langle v\theta\rangle$, $\langle v\theta\rangle^{(1)}$ S_θ, K_θ, $S_\theta^{(1)}$, $K_\theta^{(1)}$.
Bashir and Uberoi[12]	Plane jet, slot size= 3.175×127 mm $\Theta_j=60$°C; $U_j=15.24$ m/sec; $Re=2770$.	$\langle U\rangle$, $\langle u^2\rangle^{1/2}$ $\langle v^2\rangle^{1/2}$ $\langle w^2\rangle^{1/2}$ on centerline to $x/h=56$. f_u $x/d=40$. $\langle U\rangle$, $\langle u^2\rangle^{1/2}$ $\langle v^2\rangle^{1/2}$ $\langle w^2\rangle^{1/2}$ along centerline for $AR=20$ and 144.	$\langle\Theta\rangle$, $\langle\theta^2\rangle^{1/2}$ at many axial stations to $x/h=56$. γ_T, $\langle v\theta\rangle$, $\langle v\theta^2\rangle$, $\langle\partial\theta/\partial t^2\rangle$, f_θ at $x/h=40$; $\langle\Theta\rangle$, $\langle\theta^2\rangle^{1/2}$ along centerline for $AR=20$ and 144.
Batt[13]	Plane mixing layer. $u_0=23$ and 50 ft/sec; $\langle u^2\rangle^{1/2}/u_0<0.4\%$; $\theta_0=4.5$, 35.8, 53.6°C.	$\langle U\rangle$, $\langle u^2\rangle$, f_u, δ, $P(U)$, $\langle vu\rangle$, $R_{uu}(x,\tau)$.	$\langle\Theta\rangle$, $\langle\theta^2\rangle$, γ_θ, δ, S_θ, K_θ, $P(\theta)$, f_θ, $\langle v\theta\rangle$.
Catalano *et al.*[25]	Round jet in wind tunnel. $U_e=3.20$ m/sec; $U_j/U_e=5.1$; $D=2.14$ cm; $Re=22{,}600$.	$\langle U\rangle$, $\langle u^2\rangle^{1/2}$ profiles at $x/D=2,4,6,8$. $\langle u^2\rangle^{1/2}$ at 0. Also $R_{uu}(\tau)$, f_u.	$\langle u,\theta\rangle$, $x/D=2,4,8$. γ_θ at $x/D=0,2,4,6,8$.
Chevray and Tutu[26]	Free jet. $\Theta_j=20$°C; $U_j=25$ m/sec; D=22.5 cm; $Re=423600$.	$\langle U\rangle$, $\langle u^2\rangle$, $\langle v^2\rangle$, $\langle uv\rangle$, $\langle u\theta\rangle$, $\langle v\theta\rangle$.	$\langle\Theta\rangle$, $\langle\theta^2\rangle$.
Davies *et al.*[30]	Plane jet. Slot size= 51×305 mm. $\Theta_j=14.6$°C; U_j13.5 m/sec; $Re=51800$.	γ_u, $\langle u^2\rangle^{(1)1/2}$ at $x/h=20$. $\langle U\rangle$, $\langle U\rangle^{(1)}$ $\langle u^2\rangle^{1/2}$ at x/h: 10, 12.5, 15, 17.5, 20, 22.5, 25. y_u, U_j^2/u_0^2 vs x/h.	$\langle\Theta\rangle^{(1)}$ γ_θ, $\langle\theta^2\rangle^{(1)1/2}$ profiles at $x/h=10$. $\langle\Theta\rangle$, $\langle\theta^2\rangle^{1/2}$ $\langle\Theta\rangle^{(1)}$ at 10, 12.5, . . ., 25. y_θ, y_γ along centerline.
Fielder[45]	Axisymmetric mixing layer $u_0=8$ m/sec; $\Theta_0=26$°C.	$\langle U\rangle$, $\langle V\rangle$, γ_w.	$\langle\Theta\rangle$, $\langle\theta^2\rangle$, S_θ, K_θ, f_θ, $R_{\theta\theta}(\tau)$, $\langle\Theta\rangle^{(1)}$ $\langle\theta^2\rangle^{(1)}$.
Fielder *et al.*[46]	Axisymmetric mixing layer. $u_0=10$ m/sec; $\Theta_0=26$°C.		$\langle\Theta\rangle$, $\langle\theta v\rangle$, $\langle v\theta^2\rangle$, $\langle\theta^2\rangle$.
Jenkins and Goldschmidt[53]	Plane jet. Slot size= 1.27×30.4 cm.	$\langle U\rangle$ on centerline and y_u to $x/h=70$. $\langle U\rangle$ profiles at $x/h=$ 25,35,45,55.	$\langle\Theta\rangle$ on centerline and y_θ to $x/h=70$. $\langle\Theta\rangle$ profiles at $x/d=$ 25,35,45,55.
Keagy and Weller[54]	Free jets of He, N_2 and CO_2 ($R=7.25$, 1.04, 0.63); $D=0.128$ in., $U_j=400$ ft/sec; $Re=3600$, 27700, 54700.	$\langle U\rangle$ on centerline, radial profiles at $x/D=$ 8, 16, 24.	
Sreenivasan *et al.*[78]	Axisymmetric mixng layer (initial region of large free jet, $D=48$ mm). $\Theta_j=13$°C; $U_j=15.1$ and 4.8 m/sec; $\langle\theta^2\rangle_j^{1/2}/\Theta_j<1\%$.	$\langle U\rangle$. For $P(u)$, $\langle u^2\rangle^{1/2}$, S_u, K_u and $\langle\theta u\rangle$ both conditioned and unconditioned results reported.	$\langle\Theta\rangle$, $P(\theta)$. For $\langle\theta^2\rangle^{1/2}$, S_θ and K_θ both conditioned and unconditioned results reported.
Venkataramani *et al.*[82]	Round jet. $D=22.5$ cm; $Re=3\times10^5$	$P(U)$, $P(V)$ $P(U,V)$, $P(V,\theta)$ at $x/d=15$, $r/D=0$, 1.0, 1.89. $P(U,\theta)$ at $r/D=0$.	$P(\Theta)$, γ_θ at same locations.
Wilson and Danckwerts[84]	Round jet. $\Theta_j=200$, 181, 144, 123, 99, 79, 52, 21, 12°C. $U_j=\leq100$ m/sec; D=0.5 in.; $Re=20{,}000$–$40{,}000$.	$\langle U\rangle$ on centerline and radial profiles. r_u and u_0 reported also.	$\langle\Theta\rangle$ and $\langle\theta^2\rangle^{1/2}$ centerline and radial profiles. r_θ and Θ_0 also reported.

Other	Probe characteristics	Comments
	Constant temperature hot-wire for velocity, compensated (to 20 kHz) cold-wire for temperature.	$\langle uv \rangle$ and $\langle \theta v \rangle$ inferred from data by calculation.
Budgets	Constant temperature X hot-wire, compensated cold-wire.	Temperature used to obtain I. First moments are similar; higher moments are not. Data only at one axial station, $x/d = 59$.
	Constant temperature hot-wire for velocity and cold-wire for temperature. Temperature checked with thermocouple.	There is significant variation in centerline decay with AR. May be the result of 3-dimensional effects.
$\langle C_{NO_2} \rangle$, $\langle c^2_{NO_2} \rangle^{1/2}$ δ, $P(C_{NO_2})$, f_{NO_2}.	Constant temperature hot-wire for velocity, 5 kHz response; cold-wire for temperature, 1 kHz response. NO_2 by fiberoptic probe, vol. = $0.1 \times 0.1 \times 0.039$ in., flow visualization.	$N_2 + N_2O_4 \leftrightarrow 2NO_2 + N_2$ reaction studied. NO_2 probe is large and has poor spatial resolution.
	LDV and marker nephelometry.	dp/dx not given. Jet marked with dioctylphthalate.
	Constant temperature hot-wire for velocity. Cold-wire for temperature	Conditional and unconditional measurements at one x/D, $x/D = 15$.
	Single constant temperature hot-wire and cold-wire for velocity and temperature 2 kHz frequency response.	
	Parallel constant temperature hot-wire for velocity and cold-wire compensated to 2 kHz for temperature.	Initial mixing layer of free, axisymmetric jet. Self-preserving first moments for $x/D > 5/3$. Acoustic excitation of mixing layer studied.
	Pitot-probe and constant temperature hot-wire for velocity. Cold-wire for temperature.	No influence of varying Θ_j observed. Reported axial variation of θ_0 does not follow similarity. See Table 1a.
$\langle C \rangle$ on centerline and at $x/D = 8, 16, 24$.	Pitot and gas sampling probes.	Sensitivity of $\langle C \rangle$ to sampling rate found negligible.
	Pitot probe and constant temperature hot-wire for velocity. Cold-wire for temperature, 6 kHz frequency response.	Transition to turbulence occurred at $x/D = 0.25$.
	Constant temperature hot-wire and cold-wire used.	Limited spatial information. Moments of pdf's reported.
	Pitot probe for velocity and cold-wire for temperature.	Θ_0 and u_0 correlated by form of $C^e\sqrt{R(x/D - x_0/D)}$.

Plane Jets:

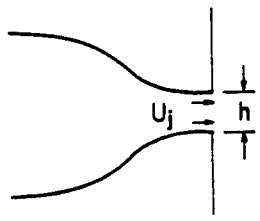

a.

ANTONIA & COWORKERS, 1983 - 84
BASHIR & UBEROI, 1975
JENKINS & GOLDSCHMIDT, 1973

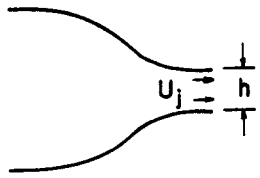

b.

DAVIS, et al., 1975

Round Jets:

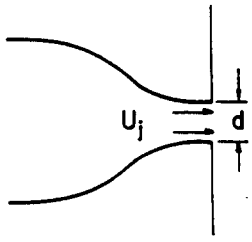

CHEVRAY & TUTU, 1978
CORRSIN & UBEROI, 1950
VENKATARAMANI, et al., 1975
WILSON & DANCKWERTS, 1964

a.

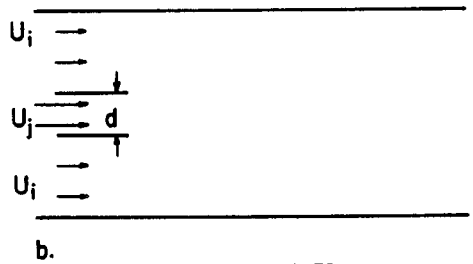

b.

ANTONIA, et al., 1975
ANTONIA & BILGER, 1976
CATALANO, et al., 1976

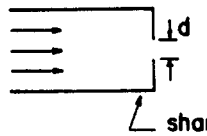

c.

KEAGY & WELLER, 1950

Mixing Layers:

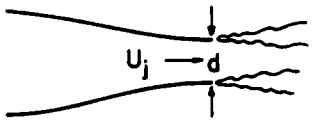

a. FIELDER, 1974
FIELDER, et al., 1977
SREENIVASAN, et al., 1977

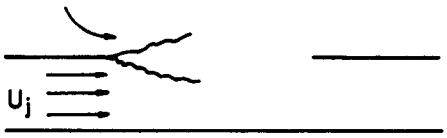

b. BATT, 1977

find different centerline variations in all three cases. This may be the result of three-dimensional effects arising in the downstream portion of the jet. Krothapalli *et al.*[57] have studied the effect of nozzle aspect ratio on the development of plane jets. The plane jet is divided into three regions—an initial mixing region, a two-dimensional region, and finally, far downstream, a three-dimensional region in which the plane jet evolves into an axisymmetic jet. As noted above, if the nozzle aspect ratio is too small, the two-dimensional region may not be large enough for a similar flow to develop in that region. Even if a similar, two-dimensional flow exists, care must be taken to distinguish the similar region from adjoining regions both upstream and downstream. The exact cause of the variations observed by Bashir and Uberoi is not clear. Unfortunately, data for the 20 and 144 aspect ratio cases are too sparse to detect different regions of jet growth by changes in the centerline variations of u_0 and θ_0. Everitt and Robins[42] also report aspect ratio effects in data for the spread of plane jets (see Table 1a).

Of the data in Table 3 the plane-mixing layer data of Batt[13] and the round-jet data of Antonia and Bilger[5] seem the most useful. However, Batt's optical probe was quite large, raising concern about spatial resolution and possible flow distortion. In addition, the boundary conditions in the experiment are not well defined. The shear flow is obtained by essentially removing one wall of a wind tunnel and entraining ambient air. This type of flow is not as cleanly defined as is a two-dimensional shear flow generated by a splitter plate. Antonia and Bilger[5] present data obtained in coflowing streams with varying U_j/U_1 over a good range of x/D. As the data verify, these flows do not achieve similarity, and thus they cannot be checked against the data in Table 1. On the other hand, in coflowing streams, accurate velocity measurements can be made to large x/D and r/D without encountering error associated with low mean velocities and high turbulent intensity, e.g. instantaneous flow reversal; an advantage for measurements in coflowing streams. Antonia and Bilger[5] present a somewhat limited set of turbulence data, u^2, $u\theta$ and θ^2, while uv is inferred from the mean flow data. It should be noted that there are other round-jet, coflowing stream data from Antonia, Bilger and coworkers (Antonia and Bilger[6] and Antonia *et al.*[10]) obtained in the same wind tunnel facility. However the data are for different initial jet diameters (D) and therefore, while they complement the data of Antonia and Bilger,[5] they do not supplement it.

Recently, Antonia and co-workers have presented a series of papers containing extensive data for a free, plane jet which appear to be well suited for model development and evaluation (Browne *et al.*;[24] Browne and Antonia;[22] Antonia and Browne;[7] Antonia *et al.*;[8,9] Brown *et al.*;[23] Antonia *et al.*[11]). Inlet and boundary conditions are well characterized, and a broad range of turbulence data are available as well as profiles of mean velocity and temperature. The initial flow is laminar ($(\overline{u^2})^{1/2}/U_j$ and $(\overline{\theta^2})^{1/2}/\Theta_j$ values measured at $x/h=0$ vary slightly from paper to paper but are less than 0.002 in all cases) with laminar boundary layers (0.23 mm momentum thickness). Turbulence data presented in the various

papers include lateral profiles of $\overline{q^2}$, $\overline{\theta^2}$, $\overline{uv}$, $\overline{v\theta}$ at as many as 8 axial locations to $x/h=40$. Similarity is found to obtain for $x/h>20$. The lateral profiles are carried to $y/y_u=1.4$; beyond this point high turbulence intensity precludes accurate measurements. $P(\theta)$, S_θ, K_θ, f_θ, and correlation data are also presented for many locations in the flow. Antonia and Browne[7] present data on the dissipation of $\overline{\theta^2}/2$ which include terms such as $\overline{v\theta^2}$. Data for centerline properties are presented to $x/h=40$, while several lateral profiles are reported up to $x/h=40$. Additional lateral profiles at larger x/h would be desirable especially to see if the evolution of the turbulence properties to similarity is complete.

With a laminar initial flow, transition to turbulence occurs in the calculation domain. For models which do not calculate transition, as is generally the case, some manipulation of the initial conditions is required but certainly is not desirable. Another problem with these data with regard to model validation and evaluation, is the presence of large-scale fluctuations at the end of the potential core region and beyond. Several investigators have reported such fluctuations in free-plane jets, and Antonia *et al.*[8] present considerable information on the nature of the fluctuations in their jet. (N.B., fluctuations have also now been observed in two-dimensional wake flows up to a very high Reynolds number[81] where previously they were thought not to exist. One wonders how long it will be before they are found regularly in round free jets.) Relative to other plane-jet experiments, the aspect ratio of the Antonia and coworker's jet (19.7) is rather small (see Table 1a) as is the initial Reynolds number (7620) based on h. Also the flow constants, C_u and C_θ, are low relative to other results. At this point one cannot say for sure that the data of Antonia and coworkers are free of three-dimensional effects stemming from a low aspect ratio. In spite of these drawbacks these data appear, because of their breadth, to be the most useful data for model development and evaluation available at the present time.

Constant temperature hot-wires were used by Antonia and coworkers to obtain velocity data. Three different configurations were used: single wire, X-wires, and two parallel wires for gradient measurements. A constant current, cold-wire was used for temperature measurements. The spatial resolution of these measurements appears to be less than 1 mm. Brown *et al.*[24] present accuracy estimates for their measurements; these are reproduced here:

$\overline{U}=\pm 1.5\%\ldots\ \overline{\Theta}=\pm 3\%$.

$\sqrt{\overline{u^2}}=\pm 3\%\ldots\sqrt{\overline{v^2}},\sqrt{\overline{w^2}}=\pm 4\%\ldots$
$\sqrt{\overline{\theta^2}}=\pm 4\%$.

$\overline{uv}=\pm 7\%\ldots\overline{v\theta}=\pm 12\%$.
$Pr_t=\pm 14\%$.

Although perhaps unnecessary, it should be noted that the comments made in this review do not constitute a general evaluation of the quality and value of the experimental data reviewed. Model evaluation is only one of many applications for experimental data and a rather new application. In most of the reviewed research, model evaluation was not a consideration or was only one of several considerations in the design and the conduct of the experiment.

TABLE 4.

Data Summary

Flow Free plane jet
Data Evaluators Gouldin and Johnston
Case Antonia and Coworkers
Geometry
Re: 7,620
Aspect ratio 19.7
$h=12.7$ mm
Mean dp/dx: practically zero

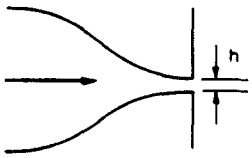

Mean quantities measured

U and Θ on centerline up to $x/h=40$. Lateral profiles at $x/h=5,7,8,9,15,20$ and 40.

Turbulence quantities measured

$\overline{u^2}$, $\overline{v^2}$, $\overline{w^2}$, $\overline{uv}$, $\overline{\theta^2}$, $\overline{v\theta}$ on centerline up to $x/h=40$ and lateral profiles at $x/h=5,7,8,9,15,20$ and 40.
$p(\Theta)$ and S_θ, K_θ, on centerline up to $x/h=20$.

Budget for $\frac{1}{2}\overline{\theta^2}$ and for data for $u\dfrac{\partial\overline{\theta^2}}{\partial x}$ and $v\dfrac{\partial\overline{\theta^2}}{\partial x}$ at $x/h=40$.

Initial conditions

Measured.

Notes

Initial flow is laminar.
Flow oscillations and large scale structures observed in initial growth region of the jet.

2.3. *Recommended Case*

For reasons given above, the recommended case for constant density flows is the plane jet case of Antonia and coworkers.[7-9,11,22-24] A summary of the flow conditions and the extent of the data taken is presented in Table 4. Data for comparison with model predictions should be taken from the literature.

As an aid to the reader some of the Antonia, Browne and coworker data are reproduced here. A schematic diagram of the apparatus is shown in Fig. 1. The aspect ratio of the nozzle is 19.7. The initial velocity profile is flat except for small wall boundary layers; $U_j = 9$ m/sec and the initial temperature difference between jet fluid and ambient air is 25 K.

Axial variations of mean temperature and mean axial velocity half-widths are presented in Fig. 2. In the downstream region their variation follows similarity form:

$$\frac{L_u}{h} = 0.104\left(\frac{x}{h} + 5\right)$$

and

$$\frac{L_\theta}{h} = 0.128\left(\frac{x}{h} + 5\right).$$

In Fig. 3 $(U_j/u_0)^2$ and $(\Theta_j/\theta_0)^{1/2}$ are plotted vs x/h. The velocity data at larger x/h satisfy similarity:

$$(U_j/u_0)^2 = 0.143(x/h + 9).$$

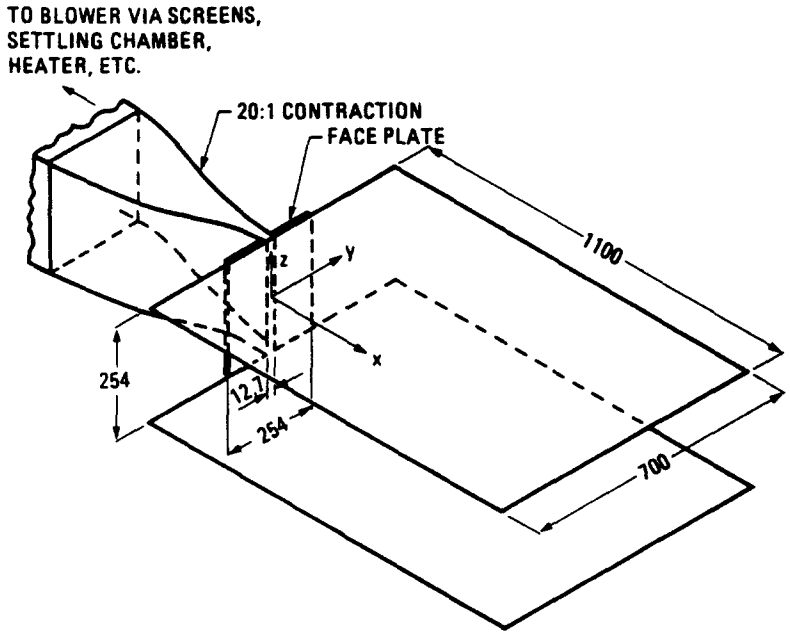

FIG. 1. Schematic diagram of flow apparatus. Dimensions are in mm. From Antonia *et al.*[8]

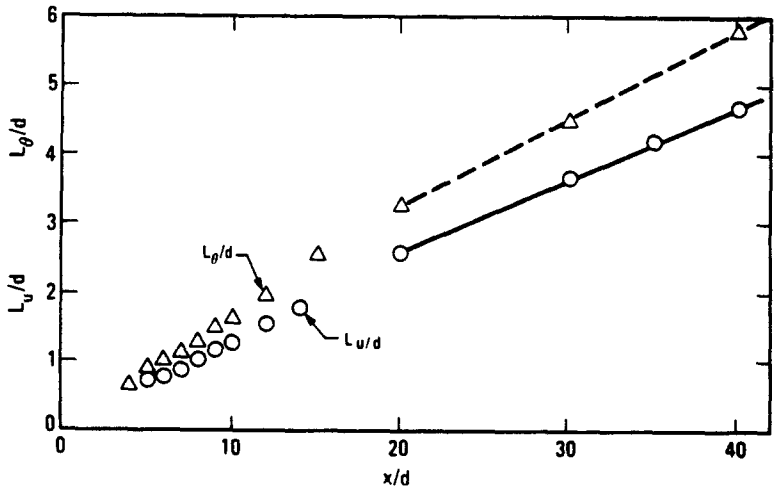

FIG. 2. Axial variation of the mean velocity and mean temperature profile half-widths from Browne *et al.*[23]

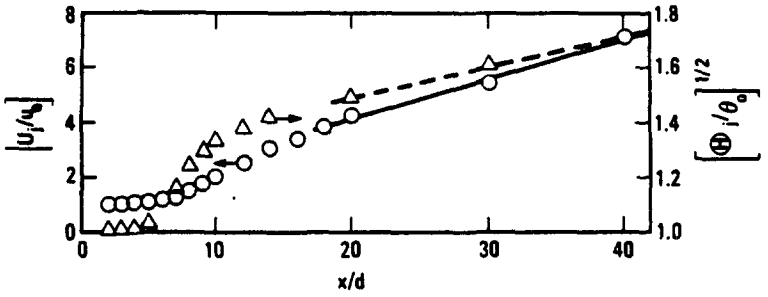

FIG. 3. Axial variation of centerline mean velocity and mean temperature from Browne *et al.* [23]

Jenkins and Goldschmidt[53] report their temperature data as $(\Theta_j/\theta_0)^{1/2}$ and these data are presented in the same way. The appropriate similarity form is $(\Theta_j/\theta_0)^2$, and from Browne *et al.*[24]

$$\left(\frac{\Theta_j}{\theta_0}\right)^2 = 0.18\left(\frac{x}{h}+8\right).$$

To complete this description of centerline properties, axial variations of $(\overline{u^2})^{1/2}$, $(\overline{v^2})^{1/2}$, $(\overline{w^2})^{1/2}$, $(\overline{\theta^2})^{1/2}$ and of $\overline{u\theta}$ are presented in Figs 4 and 5.

Beyond $x/h = 20$, first moments obey similarity to a good approximation in both the axial and lateral directions, while higher moments tend to approach similarity behavior. This behavior can be seen in Fig. 6 for $\overline{U}$ and $\overline{\Theta}$ and in Figs 7, 8 and 9 for $(\overline{\theta^2})$, $(\overline{q^2})$ and for several correlations. For more detail on the flow and for information on the flow oscillations observed in the potiential core region of the jet the reader is referred to the original papers.

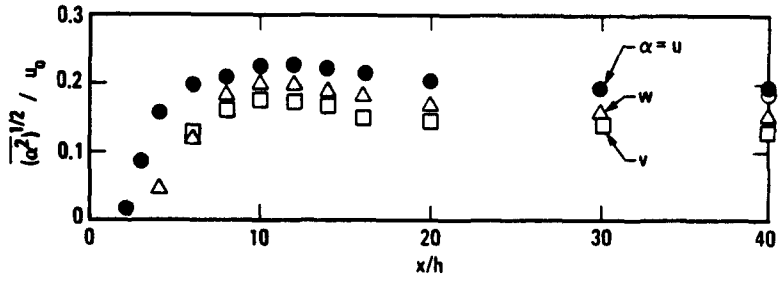

FIG. 4. Axial variations of $(\overline{u^2})^{1/2}$, $(\overline{v^2})^{1/2}$ and of $(\overline{w^2})^{1/2}$ on the centerline normalized by U_j, from Browne *et al.*[23]

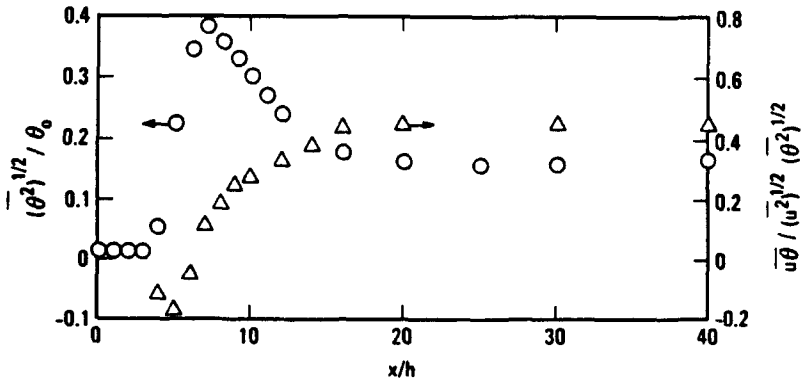

FIG. 5. Axial variation on the centerline of $(\theta^2)^{1/2}/\theta_0$ and $\overline{u\theta}/(\overline{\theta^2})^{1/2}(\overline{u^2})^{1/2}$ from Browne, *et al.*[23]

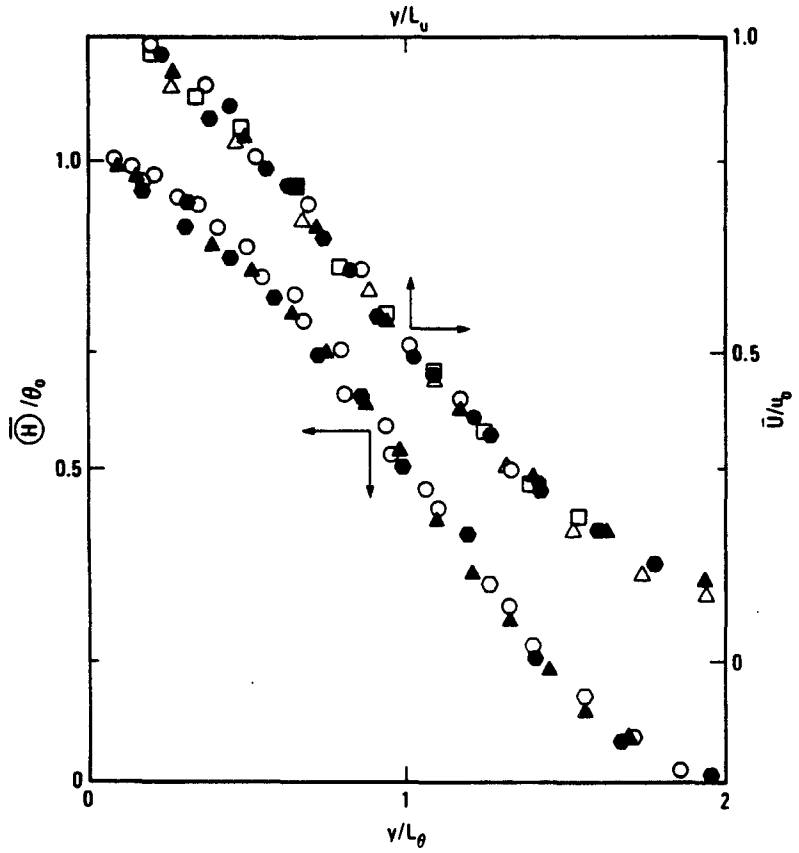

FIG. 6. Lateral profiles of mean temperature and velocity from Browne *et al.*[23] △, $x/h=5$; ⬢, 7; ▲, 8; ●, 9; ◇, 12; ▽, 14; □, 20; ○, 40.

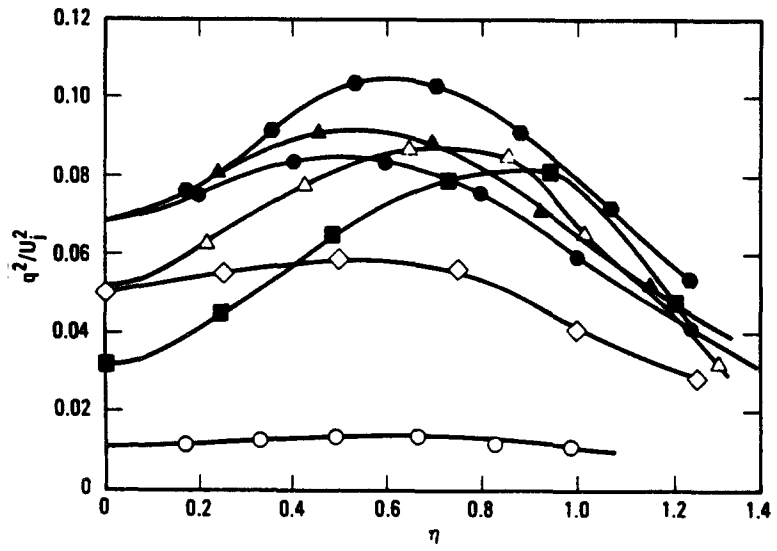

FIG. 7. Lateral profiles of $\overline{q^2}/U_j^2$ from Browne *et al.*[24] ■ $x/h=4$; other symbols are as in Fig. 6.

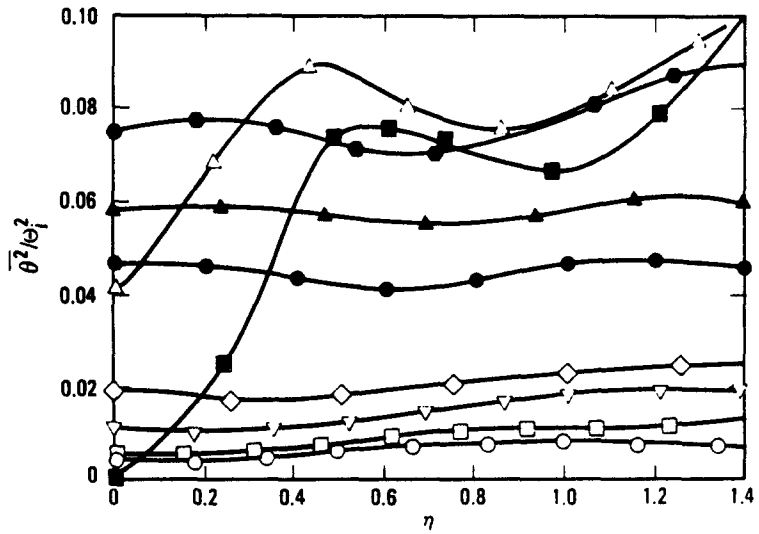

FIG. 8. Lateral profiles of θ^2/Θ_j^2 from Browne *et al.*[24] Symbols are as in Fig. 7.

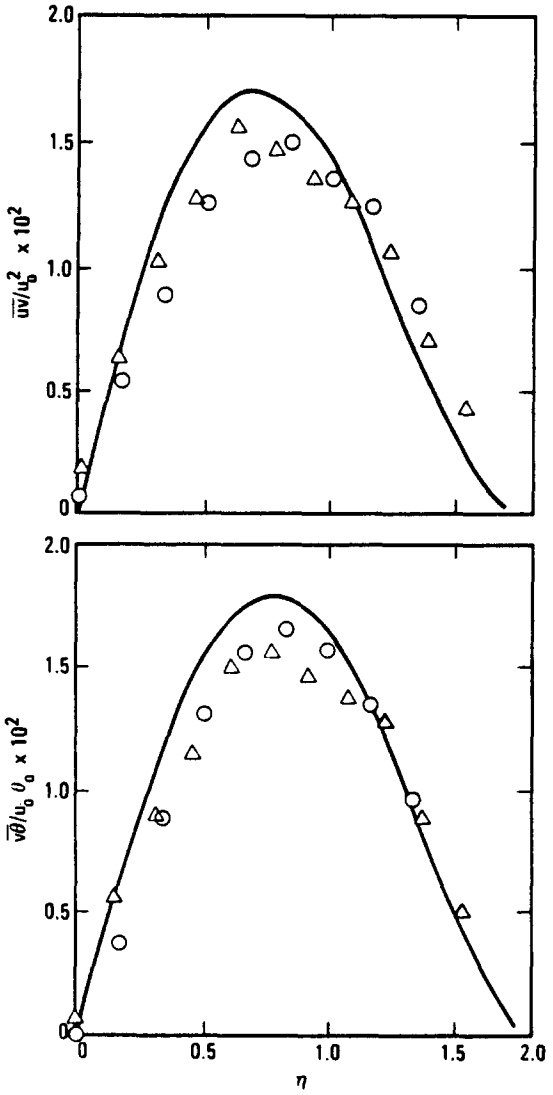

FIG. 9. Reynolds shear stress (a) and heat flux (b) profiles at two axial locations from Browne and Antonia.[22] ○, $x/h = 40$; △, 20.

3. VARIABLE DENSITY MIXING FLOWS

In this section, data for variable density, turbulent, mixing flows are presented and discussed as to their suitability for model evaluation. Additional data needs for this type of flow are recommended.

3.1. *Review of Data*

Experimental studies of turbulent, variable density flows have utilized numerous experimental techniques under widely-varying flow conditions and geometries. Based on the criteria set forth in the previous section, a summary of those studies most revelant to the present report is presented in Tables 5 and 6. The two major categories of variable-density nonpremixed flows to be considered in the following discussion are axisymmetric and planar jets (Table 5) and two-dimensional shear layers (Table 6). Turbulent jets (both axisymmetric and planar) provide a simplified flow geometry that is well suited to modeling. Unfortunately, initial density variations rapidly decrease with axial distance in these flows. Two-dimensional shear layers have recently received greater attention and provide a mixing region in which density differences are more easily maintained over the experimental region of interest. However, recent measurements have identified the possible importance of large-scale structures in the mixing process. The application of current modeling calculations to flows where large-scale structures play an important role in the mixing process could prove to be difficult.

The experiments presented in Table 5 correspond to a jet of density ρ_j flowing into either a quiescent or a coflowing gas of different density ρ_1. This class of flows is further subdivided on the basis of geometry into axisymmetric round jets (Table 5a) and two-dimensional planar jets (Table 5b). It should be noted that the term "two-dimensional" strickly applies only

to the test section geometry since the three-dimensionality of turbulent flowfields is well known. The range of density ratios studied varies from the helium jets of Keagy and Weller[54] and Aihara *et al.*[2] flowing into air (corresponding to a density ratio ρ_j/ρ_1 of 0.14) to the studies of Dyer[40] and of Schefer *et al.*[73] in which a propane jet into coflowing air was used ($\rho_j/\rho_1 = 1.6$). All flows considered in Table 5 are parabolic except for perhaps in the region immediately downstream of the jet exit rim where, depending on the rim thickness, parabolic flow assumptions may be invalid due to flow disturbances and small recirculation zones caused by the jet rim. It is likely that these disturbances rapidly disappear downstream where the majority of mixing occurs. In either case modeling assumptions can be made for this region and its influence on downstream mixing can be quantified. Only four of the references in Table 5a for axisymmetric jets report measurements of both a scalar and velocity.

Keagy and Weller[54] report measurements in 3.25-mm dia helium and carbon dioxide jets flowing into still air with a jet velocity of 122 m/sec. Concentration and velocity profiles were measured along the centerline, and radial profiles were obtained at three axial locations. The measurements were obtained with a pitot tube for velocity and a sampling probe for concentration and are therefore limited to mean values.

Aihara *et al.*[2] studied the effects of coflowing air on the spreading rate and turbulent transport rates in a 1-mm dia helium jet. A hot-wire probe was used to measure velocity and concentration and the latter measurements were compared with sampling probe measurements to verify the hot-wire results. Detailed radial profiles of concentration and velocity and the correlations between velocity and concentration fluctuations are presented at several downstream locations. The results are limited to low Reynolds number conditions ($Re = 2950$) where the flow may not be fully turbulent.

Extensive scalar measurements have been made in methane jets but velocity data are somewhat limited. Chigier and Strokin[27] used a gas sampling probe to obtain concentration measurements in a methane jet with low velocity coflowing air. Mean velocity was determined from the measured density and concentration and the dynamic pressure. A gas tracer method was used to calculate the turbulence intensity. The effects of combustion on turbulent diffusion were studied by comparing results in a reacting jet with those in a cold-flow case. Mean concentration and velocity measurements are limited to centerline profiles for the cold-flow case.

Recent studies of methane jets have concentrated on the use of nonintrusive optical diagnostic techniques. Pitts and Kashiwagi[66] used Rayleigh scattering for the measurement of methane concentration (on a mass and mole fraction basis) in a turbulent round jet and presented extensive comparisons between constant and variable density jets. One radial concentration profile and a centerline profile of methane concentration were obtained but no velocity data were presented. The jet exit Reynolds number was also somewhat low ($Re = 4130$) for fully-turbulent flow. Birch *et al.*[18] used laser-Raman scattering to measure detailed radial profiles and an axial profile of the mean methane concentration and higher moments (up to the fourth moment). Velocity measurements were limited to axial velocity fluctuations along the centerline and comparisons were made with the centerline concentration fluctuations. This data provides a suitable data set for modeling calculations in methane jets.

The temperature distribution throughout the flowfield of a heated air jet ($T_j = 225°C$) was measured by Lockwood and Moneib[62] using a 12.7-μm thermocouple. Extensive data were obtained on the mean and higher moments, pdf's, and spectral density distributions, and comparisons were made with results in the literature. No velocity measurements were, however, made.

Recent data has been obtained by Schefer and co-workers in an axisymmetric propane jet with coflowing air (Schefer *et al.*,[73,74] Dibble *et al.*[33,34]). The data are extensive, include both a scalar quantity (propane mixture fraction) and velocity, and are well suited for model evaluation. Axial and radial velocities were measured using two-color laser velocimetry (LV). Velocity statistics conditioned on fluid originating from the jet and air streams were obtained by alternately seeding only the jet and the coflowing air with LV seed particles. The results thus represent the extremes of biasing errors commonly encountered due to unequal seeding of the jet and air streams. Unconditional velocity statistics can be calculated from the intermittency profiles measured using Rayleigh scattering in the same flow. Concentration measurements were obtained from Rayleigh scattering (density and propane mixture fraction) and laser Raman scattering (density and mixture fraction). Time histories, power spectra, and mixing length information were obtained from the Rayleigh scattering measurements. In addition, the Raman and LV systems were combined to measure simultaneously two velocity components and the conserved scalar.

The flows listed in Table 5b consist of planar two-dimensional jets issuing into coflowing air. They are similar to the studies shown in the previous table in that two initially separated streams of different densities and velocities form a mixing layer downstream of the inlet section. Most apparent are the limited data that are available on plane mixing layers. Only two studies were found with sufficient data to make comparisons with modeling calculations. Anderson *et al.*[4] used a two-sensor hot-wire probe to measure mean and fluctuating velocity and concentration in a helium jet discharging into a coflowing air stream. Spatial resolution of the probe

TABLE 5a. Round jets

Reference	Flow	Measurements reported: Velocity	Measurements reported: Temperature
Keagy and Weller[54]	Free round helium and CO_2 jet. $U_j = 122$ m/sec; $D = 3.25$ mm.	$\bar{U}$: one centerline + 3 transverse profiles.	
Aihara *et al.*[2]	Free round helium jet with and without an air co-flow. $Re = 2.95 \times 10^3$, $D = 1$ mm, [Air]/[He] = 7.	$\bar{U}$, u', v', $u'v'$: 3 transverse profiles.	
Chigier and Strokin[27]	CH_4—diffusion flame. $D = 0.005$ m, $R_e = 6600$ $U_j = 20.5$ m/sec $U_e = 0.6$ m/sec.	U, u': one centerline and 2 transverse profiles.	
Birch *et al.*[18]	Free round CH_4-jet in air $R_e = 160000$, $D = 0.0126$ m, $U_e = ?$ $[CH_4]/[Air] = 0.55$.	u': one centerline profile.	
Dyer[40]	Free round C_3H_8-jet in air $R_e = 9790$, $U_j = 21.1$ m/sec, $U_e = 0.7$ m/sec (air), $[C_3H_8]/[Air] = 1.52$.		
Lockwood and Moneib[62]	Heated round jet. $R_e = 5000$, $D = 19.3$ mm, $T_j = 225$°C.		$\bar{T}$, T', higher moments: one centerline +8 transverse profiles; pdf's of T: 4 transverse profiles; power spectra.
Long *et al.*[63]	Free round jet. $R_e = 3240$, 4160, [Air]/[Air] = 1.0.		
Pitts and Kashiwagi[66]	Round CH_4-jet in air $R_e = 4130$, $U_j = 10.2$ m/sec, $U_e = 0.34$ m/sec, $[CH_4]/[Air] = 0.55$.		
Schefer *et al.*[73, 74]	Round C_3H_3-jet in air. $Re = 68000$, $D = 5$ mm. $U_j = 53$ m/sec; $U_e = 9.2$m/sec, T_0 ambient, $[C_3H_8]/[Air] = 1.6$.	$\bar{U}$, $\bar{V}$, u', v', $u'v'$ and pdf's: one centerline +3 transverse profiles.	
Dibble *et al.*[34]			
Dibble *et al.*[33]			

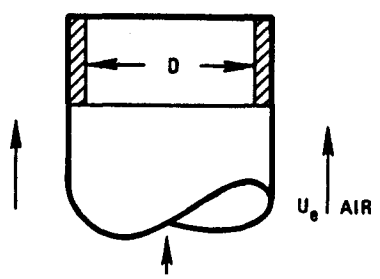

Other	Probe characteristics	Comments
Concentration ($\bar{C}$): one centerline +3 transverse profiles.	Pitot tube, sampling probe, 0.762 mm bore	Low Reynolds number.
Concentration ($\bar{C}$, c', $\overline{u'c'}$, $\overline{v'c'}$): 3 transverse profiles.	Hot wire for velocity and concentration. Sampling probe for mean concentration, 0.3 mm bore.	Low Reynolds number.
Dynamic pressure ($\overline{pu^2}$): one centerline profile. Concentration ($\bar{C}$): one centerline +4 transverse profiles.	0.12-mm coated thermocouple. Probe, 0.2-mm bore.	Flame and cold flow.
Concentration ($\bar{C}$, c') higher moments, integral time scales: one centerline +3 transverse profiles; autocorrelation, power spectra, pdf's: one transverse profile.	Raman spectroscopy probe volume 0.2 mm × 2 mm.	Some velocity measurements density can be inferred from concentration measurement. Axial velocity, mean and rms. No direct density measurements
Mole fraction ($\bar{X}_{C_3H_8}$): 3 transverse profiles ($x/D =$ 15, 20, 30); rms: one transverse profile ($x/D = 20$).	Rayleigh scattering, probe volume 0.2 mm × 1 mm.	No velocity or density measurements.
	12.7 μm bare-wire thermocouple.	Classical experiment. No density measurement. Density fluctuations small. Lots of data. No velocity.
Jet Fluid Concentration ($\bar{C}$, c'): contours $x/D =$ 3–8; two-point covariance.	Lorentz/Mie scattering (seed). Technique demonstration.	Constant density mixing. No velocity, limited spatial regime.
Mass and mole fraction ($\bar{C}$, c'), higher moments, conditional moments, intermittency power spectra: one centerline +1 transverse profile ($x/D = 35$).	Rayleigh scattering, time-resolved concentration probe, probe volume 0.035 mm × 0.27 mm.	No velocity or density measurements. Small density variation. Time resolution 5000 Hz, 200 μsec. Confined, no pressure gradient.
C_3H_8 mixture fraction density ($\bar{C}$, $\bar{P}$, C', P'), higher moments, pdf's, power spectra: one centerline +3 transverse profiles.	2-color LDV, Rayleigh scattering, probe volume 0.2 mm × 1 mm.	Small density variation. Publication in preparation.
C_3H_8, O_2, N_2 concentration ($\bar{C}$, c', $\overline{u'c'}$, $\overline{v'c'}$), joint pdf's: 4 locations.	Simultaneous LDV—laser Raman spectroscopy.	
Instantaneous radial profiles of mixture fraction.	One-dimensional Rayleigh imaging.	

TABLE 5b. Planar jets

Reference	Flow	Measurements reported: Velocity	Measurements reported: Temperature
Anderson *et al.*[4]	Two-dimensional jet of helium discharging into moving airstream, U_j = 120 m/sec, U_e = 4/6 m/sec.	$\bar{U}$, u': several streamwise locations.	
LaRue and Libby[60]	Boundary layer with He-injection, U_j = 5 m/sec, U_e = 2 m/sec.	$\bar{U}$, u', v', $u'v'$: 6 transverse profiles.	

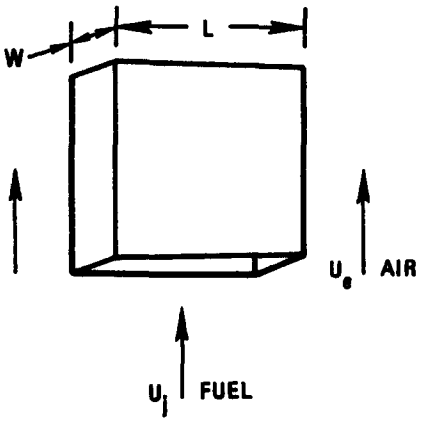

Anderson *et al.*[4]

TABLE 6. Plane mixing layer

Reference	Flow	Measurements reported: Velocity	Measurements reported: Temperature
Rebollo[69]	Plane mixing layer N_2–He at p = 4 atm.	$\bar{U}$, u': transverse profiles.	
Brown and Roshko[21]	Plane mixing layer, N_2–He, [N_2]/[He] = 7, p = 7 atm. U_{He} = 5 m/sec; U_{N_2} = 1.9 m/sec.	U: transverse profiles.	
Konrad[89]	Plane mixing layer + wakes, N_2–He, Ne–He + Ar.		
Keller[55]	Plane mixing layer U_1 = 15 m/sec, U_2–5 m/sec, T_2/T_1 = 6.	U, V, u', v' $u'v'$, moments: transverse profiles.	

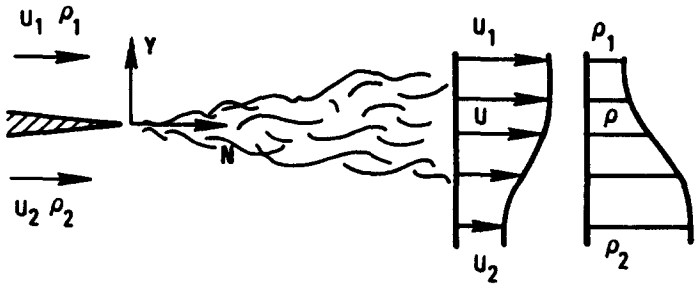

Other	Probe characteristics	Comments
Concentration (C, c'): several streamwise locations.	Hot wire for velocity and concentration.	
Concentration (C, c', $c'v'$).	Hot wire for velocity and concentration.	Geometry difficult. Helium injected into boundary layer.

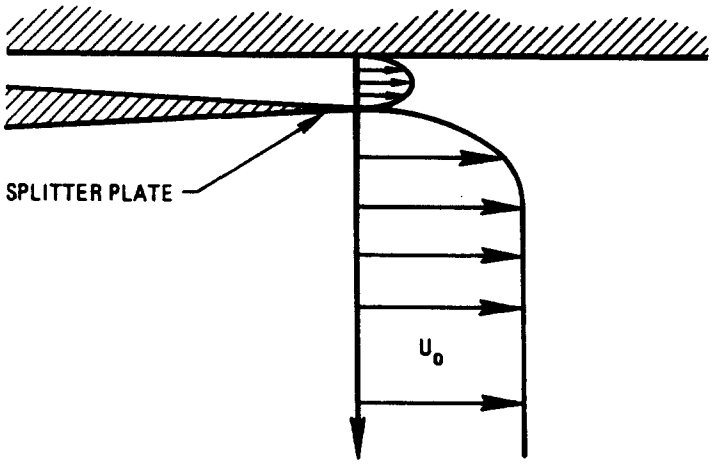

LaRue and Libby[60]

Other	Probe characteristics	Comments
Density (ρ, ρ'): transverse profiles.	Pitot probe for velocity Brown–Roshko probe for density.	
Density (ρ): transverse profiles.	Probe, visualization Pitot probe for velocity Brown–Roshko probe for density.	Low R_τ. Mean values.
Concentration pdf's.	Probe.	
	2-color LDV forward scatter, probe volume 0.13 mm × 1.8 mm.	Not clear that flow was parabolic (maybe elliptic) No scalar measurements.

was on the order of three times the estimated Kolmogorov length scale (approximately 0.5 mm). Mean and fluctuating streamwise velocities and the mean and fluctuating concentration were presented at several streamwise locations. Range-conditioned point statistics were determined to provide the distribution of velocity and concentration statistics in the turbulent fluid elements at several locations.

LaRue and Libby[60] used a three-sensor probe (the Way–Libby probe) to obtain velocity and concentration measurements in a turbulent wall boundary layer of air with helium injection through a slot adjacent to the outer wall. Measurements were reported of the streamwise and transverse velocity components, helium concentration, and density and their higher order correlations. Comparisons were also made between conventionally-averaged and Favre-averaged statistics. The boundary conditions are more complex than those for conventional axisymmetric and planar jets but the extensive data available make this a suitable case for the evaluation of computational models.

The flows of Table 6 correspond to two-dimensional shear layers in which two initially separated streams of different density and velocity form a mixing region downstream of a splitter plate. These flows may be subject to organized large-scale structures which complicate comparisons with current modeling approaches. They would, however, provide excellent test cases for emerging modeling approaches (e.g. vortex dynamics or hybrid schemes involving both vortex dynamics and large-eddy simulation) which attempt to calculate such large-scale structures.

Rebollo[69] obtained measurements in a plane mixing layer of nitrogen and helium at a pressure of 4 atm. A pitot probe and a fast-response density probe were used to measure mean streamwise velocity and mean and fluctuating density, respectively. Transverse profiles at several streamwise locations were measured. Similar measurements were made by Brown and Roshko[21] in a nitrogen and helium mixing layer at a pressure of 7 atm., although only mean transverse velocity and concentration measurements were presented. Flow visualization studies were made showing the existence of large coherent structures which control the mixing layer development in this type of flow. These measurements were extended by Konrad[89] who mixed argon with the helium flow to study the effects of density ratio.

The velocity measurements of Keller[55] were made in a mixing layer of high-temperature combustion products and air ($T_2/T_1 = 6$). A two-color LV system was used to obtain pdf's of the streamwise and transverse components of velocity. From these pdf's, transverse profiles of the means and higher moments (up to the fourth moment) and the Reynolds shear stress were determined at several streamwise locations. No scalar measurements are reported and it is not certain that the flow was truly parabolic.

3.2. *Recommended Case: Variable Density Flows*

The recommended case for variable density flows is the nonreacting round jet of propane into coflowing air (Schefer *et al.*;[73,74] Dibble *et al.*[33,34]). A summary of the flow conditions and the extent of the data taken is shown in Table 7. Since these data have not yet been published in the literature, an expanded discussion of the experimental results is provided in Section 4 of this report. To facilitate comparisons with modeling calculations a complete tabulation of the available experimental data for this flow can be found in Schefer *et al.*[76] The tabulated results include measurements of mean and fluctuating quantities, higher moments, and prob-

TABLE 7.

Data Summary

Flow Propane jet (round)
Data evaluators Schefer and Johnston
Case Schefer, Dibble and Hartman
Geometry
Re: 68,000
Mean dp/dx: 6 Pa/m
Mean quantities measured
$\bar{u}$ and $\bar{f}$ on centerline up to $x/D = 80$. Radial profiles at $x/D = 15,30,50$.
Turbulence quantities measured
$\overline{u'^2}$, $\overline{v'^2}$, $\overline{u'v'}$, $\overline{f'^2}$, $\overline{f'^3}$, $\overline{f'^4}$, $p(u,v)$, $p(f)$ on centerline up to $x/D = 80$.
Radial profiles at $x/D = 15,30,50$. Also $p(u,v,f)$ at $x/D = 30,50$ on $r/D = 0.2$.
Initial conditions
$\bar{U}_e = 9.2$ m/sec, $\overline{u'^2}/\bar{u} = 0.02$ $\bar{U}_j = 53$ m/sec and u, $\bar{u'} \rightarrow f, \bar{f'}$ at $x/D = 4$.
Notes
No flow visualization.
Vertical tunnel.
Density obtainable from mixture fraction.

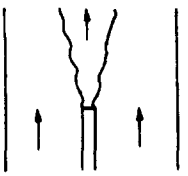

TABLE 8. Experimental diagnostics

Diagnostic	Quantity measured
CW Rayleigh scattering	Single-point density and mixture fraction
Laser-Doppler velocimetry	Simultaneous single-point axial and radial velocities
Raman scattering	Simultaneous single-point species concentrations (C_3H_8)
Combined LDV-Raman	Simultaneous single-point species concentrations and two-velocity components
One-dimensional Rayleigh imaging	Instantaneous radial profiles of density and mixture fraction

ability density distributions. Copies of the tabulated data are currently available on magnetic tape and can be obtained from the authors through Sandia National Laboratories, Livermore, CA 94550.

4. DATA BASE: NONREACTING PROPANE JET

In the following sections the experimental results obtained by Schefer and coworkers in a nonreacting propane jet into coflowing air are described. Typical experimental data are presented and compared with data for constant density and variable density jets found in the literature.

4.1. *Experiment*

4.1.1. *Test facility*

All measurements were performed in the Sandia Turbulent Diffusion Flame Facility. A complete description of the facility is given by Dibble *et al.*[32] This facility is similar to that used in previous studies (Driscoll *et al.*,[38] Schefer and Dibble[75]) with the exception that the axis of the test section has been oriented vertically instead of horizontally to eliminate flame asymmetry (for combustion measurements) due to buoyancy effects. The experimental diagnostics used in the study and the corresponding quantities measured are summarized in Table 8. The experimental methodology followed in the investigation is illustrated by the order in which the diagnostic techniques and measurements are listed in the table. Test section dimensions and the inlet conditions are summarized in Table 9. Velocity measurements at the test section inlet using laser velocimetry showed that the maximum velocity at the centerline of the jet exit ($u_{j,\,max}=69$ m/sec) is consistent with fully-developed, turbulent pipe flow ($u_{j,\,max}=1.28\ u_{j,bulk}$). A thin boundary layer was also measured along the outer edge of the jet pipe with a thickness of approximately 0.3 jet diameters at the exit plane of the jet. A more complex description of the inlet conditions can be found in Appendix A.

4.1.2. *Rayleigh scattering system*

Rayleigh scattering was used for single-point density and propane mixture fraction measurements.

TABLE 9. Test section dimensions and inlet conditions

Test section	30 cm × 30 cm
Jet tube exit	0.52 cm (I.D.) 0.90 cm (O.D.)
Length of jet straight section prior to exit	2 m
Jet velocity (Bulk)	53 m/sec
Coflow air velocity	0.2 m/sec
Reynolds number (based on jet exit dia)	68000
Coflow air turbulence	0.4 %
Axial pressure gradient	6 Pa/m

A complete description of the experimental system is given in Schefer and Dibble.[75] Briefly, the Rayleigh scattering measurements were made using a 6 W CW argon-ion laser operating at $\lambda=488$ nm. The laser beam was focussed with a 35-cm focal length lens to a 200-μm waist diameter. The measurement volume, defined by the entrance slit to the photomultiplier tube (3-mm wide, 2-mm high) and the laser beam diameter, was 1 mm in length by 0.2 mm in diameter. At each spatial location 64,000 measurements were taken at a sample rate of 16,000 samples/sec. This sample rate resulted in frequency components up to 8 kHz contributing to the mean and fluctuating Rayleigh signal.

In addition, the single-point Rayleigh scattering measurements were extended to one-dimensional measurements using an optical multichannel analyzer (OMA) to obtain information on instantaneous gradients in the flowfield. These data have been published elsewhere (Dibble *et al.*[33]) and will not be discussed further.

4.1.3. *Laser velocimeter*

Velocity measurements were made using a two-color laser velocimeter. The LV system (see Schefer *et al.*[74]) includes a two-color, dual-beam, real-fringe system with a measurement volume, as defined by the image of the pinhole on the beam crossing, 0.3 mm long by 0.25 mm in diameter. Coincidence of the radial and axial velocity measurements was verified using a multichannel interface with a variable time window set at 10 μsec to assure that the velocity

measurement in each direction was from the same seed particle.

The velocity data are presented as mean and fluctuating velocity components (axial and radial velocity) and their correlation, conditional on fluid originating from the jet or the air stream. In the analysis of the velocity data, it is assumed that the seed particles (0.85 μm follow the motion of the fluid and that the difference between the diffusivity of the particle and the fluid is negligible. These assumptions are asymptotically valid in the limit of large Reynolds number (Bilger and Dibble[17]). With these assumptions, the motion of a seed particle is identified to the motion of a fluid element and fluid originating from the jet can be distinguished from fluid originating from the coflowing air. Thus by alternately seeding only the jet and the coflowing air streams, velocity statistics conditional on the jet fluid and on the coflowing air fluid can be obtained.

4.1.4. *Raman scattering system*

The data were extended to include simultaneous measurements of two velocity components and species concentrations by combining the two-color LV system with a Raman scattering system (Dibble *et al.*[32]). Information on important turbulent transport terms used in modeling equations can be obtained from these data. Raman measurements of gas species concentrations were made using a high-power pulsed dye laser (1 J/pulse, 2 μsec pulsewidth, $\lambda = 514.5$ nm, $\Delta\lambda = 0.4$ nm). Further details of the Raman scattering system can be found in Dibble *et al.*[32] The beam was focussed to a 500 μm waist diameter which was aligned to overlap the LV measurement volume. The width of the spectrometer entrance slit determined the length of the Raman probe volume (1 mm), while the height of the probe volume was determined by the laser beam diameter. The vibrational Raman-scattered light from C_3H_8 was separated from the collected light with a 3/4-m grating spectrometer and measured on a photomultiplier tube at the exit plane of the spectrometer. At each spatial location a minimum of 2500 simultaneous pairs of axial and radial velocity and of mixture fraction were measured.

4.2. *Error Analysis*

4.2.1. *Rayleigh scattering*

Rayleigh scattering has been used to measure concentration, temperature, and density (Johnston *et al.*[58]). In addition, recent studies have demonstrated its applicability to both nonreacting and reacting turbulent flows (Dibble and Hollenbach;[31] Pitts and Kashiwagi;[66] Schefer and Dibble[75]). In a two-component, isothermal flow such as the nonreacting propane jet reviewed here, the Rayleigh signal intensity is directly related to the propane mass fraction. The primary sources of error in the Rayleigh scattering measurements are background scattering and shot noise. The major source of background scattering is laser light scattered from the test section windows. Background scattered light was measured by moving the collection optics off the laser beam (thus eliminating the Rayleigh scattered light contribution to the total signal). Using this technique the background signal was found to be approximately 4% of the Rayleigh signal measured in air. At each measurement location the contribution of background scattering was eliminated by subtracting its value from the measured signal. Particle (Mie) scattering was effectively eliminated as a source of background scattered light by filtering particles from the coflow air upstream of the test section inlet. Detailed discussions of shot noise and its affect on the measurement of turbulent quantities can be found elsewhere (Pitts and Kashiwagi[66]). Electronic shot noise contributes to the measured concentration fluctuations. An estimate of the shot noise contribution was made from Rayleigh scattering measurements in air and found to be 3% of the total air signal. The uncertainty in the mixture fraction measurements using Rayleigh scattering was estimated from calibration data and from the scatter measurements for several different experimental runs. The estimated uncertainty in the data is: $f = \pm 2\%$, $\sqrt{f^2} = \pm 3\%$.

4.2.2. *Laser velocimetry*

Conditional statistics were obtained for the mean and fluctuating velocities and the correlation between the axial and radial velocity $u'v'$. At each measurement location a minimum of 3,000 velocity measurements were obtained. This was estimated to be sufficient for the first two moments of the velocity. The correlation $u'v'$ calculated from 3,000 measurements was found to agree within 1% of the value calculated from up to, 10,000 measurements. The primary source of error that must be considered is bias due to the proportionality of particle flux, through the measurement volume, to the instantaneous velocity. This may give rise to a statistical bias toward higher velocities when number-weighted averages are used to calculate stationary statistics. Razdan and Stevens[68] have shown in a comparable jet flow that for velocity fluctuations up to 10% the errors are negligible. As the fluctuations increase the velocity statistics are increasingly biased toward higher velocities. At the maximum fluctuation levels measured a maximum bias error of 3% in the mean is estimated. The velocity data presented are not corrected for the effects of velocity bias.

Additional sources of error have also been estimated. The error due to velocity-gradient broadening was estimated to be less than 0.3%. Errors in time measurement with a counter processor having 0.5 nsec resolution are less than 0.2% at the highest burst frequencies measured. Since the velocity of a particle is actually measured with laser velocimetry, particle-velocity lag must also be considered. Using

the estimates of Durst *et al.*,[39] a 0.85 micron particle can follow the flow up to a frequency of 8 kHz with a slip velocity of 1 %. Based on previous measurements in the current flow this frequency response is sufficient.

The estimated uncertainty in the velocity measurements was inferred from calibration data and from the scatter in measurements from different experimental runs. The resulting uncertainties (based on data set consisting of 3,000 measurements) are as follows:

$$\bar{U} = \pm 1\% \ldots \bar{V} = \pm 15\%$$
$$\sqrt{\overline{u^2}} = \pm 2\% \ldots \sqrt{\overline{v^2}} = \pm 2.5\% \ldots$$
$$\overline{uv} = \pm 5\%.$$

4.2.3. *Raman scattering*

The primary sources of error in the Raman scattering measurements are calibration of the light collection system, shot noise, and background fluorescence (primarily from the windows where the laser beam enters and exits the test section). Calibration of the Raman system was done in mixtures of C_3H_8 and N_2. As a measure of the overall efficiency of the collection system, 6,000 photoelectrons/J of laser light were collected from N_2 in room air. The background fluorescence contribution to the Raman signal was measured by scanning the spectrometer away from the Raman line and was determined to be less than 0.5 % of the Raman signal from N_2 at STP.

4.2.4. *Data consistency checks*

Several checks on the data were performed to assess the accuracy of the measurements. Conservation of propane (on a mass basis) was verified by integrating the velocity and the propane mass fraction measurements across the flowfield. The integrations were carried out at three axial locations ($x/D = 15$, 30 and 50) and the total propane mass flux was compared with the calibrated value based on the mass flowmeter reading. The total propane mass flux at the jet exit was 2.3 g/sec, and the mass flux calculated at each axial location agreed with this value within 5 %. In addition to the conservation of propane, momentum must also be conserved across the flowfield. Integration of the total momentum at the above three axial locations was found to agree within 3 % of the inlet value. A further check on the data and experimental techniques has been provided by comparisons with published measurements where possible.

4.3. *Discussion of Data*

Selected mixture fraction and velocity data are presented and discussed in the following sections. Included in the discussion are axial and radial profiles, probability distributions, and joint probability distributions of propane mixture fraction and velocity. Publications more fully describing these data and containing more extensive comparisons with published results are in preparation.

4.3.1. *Mixture fraction measurements*

4.3.1.1. Mean and fluctuating quantities. The centerline variations in the mean and fluctuating component of the mixture fraction are shown in Fig. 10. Axial distance x is normalized by the jet exit diameter D. The rms of the mixture fraction fluctuations $(\overline{f'^2})^{1/2}$ is normalized by the mixture fraction at the centerline $\bar{f}_{cl}$. The mean mixture fraction $\bar{f}$ remains nearly constant over the potential core region, which extends approximately 4 jet diameters downstream of the jet exit, before decreasing rapidly as coflowing air is entrained by the high velocity jet and mixes with the propane. After the initial core region, the fluctuations increase rapidly downstream of the jet exit. In the downstream region, the fluctuations continue to increase but at a slower rate.

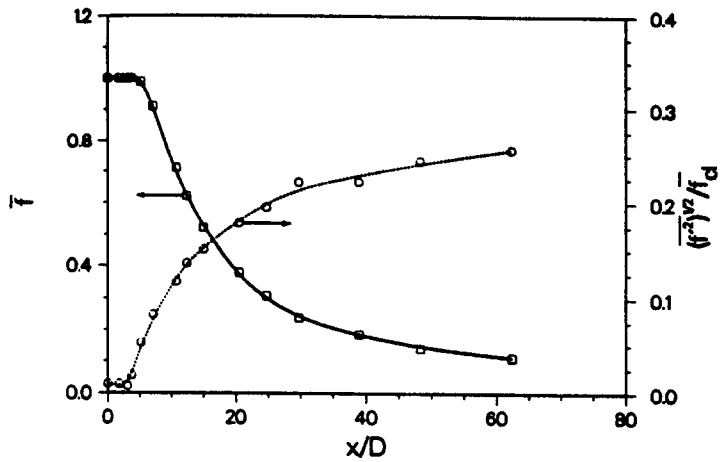

FIG. 10. Mean mixture fraction and mixture fraction fluctuations measured along centerline in turbulent nonreacting propane jet. Bulk jet velocity = 53 m/sec; coflowing air velocity = 9.2 m/sec.

Centerline variations in mean mixture fraction for nonreacting jets can be correlated with distance from the virtual origin $x_{0,1}$ (see discussion in Section 2). This correlation can be expressed as

$$\frac{\bar{f}_j}{\bar{f}_{cl}} = \frac{C_f^e(x - x_{0,1})}{D(\rho_{jet}/\rho_{air})^{1/2}}, \tag{14}$$

where $\bar{f}_j$ is the value of the mixture fraction at the jet exit ($f_j = 1$ for pure propane), and C_f^e is a constant independent of the jet density ratio. The centerline variation in the reciprocal mean mixture fraction is replotted in Fig. 11 as a function of distance from the virtual origin $(x - x_{0,1})$ times the square root of the density ratio. The solid line is the result of a least-squares-fit to the data for $x/D > 25$. Also shown for comparison are results for the CH_4–air jet of Pitts and Kashiwagi[66] and the air–air jet of Becker *et al.*[14] The propane jet results agree well with results obtained in the air–air jet, but fall below those obtained in the CH_4–air jet, which has a significantly higher centerline decay rate.

Further comparisons of C_f^e and $x_{0,1}$ are shown in Table 10. The results of Schefer *et al.*[73] give the location of the virtual origin at $x/D = 3.0$ and $C_f^e = 0.185$. Although the values of $x_{0,1}$ listed in the table show considerable scatter, such variations are not unexpected since the location of the virtual origin is dependent on initial conditions which are

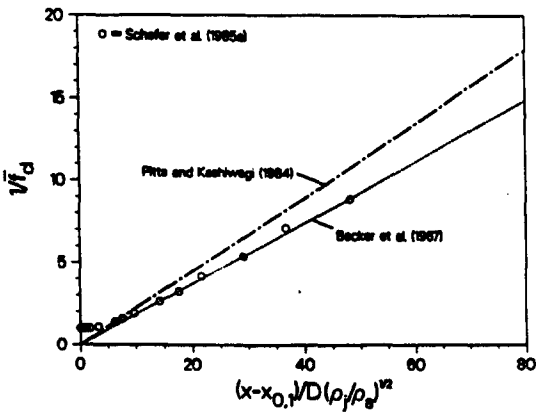

FIG. 11. Reciprocal mean mixture fraction along centerline in turbulent nonreacting propane jet. Bulk jet velocity = 53 m/sec; coflowing air velocity = 9.2 m/sec.

likely to vary between experimental systems. The values of C_f^e obtained by Schefer and coworkers compare well with the earlier results of Dyer[40] for a C_3H_8 jet and, as noted above, with the results of Becker *et al.*[14] for an air jet, but are up to 30% lower than the values obtained for CH_4 jets.

The data in Fig. 11 and the C_f^e values in Table 10 may appear to cast doubt on the density correction, but on closer examination this does not appear reasonable. The density correction has been tested extensively by Wilson and Danckwerts[84] and more recently by Pitts[65] with good results. Wilson and Danckwerts[84] studied heated jets where the only change in experimental conditions was the initial jet fluid temperature. Pitts studied jets of different fluid—CH_4, C_3H_8, CF_4—in a coflowing air stream and a jet of C_3H_8 in CO_2 all in the same apparatus with the same flow conditions. The results of both of these studies support the validity of Eq. (14).

When the results for C_f^e from different laboratories are compared there is some scatter evident. Looking at $C_{f_0}^e$ from Table 2 and C_f^e from Table 10, one notes that Lockwood and Moneib[62] compare favorably with Pitts and Kashiwagi and with Birch *et al.*, while Wilson and Danckwerts compare well with Becker *et al.* These differences suggest systematic variations between experiments. In view of the results of Wilson and Danckwerts and of Pitts cited above it is unlikely that they stem from an inadequacy in the density correction. One of the differences between experiments is the higher coflow velocity in Schefer *et al.* Their results should show a slower axial decay of mean concentration, as they do when compared to Pitts and Kashiwagi, Birch *et al.* and Lockwood and Moneib. That the Schefer and Dibble result is comparable to that of Wilson and Danckwerts and Becker *et al.* is most likely a coincidence. Becker *et al.* and Wilson and Danckwerts use nozzles to obtain a nearly uniform initial velocity profile in their jets, and the Wilson and Danckwerts jet issues from a hole in a flat surface. On the other hand Lockwood and Moneib, Pitts and Kashiwagi and Birch *et al.* study jets issuing from free-standing tubes with fully-developed turbulent pipe flow as the initial flow condition in the jet. These differences may explain the observed differences in C_f^e. More work on the subject is required.

A comparison of the mixture fraction fluctuation intensity $(\overline{f'^2})^{1/2}/\bar{f}_{cl}$ with results for the CH_4–air of

TABLE 10. Experimentally determined constants for Eqs (14)–(15)

Flow	C_f^e	$x_{0,1}/D$	C_{Lf}	$x_{0,2}/D$	Ref.
C_3H_8–air	0.185	3.0	0.120	−1.0	Schefer *et al.*[73]
C_3H_8–air	0.180	0.15	—	—	Dyer[40]
CH_4–air	0.224	−1.0	0.208	0.0	Pitts and Kashiwagi[66]
CH_4–air	0.250	5.8	0.194	0.0	Birch *et al.*[18]
Air–air	0.186	2.4	0.212	2.4	Becker *et al.*[14]

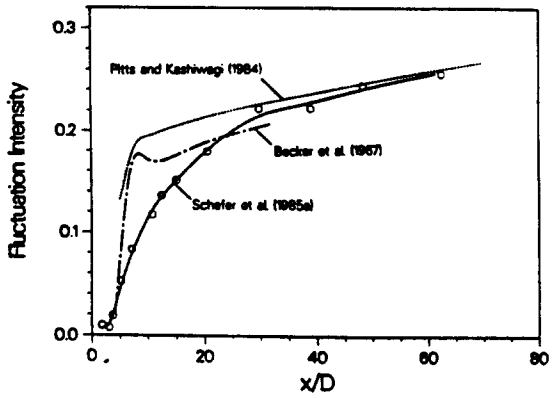

FIG. 12. Mixture fraction fluctuations along centerline in turbulent nonreacting propane jet. Bulk jet velocity = 53 m/sec; coflowing air velocity = 9.2 m/sec.

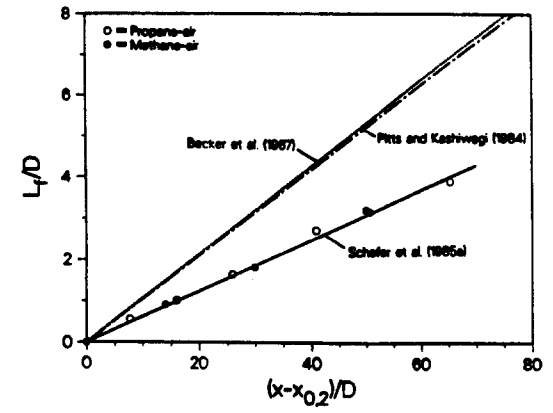

FIG. 13. Variation of mixture fraction half radius with axial distance in turbulent nonreacting propane jet. Bulk jet velocity = 53 m/sec; coflowing air velocity = 9.2 m/sec. ⊙, C_3H_8 jet; ●, CH_4 jet.

Pitts and Kashiwagi[66] and the air–air jet of Becker *et al.*[14] is shown in Fig. 12. The initial increase in fluctuation intensity is considerably more rapid for the CH_4–air and air–air jets. At downstream locations, however, the data for the variable density jets show good agreement and approach a considerably higher value than the constant density air–air jet. The propane jet results thus support the conclusions of Pitts and Kashiwagi and Birch *et al.* that centerline scalar fluctuations are higher in variable density jets than in constant density flows.

The jet spreading rate can be determined from the mean mixture fraction profiles and is typically characterized by the mixture-fraction half radius, L_f, defined as the radial location at which the mixture fraction is equal to half its value at the centerline. The variation in L_f (normalized by the jet exit diameter) with axial distance is shown in Fig. 13. For distances sufficiently far downstream L_f is proportional to the distance from a virtual origin $x_{0,2}$. This dependence can be written as

$$\frac{L_f}{D}=\frac{C_{L_f}}{2}\left(\frac{x}{D}-\frac{x_{0,2}}{D}\right). \tag{15}$$

A fit of the propane data in Fig. 13 (solid line) gives a value of $x_{0,2}/D=-1$ and $C_{L_f}=0.120$. The spreading rate obtained in the propane jet is considerably less than that measured in a CH_4–air jet (dotted line) or an air–air jet (dashed line). Values of $x_{0,2}$ and C_{L_f} obtained in other jet studies are also listed in Table 10. Although the results of Birch *et al.*[18] are based on only one axial location, the values for the CH_4–air jets and the air–air jet agree to within 7% while results in the C_3H_8–air jet are approaximately 40% lower.

The discrepancy between the propane jet results and those obtained in the CH_4–air and air–air jets could be attributed either to (1) the effects of variable density or (2) the effects of coflowing air. The good agreement between the CH_4–air and air–air jets indicates that the spreading rate is not affected by variable density. To verify this observation the spreading rate measurements were repeated under identical inlet conditions ($U_j=53$ m/sec, $U_e=9.2$ m/sec) using methane instead of propane as the jet fluid. These methane data are displayed in Fig. 13 (solid points) and show good agreement with the propane results, indicating that the spreading rate of a jet is independent of the initial density ratio. Since the velocity ratio U_e/U_j is very small in Pitts and Kashiwagi's work, if spreading rate, as measured by L_f and C_{L_f}, is independent of density differences then their results should approach the free jet results of both Becker *et al.* and Birch *et al.*, which is seen to be the case. A physical explanation of this independence in spreading rate can be offered. Density fluctuations in the jet rapidly diminish with increasing downstream distance in the initial mixing region of the jet. Therefore, in the fully-developed region all flows evolve in a manner similar to that of a constant density jet. This course is the same argument used previously to obtain the correction term $(\rho_j/\rho_1)^{1/2}$, and thus the results in Fig. 13 support the validity of this correction. Note that the $(\rho_j/\rho_1)^{1/2}$ term is added to the constant density similarity results to correct for differences in the initial momentum and mass fluxes between the truely constant density case and the pseudo-constant density case (i.e. $\rho_j\neq\rho_1$).

The above argument can be made quantitative. For mass conservation with $\overline{f'u}$ neglected,

$$M=(\pi D^2)\rho_j\bar{f}_j V_j=\int_0^\infty \rho_1\bar{f}\bar{U}2\pi r\,dr$$

where V_j is the volume-averaged velocity at the nozzle exit. Now assume similarity in the downstream region where density fluctuations may be neglected and, as required by strict similarity, let $L_f=L_u=L$. The above equation can be rewritten in similarity variables, and after some manipulation

takes the form

$$(\rho_j/\rho_1)(V_j/U_j)(C_u C_f/C_L^2)=\sqrt{2}\int_0^\infty f_f(\xi)f(\xi)\xi\,d\xi$$
$$=\text{constant}$$

where $\xi=r/L$, and $L/D=(C_L/2)(x/D)$. Expressing C_u and C_f in terms of C_u^* and C_f^* one obtains

$$(V_j/U_j)(C_u^* C_f^*/C_L^2)=\text{constant}$$

from which it can be seen that C_L is independent of initial density differences. Note that V_j/U_j appears in this expression because initial mass flow scales with V_j and not with U_j and that $(V_j/U_j)C_f^*$ should be independent of both density and the initial velocity profile in the jet.

The major differences in spreading rate seen in Fig. 13 and in C_L, Table 10, are best attributed to the influence of coflow. The results of Birch *et al.*, Becker *et al.* and Pitts and Kashiwagi (which are free jet flows) compare favourably with each other, while the data of Schefer and coworkers exhibit a lower spreading rate. As coflow increases, i.e. U_e/U_j increases, the spreading rate decreases.

Variations in $\bar{f}$ and $(\overline{f'^2})^{1/2}$ are shown in Fig. 14 as a function of radial distance normalized by L_f. It should be noted that the use of similarity variables such as L_f is not meant to imply that flow similarity exists in variable density jets with high coflow air velocities, but rather to emphasize differences with other jet flows in the literature. The results indicate that the mean mixture fraction profiles collapse onto the same curve within 15 dia of the jet exit. The solid line in Fig. 14(a) is a Gaussian-type function of the form

$$\frac{\bar{f}}{\bar{f}_{cl}}=\exp\left(-0.693\left(\frac{y}{L_f}\right)^2\right). \qquad (16)$$

This equation has been shown to provide a good fit to data in CH_4–air jets (Pitts and Kashiwagi[66]) and provides a good fit to the propane jet data for $y/L_f<1.25$. At larger values of y/L_f, the decrease in $\bar{f}$ with radial distance is more rapid than Gaussian as was observed by Pitts and Kashiwagi for CH_4–air jets.

The mixture-fraction fluctuations normalized by the centerline value $(\overline{f'^2})_{cl}^{1/2}$ are shown in Fig. 14(b). The profile at $x/D=15$ shows consistently higher fluctuations than at the downstream locations for all radial locations. At $x/D=30$ and 50 the profiles show good agreement for $y/L_f<1$ but at larger radial distances the profile at $x/D=50$ falls slightly outside the results for $x/D=30$. This result is apparently due to the effects of the coflowing air stream since radial mean CH_4 concentration profiles at $x/D=20$, 30 and 40 in a CH_4–air jet with no coflowing air show good similarity with respect to the normalized radial distance y/L_f (Birch *et al.*[18]).

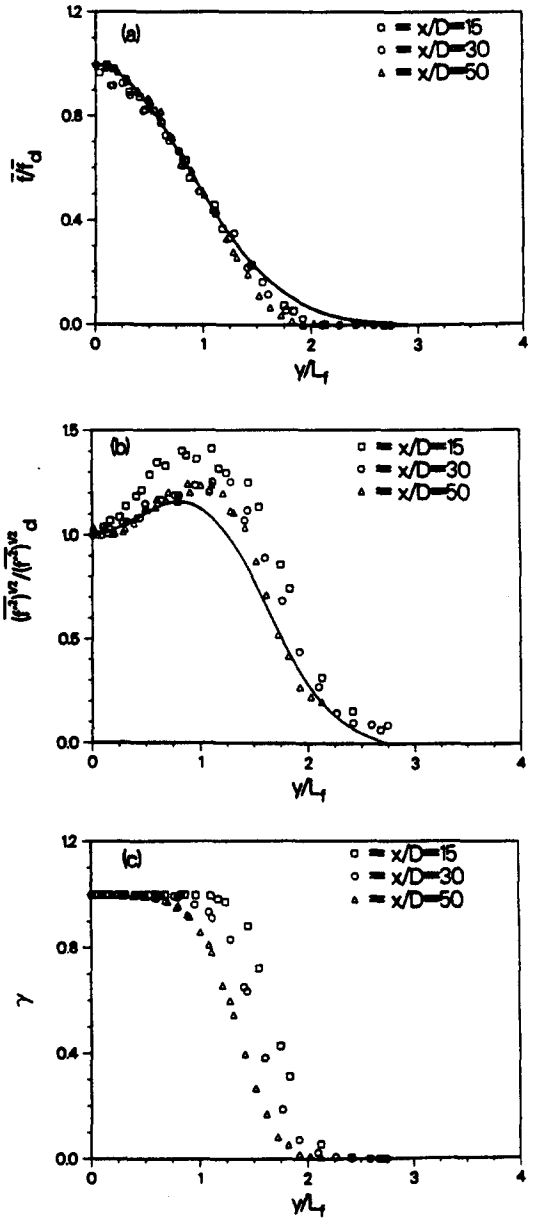

FIG. 14. Normalized radial profiles for a turbulent non-reacting propane jet at axial locations of $x/D=15$, 30 and 50. Bulk jet velocity 53 m/sec; coflowing air velocity= 9.2 m/sec; (a) mean mixture fractions; (b) mixture fraction fluctuations; (c) intermittency.

Represented as a solid line (Fig. 14(b)) are the results of Pitts and Kashiwagi[66] and Birch *et al.*[18] for CH_4–air jets. The maximum fluctuations for the CH_4–air jets are lower and occur closer to the centerline with respect to L_f. A comparison of the maximum fluctuations $(\overline{f'^2})_{max}^{1/2}$ and their radial locations is shown in Table 11. While Pitts and Kashiwagi[66] concluded that scalar fluctuations are higher in variable density jets (in agreement with the present results), any more specific conclusions on the effect of density variations are difficult to make. The lowest values of $(\overline{f'^2})_{max}^{1/2}$ occur for constant density air

TABLE 11. Maximum mixture fraction fluctuation intensities

Flow	f'_{max}/f	y_{max}/L_f	Ref.
C_3H_8–air	1.24	0.96	Schefer *et al.*[73]
C_3H_8–air	1.29	0.80	Dyer[40]
CH_4–air	1.18	0.70	Pitts and Kashiwagi[66]
CH_4–air	1.20	0.70	Birch *et al.*[18]
Air–air	1.15	0.80	Becker *et al.*[14]
Air–air	1.14	—	Shaughnessy and Morton[77]
Heated air–air	1.26	0.90	Lockwood and Moneib[62]

jets in which particles are used as markers for concentration. The maximum fluctuations increase in going from constant density jets to CH_4 and C_3H_8. Fluctuations are also higher in heated jets than in constant density jets. However, it is difficult to explain the significantly higher values of $(f'^2)^{1/2}_{max}$ obtained by Lockwood and Moneib[62] in a heated air jet ($\rho_{jet}/\rho_{air}=0.54$) than are found in CH_4–air jets ($\rho_{jet}/\rho_{air}=0.55$) where the ratios of jet to air density are nearly the same.

Radial variations in the intermittency γ are shown in Fig. 14(c). The intermittency is defined as the fraction of time that the mixture fraction is greater than a near-zero threshold (a value of zero corresponding to pure air). Typical probability density distributions in the mixing region consist of an intermittency spike associated with unmixed air and a broader distribution corresponding to mixed air and propane (probability density distributions of f are presented in the following section). The finite width of the intermittency spike often requires the somewhat arbitrary selection of a threshold value to differentiate between unmixed and mixed fluid. Bilger *et al.*[15] have shown that the finite width of the intermittency spike can be closely fitted by a Gaussian, and the area under the resulting curve provides a good estimate of $(1-\gamma)$. The threshold value of mixture fraction determined using this method was $f_{th}=0.015$. Thus for values of $f<f_{th}$ the flow is considered as unmixed air and for values of $f>f_{th}$ the flow is considered as mixed propane and air. Calculated values of γ were found to be insensitive to small variations in the threshold level (± 0.005).

At all axial locations, a region exists near the centerline for which γ is unity, indicating that turbulent mixing is insufficient to transport unmixed air into the central region. Only in a relatively well-defined mixing region for which γ is between 0 and 1 is the presence of any unmixed air observed. Thus the mixing region can be characterized as consisting of mixed propane and air, and unmixed air which is entrained by the high velocity jet. No unmixed air exists near the centerline at the axial locations shown. These observations are consistent with the view that the center of the jet is relatively well mixed while at increasing radii, engulfment of coflowing air and subsequent mixing occurs.

4.3.1.2. Higher moments. Radial variations in the third and fourth moments of the mixture fraction (skewness S and kurtosis K, respectively) are shown in Fig. 15(a) and (b). The values of S and K for a Gaussian distribution are zero and 3.0, respectively. At the centerline the skewness has a slightly negative value ($S=-0.4$) and the kurtosis is 3.5. Outward from the centerline S increases at first slowly, followed by a rapid increase at the outer edge of the mixing layer. The kurtosis initially decreases to a minimum value of 2.8 at a radial location just inside the mixing region, before rapidly increasing as the outer air flow is approached. The rapid increase in S and K in the intermittent mixing region is due to the passage of unmixed air past the measurement

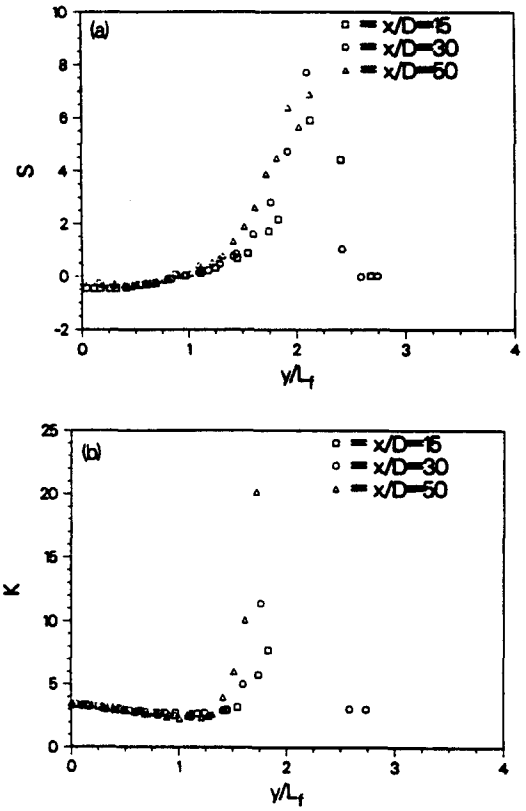

FIG. 15. Normalized radial profiles for a turbulent nonreacting propane jet at axial locations of $x/D=15$, 30 and 50. Bulk jet velocity = 53 m/sec; coflowing air velocity = 9.2 m/sec. (a) Skewness; (b) kurtosis.

volume. This results in periods of time during which the mixture fraction is zero and sharp cutoff in $p(f)$ at $f=0$.

The centerline variation in S and K can also be obtained from Fig. 15. The results show the skewness increasing from -0.45 at $x/D=15$ to -3.1 at $x/D=50$. Pitts and Kashiwagi[66] found a comparable increase in S with axial distance for a CH_4–air jet ($S=-0.6$ at $x/D=20$ and $S=-0.35$ at $x/D=60$), while Birch *et al.*[18] measured a relatively constant value of $S=-0.3$ along the centerline. The reason for the difference in centerline behaviour between these studies is not clear, however, the measurement of a non-Gaussian negative skewness along the centerline is consistent in both the C_3H_8–air jet and the CH_4–air jets. In the C_7H_8–air jet the kurtosis K shows a small decrease with axial distance from 3.4 at $x/D=15$ to 3.1 at $x/D=50$. These results are in good agreement with the range of values obtained in CH_4–air jets (Birch *et al.*,[18] Pitts and Kashiwagi,[66]).

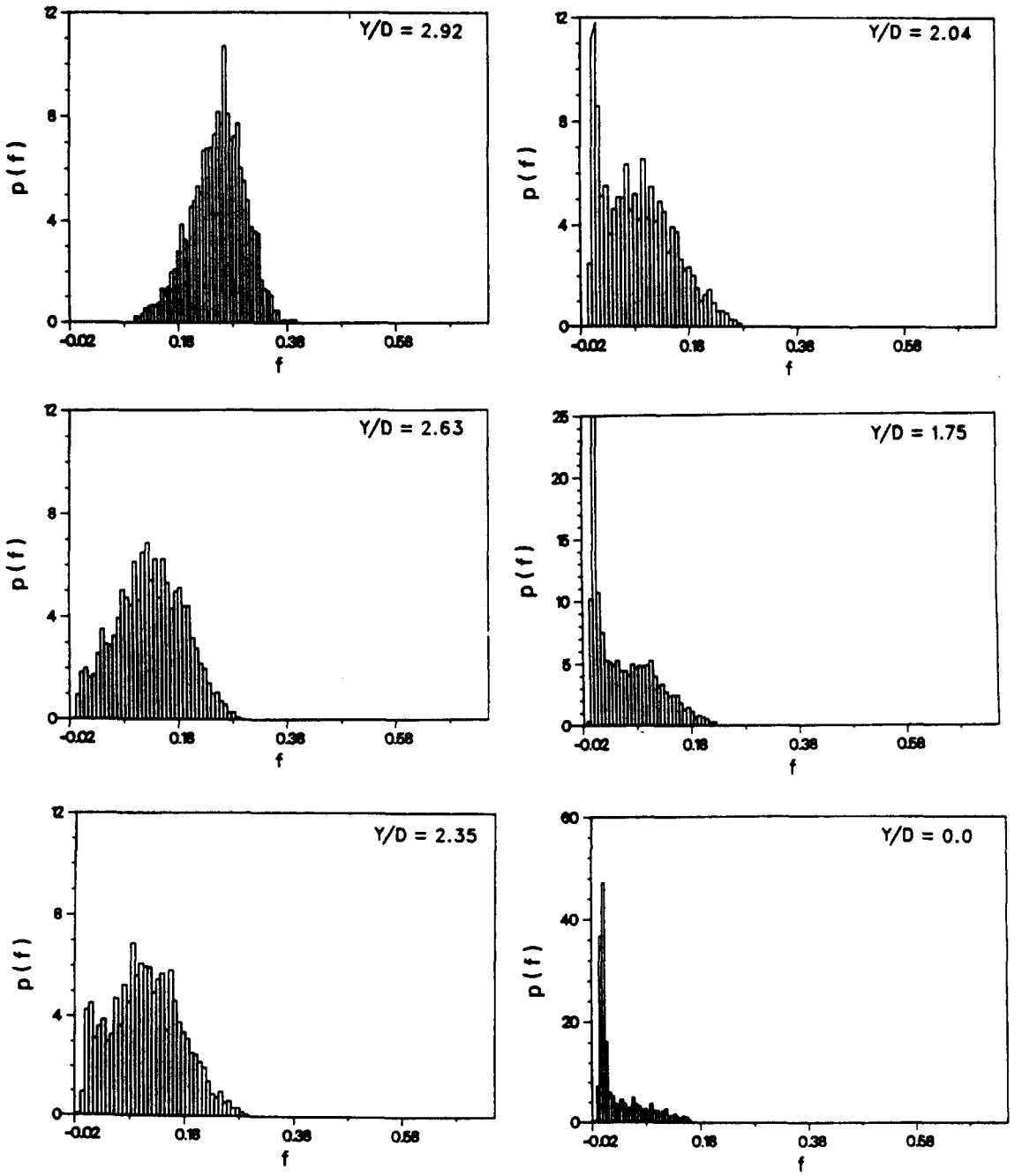

FIG. 16. Probability density distributions of mixture fraction for a turbulent nonreacting propane jet at an axial location of $x/D=30$. Bulk jet velocity = 53 m/sec; coflowing air velocity = 9.2 m/sec. (a) $y/D=2.92$; (b) $y/D=2.63$; (c) $y/D=2.35$; (d) $y/D=2.04$; (e) $y/D=1.75$; (f) $y/D=0.0$.

4.3.1.3. Probability density distributions. Probability density distributions of the mixture fraction $p(f)$ were calculated from 8,000 measurements at each spatial location using 50 bins equally spaced over the 3-sigma limits of the data. Radial variations in $p(f)$ are shown in Fig. 16 for $x/D = 30$. These distributions are quantitatively similar to conserved scalar distributions observed in nonreacting CH_4–air jets (Birch *et al.*[18]) and reacting jets (Drake *et al.*[36]). Near the centerline the distributions are dominated by a broad Gaussian-like distribution corresponding to a turbulent mixture of propane and entrained air while at outer radial locations a sharp spike corresponding to pure air at $f=0$ is observed. In the mixing region the distribution is bimodal and consists of contributions from both the unmixed air and mixed propane and air. At the axial locations shown no pure propane is indicated ($f=1$) since entrainment of coflowing air and mixing has occurred upstream. The smooth transition between the air spike and the broader distribution corresponding to mixed fluid has been attributed to the existence of a viscous superlayer between the unmixed air and the mixed propane and air zones and has led to a proposed composite distribution which includes unmixed air, fully mixed propane and air, and a contribution from the viscous superlayer (Effelsberg and Peters[41]).

4.3.2. *Velocity measurements*

4.3.2.1. Mean and fluctuating quantities. The centerline variation in mean axial velocity and the fluctuating components of axial and radial velocity are shown in Fig. 17. The axial and radial velocity fluctuations $(\overline{u'^2})^{1/2}$ and $(\overline{v'^2})^{1/2}$ are normalized by the centerline excess velocity U_{cl} where the centerline excess velocity is defined as the difference between the centerline velocity and the coflowing air velocity. The results shown were obtained with LV seed added to the jet flow only (i.e. conditional on the jet fluid). Since the average data rate on the centerline with LV seed added to the jet is considerably higher than with seed added to the coflowing air (particularly at upstream locations where differences in conditional statistics are greatest), this case provides a better comparison with conventionally-averaged statistics. The mean axial velocity remains nearly constant for approximately 2 jet diameters downstream of the jet exit, before decreasing rapidly to approach the outer coflowing air velocity of 9.2 m/sec further downstream. Both the axial and radial velocity fluctuations increase rapidly downstream of the jet exit to a maximum value of approximately 28%, and for x/D greater than 40 remain nearly constant. This value agrees well with the value of 28% obtained in isothermal jets into still air (Wygnanski and Fielder[85]) and is slightly less than the value of 30% for a heated jet with coflowing air ($u_j/u_0 = 4.5$) (Antonia *et al.*[10]). At all axial locations the axial velocity fluctuations are higher than the radial fluctuations and the initial increase is more rapid. For axial distances $x/D > 15$ (and over the range of axial distances measured, $x/D \leq 80$) the excess centerline velocity shows a hyperbolic decay rate in agreement with the results of Wygnanski and Fielder[85] for a self-preserving jet into still air, and by Antonia and Bilger[6] for nonreacting isothermal jets into coflowing air.

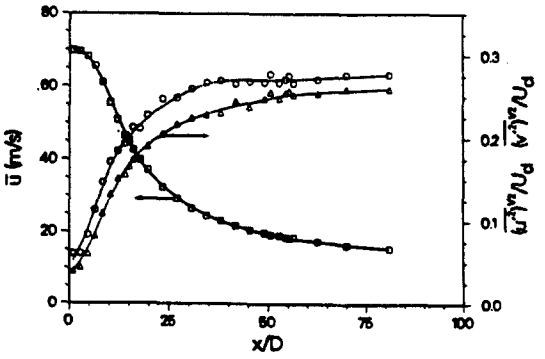

FIG. 17. Variation of mean axial velocity and normalized axial velocity fluctuations along centerline in turbulent nonreacting propane jet. Bulk jet velocity = 53 m/sec; coflowing air velocity = 9.2 m/sec. □, mean axial velocity; ○, axial velocity fluctuations; △, radial velocity fluctuations.

Radial profiles of the mean and fluctuating axial and radial velocities and their correlation in the propane jet are shown in Fig. 18 for an axial location of $x/D = 30$. The solid line indicates data collected when seed particles are added to the coflowing air stream only; the dashed line indicates data collected with only the jet seeded. The mean excess velocity, U, defined as the difference between the local mean axial velocity u and the coflow air velocity, u_1 is shown in Fig. 18(a). There is a small difference between the mean axial velocities conditioned on air seed u_{air} and on jet seed u_{jet}. This difference is smallest on centerline and increases with increasing radius. However, at all radii, u_{jet} is larger than u_{air}. Hence, on average, fluid originating from the coflow air has a smaller average axial velocity than fluid originating from the jet.

Most apparent from Fig. 18 is the difference between the conditional radial velocities v_{air} and v_{jet}, Fig. 18(b). In the sign convention adopted for the radial velocity, a positive radial velocity indicates flow outward from the centerline, while a negative radial velocity corresponds to flow inward toward the centerline. Thus both v_{air} and v_{jet} indicate net outward flow of fluid away from the centerline; however the outward radial flux of fluid originating from the jet is, on average, larger. While these differences are readily apparent, the absolute differences, $v_{jet} - v_{air}$, are comparable with the absolute differences observed in the conditionally-sampled axial velocities.

The axial velocity fluctuations $(\overline{u'^2})^{1/2}_{jet}$ and $(\overline{u'^2})^{1/2}_{air}$, Fig. 18(c), are nearly the same at the centerline. Both $(\overline{u'^2})^{1/2}_{jet}$ and $(\overline{u'^2})^{1/2}_{air}$ have a maximum

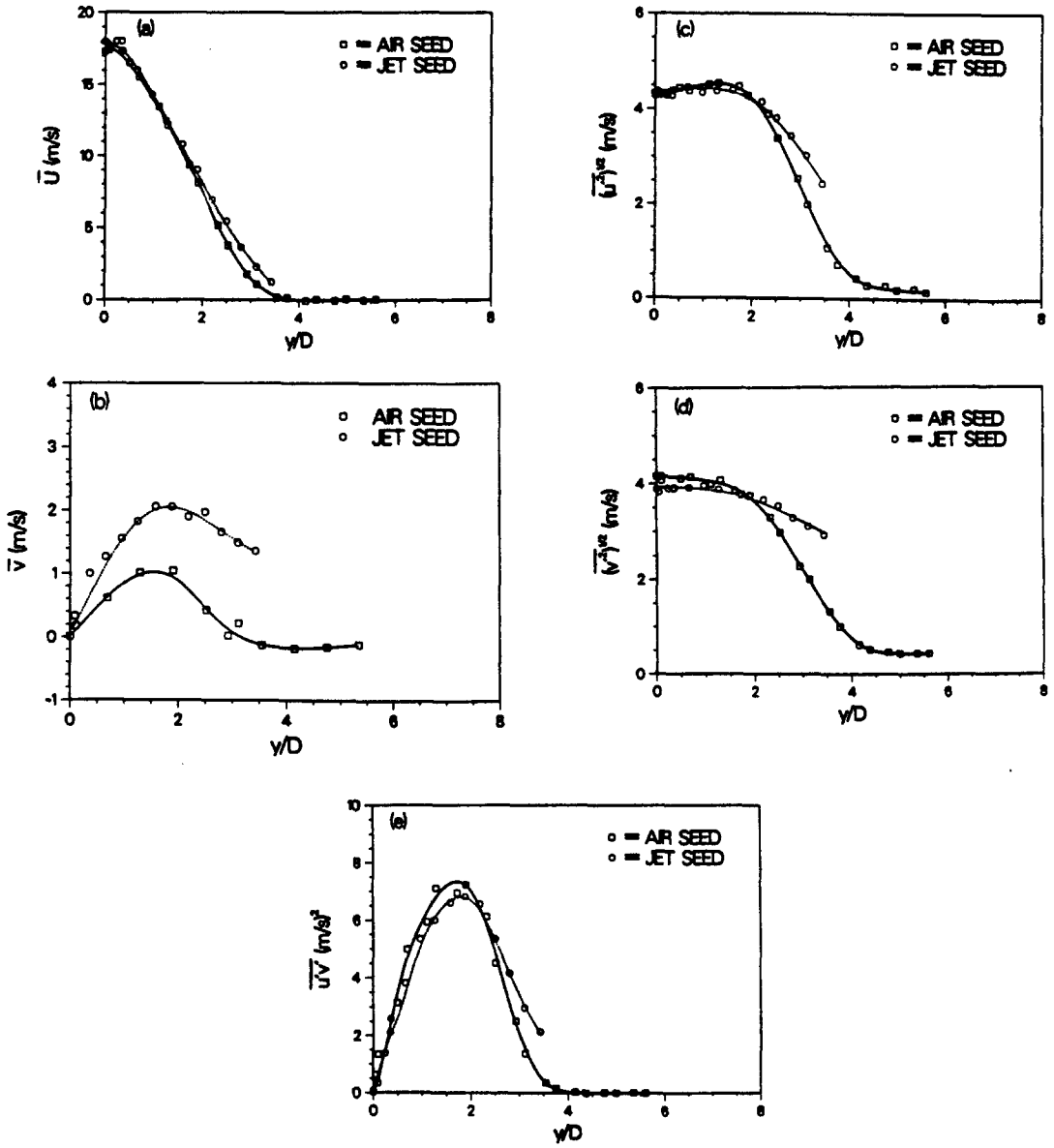

FIG. 18. Radial profiles for a turbulent nonreacting propane jet at an axial location of $x/D=30$. Bulk jet velocity = 53 m/sec; coflowing air velocity = 9.2 m/sec. Solid line indicates data collected with LV seed added to the coflowing air stream only; dashed line indicates data collected with LDV seed added to the propane jet stream only. □, Coflowing air seed only; ○, jet seed only. (a) Mean axial velocity; (b) mean radial velocity; (c) axial velocity fluctuations; (d) radial velocity fluctuations; (e) axial and radial velocity correlation.

in the mixing region between the fuel jet and the coflowing air where the gradient of the mean velocities is largest. At larger radii, $(u'^2)^{1/2}_{air}$ tends toward zero more quickly than $(u'^2)^{1/2}_{jet}$. The larger value of $(u'^2)^{1/2}_{jet}$ at large radii is explained by the fact that jet seeded fluid at these locations has, on average, emerged from the centerline region of the jet and is, therefore, generally more turbulent. When the air is seeded, fluid at large radii has, on average, originated from the coflow air which has lower turbulence. The radial velocity fluctuations $(v'^2)^{1/2}_{jet}$ and $(v'^2)^{1/2}_{air}$, Fig. 18(d), show a trend that is entirely analogous to the radial profiles of $(u'^2)^{1/2}_{jet}$ and $(u'^2)^{1/2}_{air}$. Both $(\overline{v'^2})^{1/2}_{jet}$ and $(v'^2)^{1/2}_{air}$ are comparable at the centerline and both decrease with increasing radii. As before, $(v'^2)^{1/2}_{jet}$ does not decrease as quickly with increasing radii as $(v'^2)^{1/2}_{air}$.

The correlation between the fluctuations in radial and axial velocities, $u'v'_{jet}$ and $u'v'_{air}$, Fig. 18(e), is directly related to the turbulent transport of momentum. Analogous to the previous results for axial and radial velocity fluctuations the difference is only slight near the centerline and increases at large radial distances.

All of these observations are consistent with the view that the center of the jet is relatively well mixed

while at increasing radii, the engulfment of coflowing air and subsequent mixing is occurring. Thus, the association of lower velocities with air and higher velocities with jet fluid is not unreasonable.

4.3.2.2. Probability density distributions. Probability density distributions of the axial velocity conditional on the jet fluid $p(u)_{jet}$ and on the air $p(u)_{air}$ are shown in Fig. 19 for $x/D=30$ at various distances from the centerline. The distributions shown were calclated from 3,000 velocity measurements at each spatial location using 30 bins equally spaced over the 3-sigma limits of the data. As in the previous section the solid line indicates data conditional on the air and the dotted line indicates data conditional on the jet fluid. The axial velocity distributions are in general characterized by a unimodal distribution which shifts to a higher average velocity as the centerline is approached. The axial velocity distributions conditional on the air are relatively narrow at outer radial locations with a peak value close to that of the coflowing air. Closer to the centerline the distributions become skewed toward higher velocities as fluid is accelerated by the high velocity central jet and appoach a nearly Gaussian distribution at the centerline. The distribution conditional on the jet fluid exhibits a peak close to that of the coflowing air at outer radial locations but is skewed toward higher velocities. The peak in $p(u)_{jet}$ shifts toward higher velocities and broadens nearer the centerline due to the higher turbulence associated with the jet fluid. At the centerline the distributions for both cases are closely Gaussian and nearly identical since sufficient mixing has occurred. The radial velocity distributions $p(v)_{air}$ and $p(v)_{jet}$ at $x/D=30$ are shown in Fig. 20. At the outermost radial location, $y/D=3.1$, $p(v)_{air}$ is considerably narrower than $p(v)_{jet}$. In both caes the maximums in the radial velocity distributions are centered near zero while the presence of positive and negative radial velocities indicates flow outward from the centerline and entrainment of fluid originating from both the jet and from the coflowing air. Most interesting are the positive instantaneous values of v_{air}, corresponding to previously entrained coflowing air that has subsequently mixed with jet fluid and is now flowing outward from the central region, and the negative values of v_{jet}, which correspond to re-entrainment of fluid originating from the jet. The positive mean radial velocities at this location for both cases (see also Fig. 18(b)) indicate net flow of high-velocity jet fluid outward from the centerline. The distribution $p(v)_{jet}$ is considerably more skewed toward positive velocities than $p(v)_{air}$ since fluid originating from the central jet is, on average, moving more rapidly away from the centerline.

At $y/D=2.5$ the small peak at negative radial velocity in $p(v)_{air}$ corresponds to entrainment of coflowing air inward toward the centerline. More rapid outward flow of jet fluid and previously

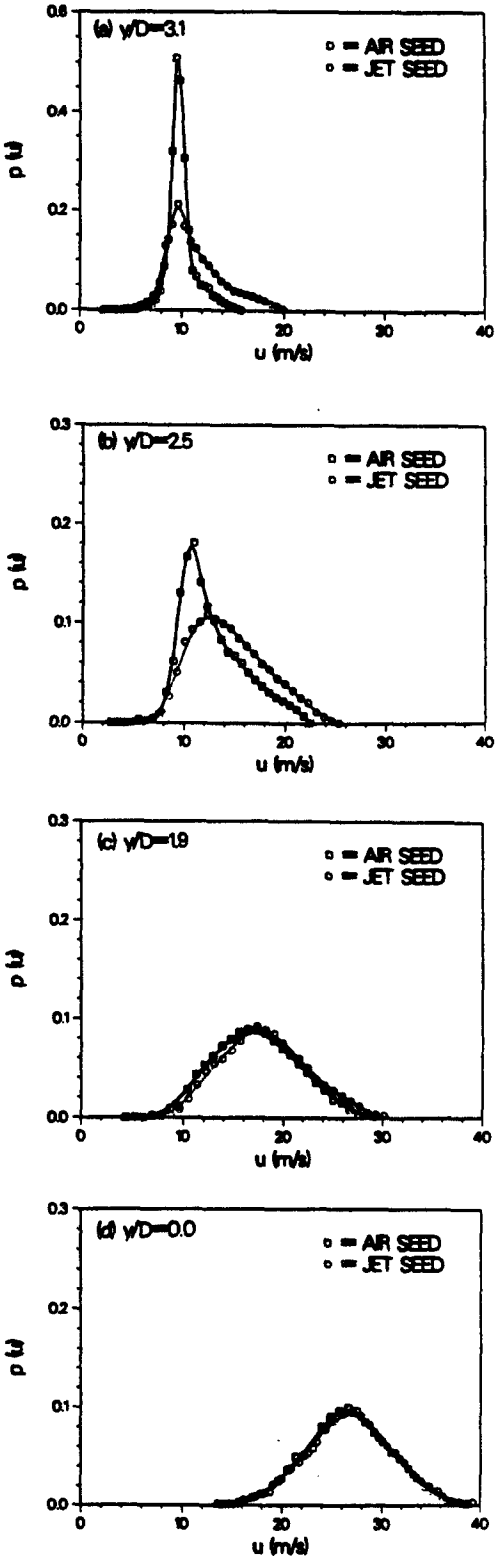

FIG. 19. Conditionally-sampled probability density distributions of axial velocity for a turbulent nonreacting propane jet at an axial location of $x/D=30$. Bulk jet velocity = 53 m/sec; coflowing air velocity = 9.2 m/sec. Solid line indicates data collected with LV seed added to the coflowing air stream only; dotted line indicates data with the LDV seed added to the jet stream only. □, Coflowing air seed only; ⊙, jet seed only. (a) $y/D=3.1$; (b) $y/D=2.5$; (c) $y/D=1.9$; (d) $y/D=0.0$.

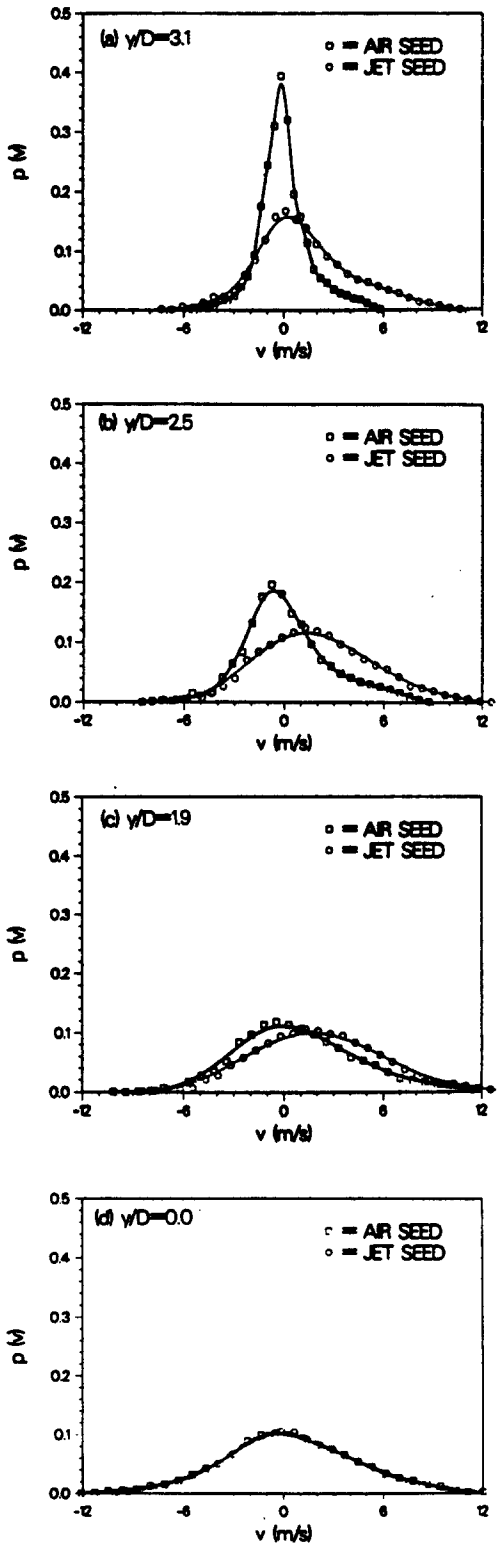

FIG. 20. Conditionally-sampled probability density distributions of radial velocity for a turbulent nonreacting propane jet at an axial location of $x/D=30$. Bulk jet velocity = 53 m/sec; coflowing air velocity = 9.2 m/sec. Solid line indicates data collected with LV seed added to the coflowing air stream only; dotted line indicates data with the LDV seed added to the jet stream only. □, Coflowing air seed only; ⊙, jet seed only. (a) $y/D=3.1$; (b) $y/D=2.5$; (c) $y/D=1.9$; (d) $y/D=0.0$.

entrained air is also shown at this radial location by the increased skewness toward positive velocities. At $y/D=1.9$ the peak in $p(v)_{air}$ has decreased considerably although entrainment of fluid originating from the air stream is still apparent. The distributions for both cases are nearly identical for positive radial velocities indicating nearly equal outward flow of fluid originating from the jet and air streams. At the centerline the distributions are closely Gaussian and nearly identical since, as was seen with the axial velocity distributions, fluid originating from both streams is well mixed in the centerline region.

4.3.2.3. Joint probability density distributions. The joint probability distributions of axial and radial velocity were calculated from a minimum of 10,000 velocity pairs at each spatial location using 20 axial and 20 radial velocity bins spaced over the 3-sigma limits of the data. The distribution shown in Fig. 21 corresponds to the mixing region where the difference in conditional velocity statistics is greatest ($y/D=2.5$). The distribution conditional on the air $p(u,v)_{air}$ exhibits a peak with the axial velocity distribution centered near the coflowing air velocity and the radial velocity centered near zero. At higher axial velocities the radial velocity distribution is highly skewed toward positive values due to the more rapid expansion of high velocity fluid originating near the centerline. The broader distribution also indicates considerably higher radial velocity fluctuations. It is likely that this is fluid originating from the air stream which has been previously entrained and mixed with higher velocity jet fluid prior to expansion outwards toward the coflowing air stream. The primary contribution to $p(u,v)_{jet}$ is from fluid moving in the axial direction near the coflowing air velocity. A maximum again exists in $p(u,v)_{jet}$ at axial velocities close to the coflowing air velocity and, at increased axial velocities, the radial distribution becomes skewed toward negative values. However, considerably more outward radial movement of the fluid is apparent and the fluctuations in both axial and radial velocities are considerably higher (higher velocity fluctuations were also seen in Fig. 18(c)).

4.3.3. *Raman/laser velocimetry results*

A scatter plot showing the correlation between mixture fraction and the axial and radial velocities in the mixing region at $x/D=30$ is shown in Fig. 22(a) and (b), respectively. These results were obtained for the case where LV seed was added to the coflow air stream only. Biasing errors in the scalar f due to preferrential seeding of the jet and air streams are fully discussed in Dibble *et al.*[34] It can be seen that a positive correlation exists between the mixture fraction and the axial velocity, and between the mixture fraction and radial velocity. Similar measurements at the centerline show that f is uncorrelated with either velocity component. From

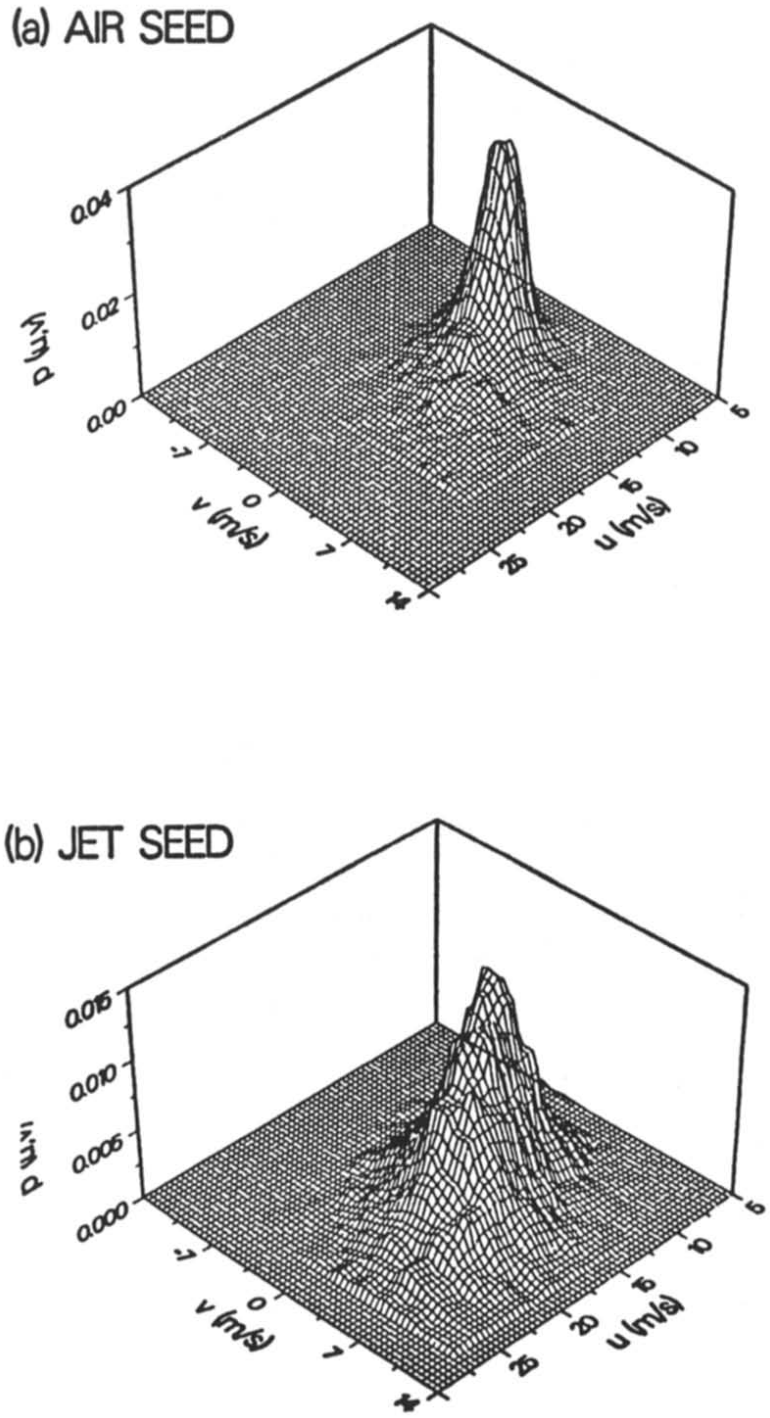

FIG. 21. Joint probability density distributions of axial and radial velocity for a turbulent nonreacting propane jet at an axial location $x/D = 30$ and a radial location of $y/D = 2.5$. (a) LV seed added to the coflowing air only; (b) LDV seed added to the jet only. Bulk jet velocity = 53 m/sec; coflowing air velocity = 9.2 m/sec.

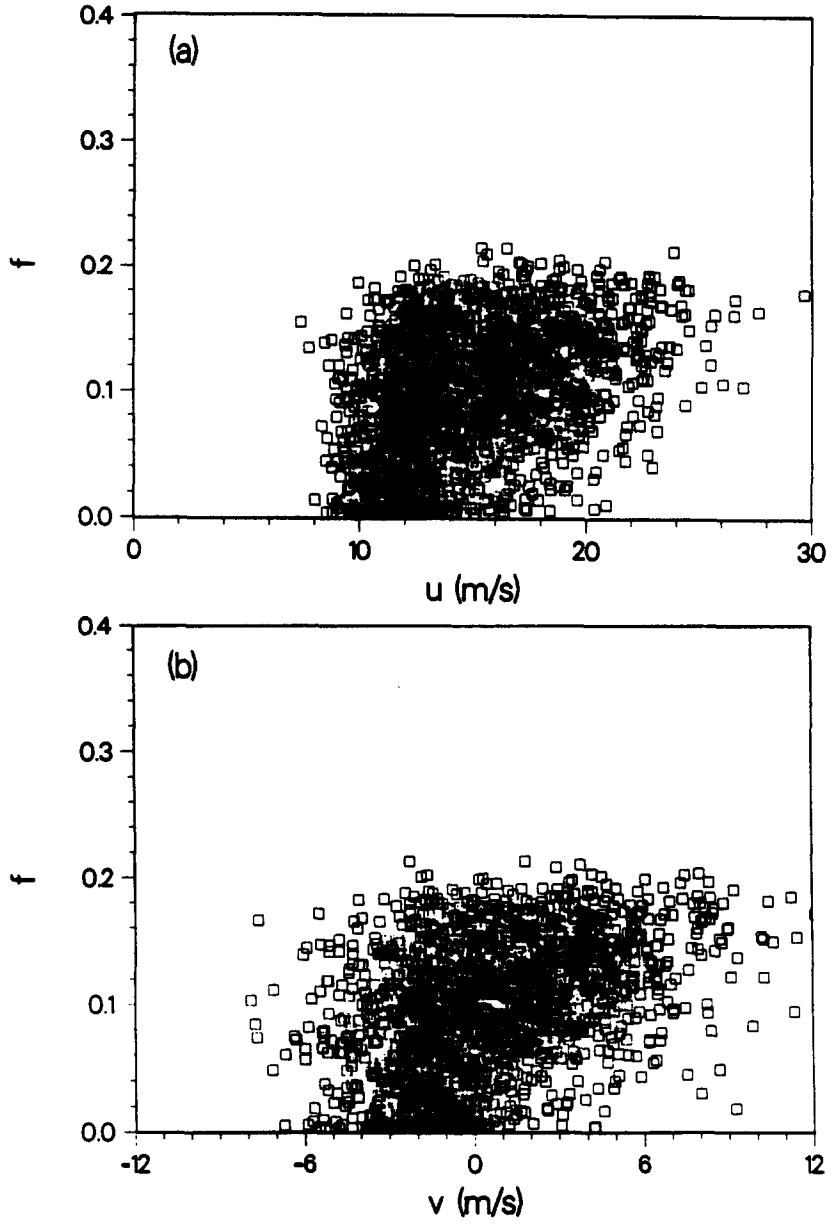

FIG. 22. Scatter plot of correlation between mixture fraction and velocity in a turbulent nonreacting propane jet at an axial location $x/D=30$ and a radial location $y/D=2.3$. LV seed is added to the coflowing air only. (a) Mixture fraction and axial velocity; (b) mixture fraction and radial velocity.

this data the following values for the correlation coefficients are obtained:

At $y/D=0.0$:

$$\overline{f'u'_{air}}=0.049\ldots\overline{f'u'_{jet}}=0.044$$
$$\overline{f'v'_{air}}=0.03\ldots\overline{f'v'_{jet}}=0.002.$$

At $y/D=2.3$:

$$\overline{f'u'_{air}}=0.077\ldots\overline{f'u'_{jet}}=0.090$$
$$\overline{f'v'_{air}}=0.065\ldots\overline{f'v'_{jet}}=0.073$$

4.4. *Data Comparison with Model Predictions*

In this section a state-of-the-art modeling approach is used to predict the data chosen for the recommended variable-density mixing case. This provides an opportunity to assess both the model and trends in the data and represents a benchmark against which other models can be compared, if desired. Since the model used is not described completely in any single reference, its essential ingredients are discussed below.

4.4.1. *The model*

The second-order closure model described in

Farshchi and Kollmann,[43] Dibble *et al.*,[35] Dibble *et al.*,[32] and Rhodes *et al.*[70] was used to calculate the isothermal round jet mixing of propane with ambient air. The model consists of transport equations for mean velocity, mean mixture fraction, Reynolds-stress components, variance of mixture fraction, scalar fluxes, kinetic energy and scalar dissipation rates. The equations are presented below in cartesian tensor form; the correct form in other coordinate systems (i.e. cylindrical form) can be obtained by proper tensor transformation. In addition, repeated indices refer to summation over all possible coordinates. The flow is isothermal and, using the ideal gas law for propane and air, we obtain for the density as a local function of mixture fraction f

$$\frac{\rho_1}{\rho(f)} = x + (1-x)f \tag{17}$$

where x is the ratio of molecular masses

$$x = \frac{M_2}{M_1}$$

and ρ_1 is the density of fluid 1 (i.e. propane). Fluctuations of pressure are neglected in the thermodynamic relations. The normalized mass fraction

$$f = \frac{Y_1 - Y_{1\infty}}{Y_{10} - Y_{1\infty}} \tag{18}$$

of fluid 1 can be taken as mixture fraction (subscript 0 refers to jet pipe exit and subscript ∞ to ambient) for the present case of isothermal mixing of two components. The pdf of the mixture fraction $P(f)$ is assumed to be a beta-function which has been found to be a good approximation for isothermal mixing flows (Rhodes *et al.*[70]). The mean density is then calculated by integration

$$\langle\rho\rangle = \int_0^1 \mathrm{d}f \rho(f) P(f). \tag{19}$$

The pdf $P(f)$ is set up using the mean $\tilde{f}$ and the variance f''^2, which determine the exponents of the beta-function uniquely (Jones[59]). The tilde indicates Favre-averaged statistics defined below.

The turbulence model includes the first-order equations for mean velocity

$$\langle\rho\rangle \tilde{D}_t \tilde{v}_\alpha'' = -\partial_\alpha\langle p\rangle - \partial_\beta(\langle\rho\rangle\overline{v_\alpha'' v_\beta''}) \tag{20}$$

and mean mixture fraction

$$\langle\rho\rangle \tilde{D}_t \tilde{f} = -\partial_\alpha(\langle\rho\rangle\overline{v_\alpha'' f''}) \tag{21}$$

in exact form. Note that Favre-averaged statistics are applied

$$\tilde{\phi} \equiv \frac{\langle\rho\phi\rangle}{\langle\rho\rangle}, \quad \phi'' = \phi - \tilde{\phi}$$

where appropriate and

$$\tilde{D}_t \equiv \partial_t + \tilde{v}_\alpha \partial_\alpha$$

abbreviates the Stokes derivative for the mean velocity. The closure of the Reynolds-stress equations includes model assumptions for turbulent flux, pressure correlations and dissipation. The following equation emerges (Dibble *et al.*[35])

$$\begin{aligned}\langle\rho\rangle \tilde{D}_t \overline{v_\alpha'' v_\beta''} = &-\langle\rho\rangle \overline{v_\alpha'' v_\gamma''}\partial_\gamma \tilde{v}_\beta - \langle\rho\rangle \overline{v_\beta'' v_\gamma''}\partial_\gamma \tilde{v}_\alpha \\ &+ \partial_\gamma\left(C_s\langle\rho\rangle \frac{\tilde{k}}{\tilde{\varepsilon}} \overline{v_\gamma'' v_\delta''}\partial_\delta \overline{v_\alpha'' v_\beta''}\right) \\ &+ \langle\rho\rangle Q_{\alpha\beta} - \langle v_\alpha''\rangle\partial_\beta\langle p\rangle - \langle v_\beta''\rangle\partial_\alpha\langle p\rangle - \frac{2}{3}\partial_{\alpha\beta}\langle\rho\rangle\tilde{\varepsilon}\end{aligned} \tag{22}$$

where the pressure correlations are modeled by (see Hanjalic and Launder[48])

$$\begin{aligned}Q_{\alpha\beta} = &-C_1 \frac{\tilde{\varepsilon}}{\tilde{k}}\langle\rho\rangle\left(\overline{v_\alpha'' v_\beta''} - \frac{2}{3}\partial_{\alpha\beta}\tilde{k}\right) \\ &- \frac{C_2 + 8}{11}\langle\rho\rangle\left(P_{\alpha\beta} - \frac{2}{3}\partial_{\alpha\beta}P\right) \\ &- \frac{8C_2 - 2}{11}\langle\rho\rangle\left(D_{\alpha\beta} - \frac{2}{3}\partial_{\alpha\beta}D\right) \\ &+ \frac{30C_2 - 2}{55}\langle\rho\rangle\tilde{k}(\partial_\alpha\tilde{v}_\beta + \partial_\beta\tilde{v}_\alpha)\end{aligned} \tag{23}$$

and

$$P_{\alpha\beta} = -\overline{v_\alpha'' v_\gamma''}\partial_\gamma v - \overline{v_\beta'' v_\gamma''}\partial_\gamma \tilde{v}_\alpha, \quad P = \frac{1}{2}P_{\alpha\alpha} \tag{24a}$$

$$D_{\alpha\beta} = -\overline{v_\alpha'' v_\gamma''}\partial_\beta \tilde{v}_\gamma - \overline{v_\beta'' v_\gamma''}\partial_\alpha \tilde{v}_\gamma, \; D = \frac{1}{2}D_{\alpha\alpha}.$$

The dissipation rate $\tilde{\varepsilon}$ of kinetic energy is determined by solving the equation

$$\begin{aligned}\langle\rho\rangle \tilde{D}_t \tilde{\varepsilon} = &\partial_\alpha\left(C_\varepsilon\langle\rho\rangle \frac{\tilde{k}}{\tilde{\varepsilon}}\overline{v_\alpha'' v_\beta''}\partial_\beta\tilde{\varepsilon}\right) \\ &- C_{\varepsilon 1}\langle\rho\rangle \frac{\tilde{\varepsilon}}{\tilde{k}}\overline{v_\alpha'' v_\beta''}\partial_\beta\tilde{v}_\alpha \\ &- C_{\varepsilon 2}\langle\rho\rangle\frac{\tilde{\varepsilon}^2}{\tilde{k}} + C_{\varepsilon 3}\frac{\tilde{\varepsilon}}{\tilde{k}}\frac{\langle\rho' v_\alpha''\rangle}{\langle\rho\rangle}\partial_\alpha\langle\rho\rangle.\end{aligned} \tag{25}$$

The statistical moments of the scalar field follow from the solutions of Eq. (20) and the equations for the variance f''^2, the scalar fluxes $\overline{v_\alpha'' f''}$ and the scalar

dissipation $\tilde{\varepsilon}_f$. The variance equation requires only one closure assumption for the turbulent flux of f''^2,

$$\langle\rho\rangle\tilde{D}_t f''^2 = \partial_\alpha\left(C_s\langle\rho\rangle\frac{\tilde{k}}{\tilde{\varepsilon}}v_\alpha''v_\beta''\partial_\beta f''^2\right) \quad (26)$$

$$-2\langle\rho\rangle v_\alpha'' f''\partial_\alpha\tilde{f} - 2\langle\rho\rangle\tilde{\varepsilon}_f.$$

The scalar flux equation is given by

$$\langle\rho\rangle\tilde{D}_t v_\alpha'' f'' = -\langle\rho\rangle v_\alpha'' v_\beta''\partial_\beta\tilde{f} - \langle\rho\rangle v_\beta'' f''\partial_\beta\tilde{v}_\alpha \quad (27)$$

$$+\partial_\beta\left[C_s'\langle\rho\rangle\frac{\tilde{k}}{\tilde{\varepsilon}}v_\beta''v_\gamma''\partial_\gamma v_\alpha'' f''\right]$$

$$-2C_{f1}\langle\rho\rangle\frac{\tilde{\varepsilon}}{\tilde{k}}v_\alpha'' f'' - 2C_{f2}\langle\rho\rangle b_{\alpha\beta}\frac{\tilde{\varepsilon}}{\tilde{k}}v_\beta'' f''$$

$$+0.8\langle\rho\rangle v_\beta'' f''\partial_\beta\tilde{v}_\alpha - 0.2\langle\rho\rangle v_\beta'' f''\partial_\alpha\tilde{v}_\beta$$

where the anisotropy tensor is defined by

$$b_{\alpha\beta} = \frac{1}{2\tilde{k}}v_\alpha'' v_\beta'' - \frac{1}{3}\delta_{\alpha\beta}.$$

Finally the scalar dissipation is obtained as a solution of

$$\langle\rho\rangle\tilde{D}_t\tilde{\varepsilon}_f = \partial_\alpha\left(C_s''\langle\rho\rangle\frac{\tilde{k}}{\tilde{\varepsilon}}v_\alpha''v_\beta''\partial_\beta\tilde{\varepsilon}_f\right) \quad (28)$$

$$-C_{P1}\langle\rho\rangle\varepsilon_f\left(\frac{f''v_\alpha''}{f''^2}\partial_\alpha\tilde{f} - \frac{C_{D3}}{C_{P1}}\frac{v_\alpha''v_\beta''}{\tilde{k}}\partial_\beta\tilde{v}_\alpha\right)$$

$$C_{D1}\langle\rho\rangle\frac{\tilde{\varepsilon}_f^2}{f''^2} - C_{D2}\langle\rho\rangle\tilde{\varepsilon}_f\frac{\tilde{\varepsilon}}{\tilde{k}}.$$

The constants are summarized in Table 12.

The numerical solution procedure was a finite-difference method solved as marching integration in the jet axis direction. The number of points in the crossflow direction was $N=60$, and about two thousand steps were required to reach $x/D=70$. Particular care was taken to describe the conditions at the jet pipe exit. The velocity profile was a turbulent pipe flow profile inside the jet pipe, a small coflow velocity for the approximation of the finite thickness of the pipe, and a profile approximating the outer coflowing stream (Fig. 23). The turbulent

TABLE 12. Model constants

C_s	C_1	C_2	C_ε	$C_{\varepsilon1}$	$C_{\varepsilon2}$
0.22	1.5	0.4	0.15	1.45	1.9
$C_{\varepsilon3}$	C_s'	C_{f1}	C_{f2}	C_s''	C_{P1}
1.45	0.22	4.7	−4.4	0.18	1.0
C_{D1}	C_{D2}	C_{D3}			
2.0	0.9	2.45			

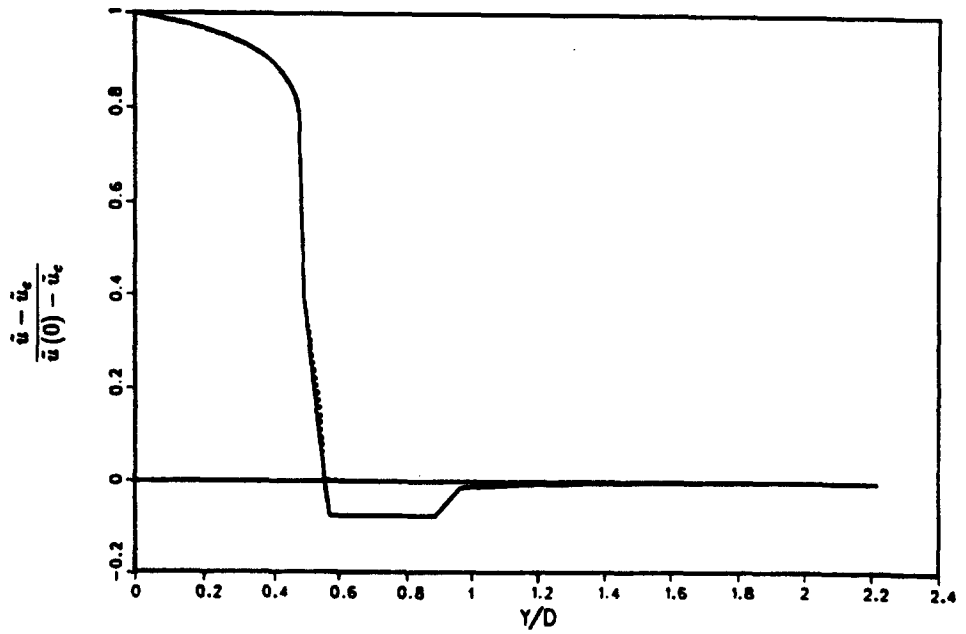

FIG. 23. Inlet velocity profile for model calculation in nonreacting propane jet.

stresses and dissipation rate are taken from the corresponding values in a fully-developed pipe, a mixing layer and a boundary layer. The boundary conditions are a Dirichlet condition (fixed value) at the outer edge of the flow and a Neumann condition (zero gradient) at the symmetry axis.

4.4.2. *Results*

The axial development of the mean velocity is shown in Fig. 24 as well as $(u''^2)^{1/2}/\Delta\tilde{u}$ in Fig. 25 and $\ln\tilde{f}$ in Fig. 26. Agreement between calculation and measurements is satisfactory. Representative radial profiles and comparisons with the data at $x/D=30$ for the mean velocity,

$$\frac{\tilde{u}(x,r)-\tilde{u}_e(x)}{\Delta\tilde{u}}$$

where $\Delta\tilde{u}=\tilde{u}(x,0)-\tilde{u}_e(x)$, are given in Fig. 27. Noting that y is normalized with the diameter D of the jet pipe, we observe that the calculated spreading rate is about 10% smaller than the experimental value. The normal stress components $(u''^2)^{1/2}/\Delta\tilde{u}$ in Fig. 28 and $(v''^2)^{1/2}/\Delta\tilde{u}$ in Fig. 29 are in good agreement with the measurements considering the uncertainties involved. The same holds for the shear stress profiles in Fig. 30. The prediction of the scalar field in terms of mean $\tilde{f}$ (Fig. 31) and the variance f''^2 (Fig. 32) is quite close to the measurements.

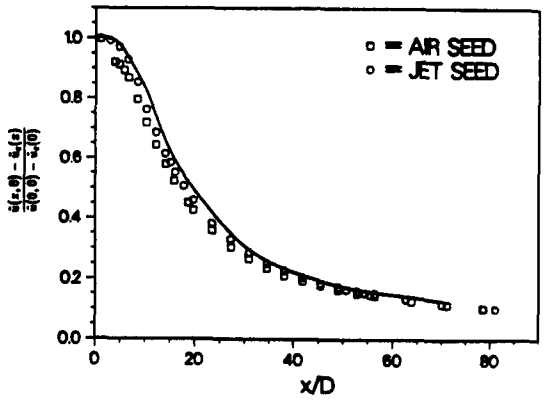

FIG. 24. Decay of mean excess velocity along centerline in a nonreacting propane jet (solid line: prediction; symbols: experiment).

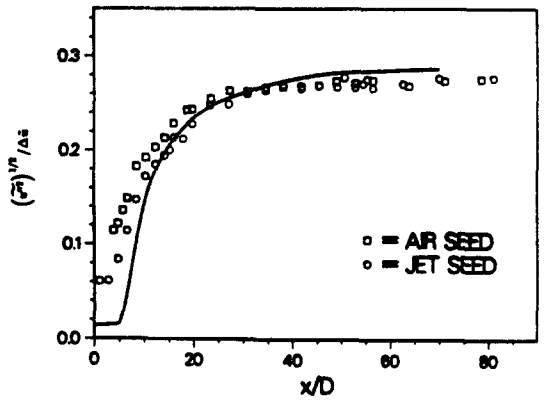

FIG. 25. Centerline variation of axial velocity fluctuations in a nonreacting propane jet.

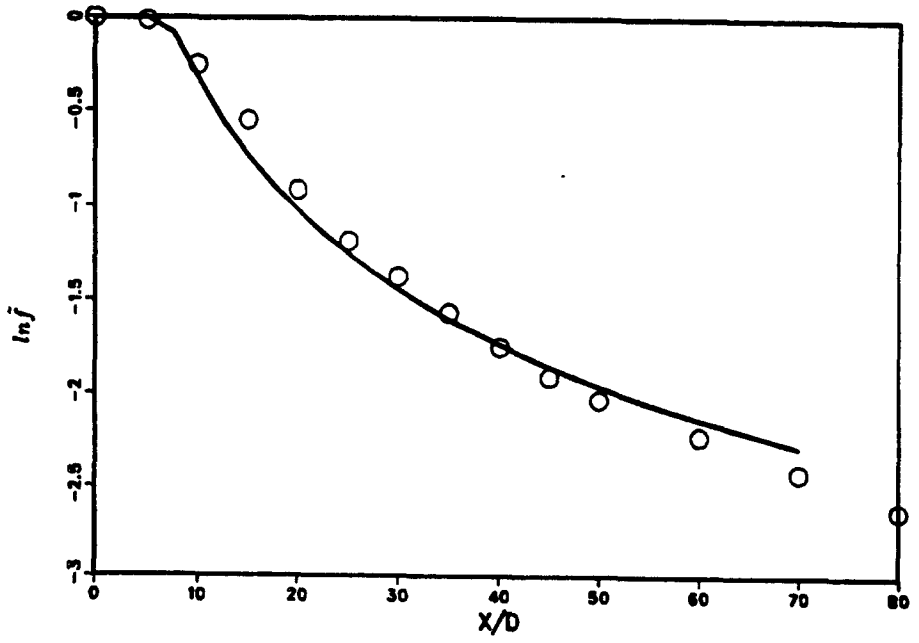

FIG. 26. Centerline variation of mean mixture fraction in a nonreacting propane jet.

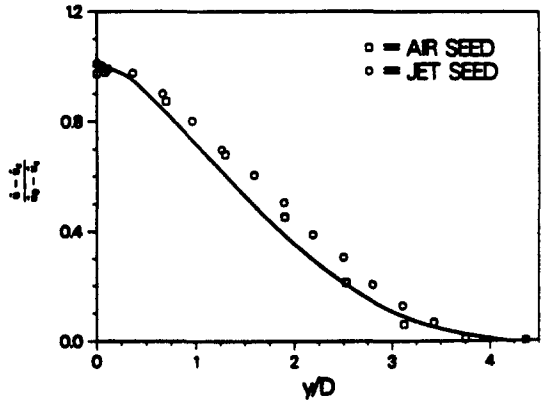

FIG. 27. Radial profile of normalized excess axial velocity at $x/D = 30$ in a nonreacting propane jet.

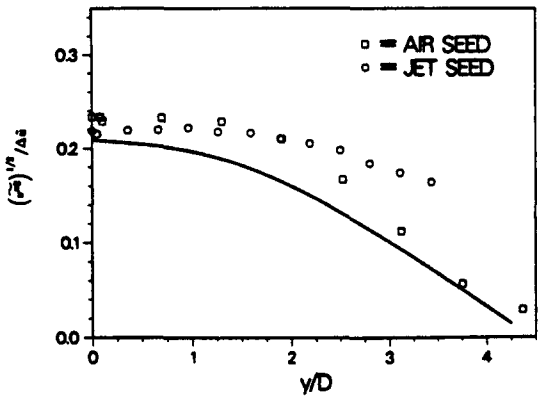

FIG. 29. Radial profile of normal stress (radial) at $x/D = 30$ in a nonreacting propane jet.

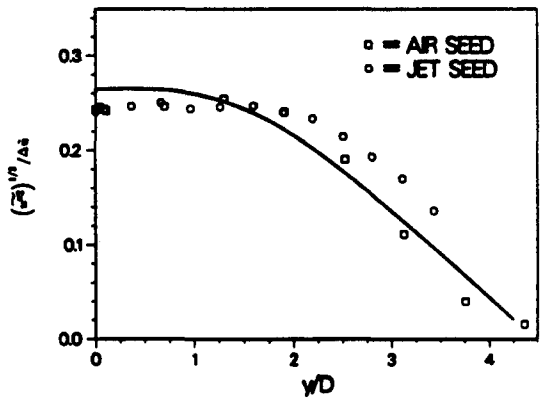

FIG. 28. Radial profile of normal stress (axial) at $x/D = 30$ in a nonreacting propane jet.

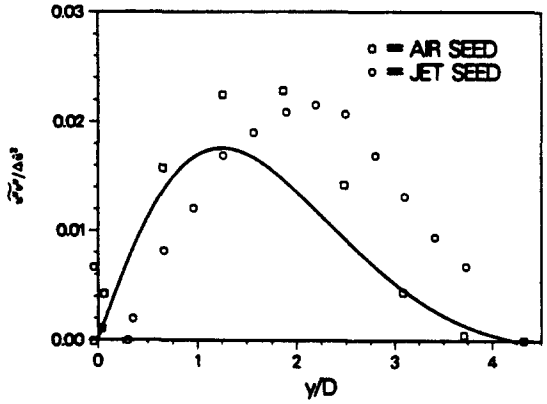

FIG. 30. Radial profile of normalized shear stress at $x/D = 30$ in a nonreacting propane jet.

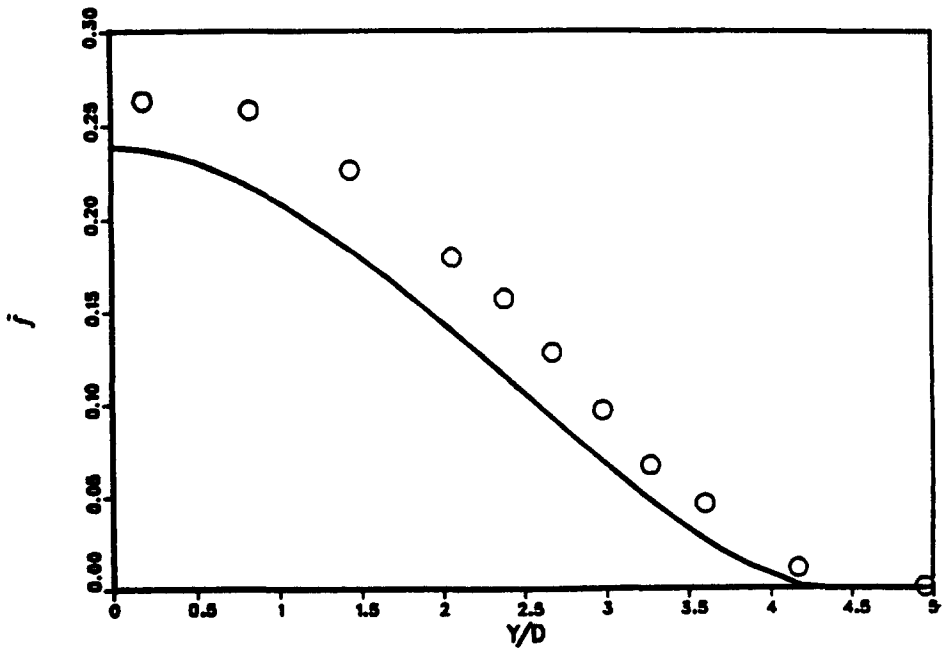

FIG. 31. Radial profile of mean mixture fraction at $x/D = 30$ in a nonreacting propane jet.

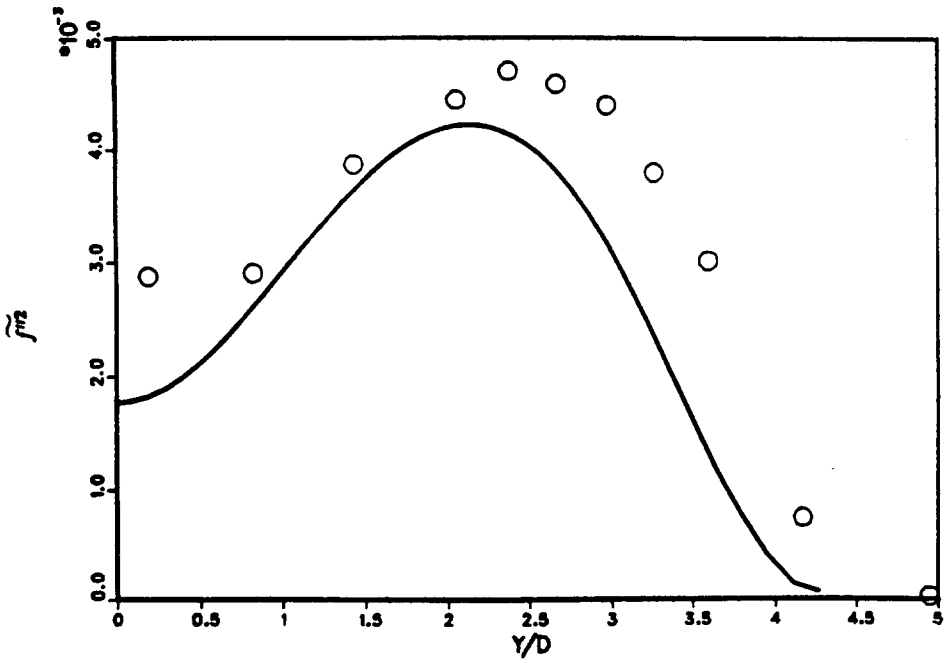

FIG. 32. Radial profile of variance in mixture fraction at $x/D = 30$ in a nonreacting propane jet.

5. ADDITIONAL DATA NEEDS

5.1. *Constant Density Flows*

The free jet data of Antonia and coworkers seem quite satisfactory for model evaluation except for the laminar initial flow conditions, possible three-dimensional effects, low Reynolds number and the presence of large-scale structures, features which are not explicitly considered in most current turbulence models. It would be helpful if questions concerning large-scale structures, the attainment of similar flow and the presence of three-dimensional flow effects were resolved. Also intermittency data for the Antonia and coworkers plane jet would be of value. Data of a similar character to those of Antonia and coworkers are clearly needed for free round jets.

In addition to a general need for more data, especially for round jets, there are several specific issues that require study. Foremost are the presence and role of large-scale structures in round as well as plane jets, the attainment of similarity, aspect ratio and three-dimensional effects in plane jets, and the influence of initial conditions and conditions in the ambient fluid on jet development and on the attainment of similarity.

Experiment has been shown consistently that radial and lateral profiles of mean velocity and mean scalar quantities are nearly Gaussian when scaled according to similarity. This result is consistent with theory from simple turbulence models (see Townsend[80]) and from more advanced turbulence models. Thus, in comparing model results for first moments with experiment, one should focus attention on the axial development of the jet as measured and calculated. For similar flows, this development for mean and second moment quantities is defined by the flow constants, C_u, C_θ, C_{L_u}, C_{L_θ}, and by the limiting values of $(\overline{u^2})^{1/2}/u_0$ and $(\overline{\theta^2})^{1/2}/\theta_0$.

Also of interest are accurate velocity measurements to larger lateral distances than have been possible in the past in order to check the form of the functions f, g and k. Finally it is noted that this review, because of time and space limitations, has essentially excluded two-dimensional shear layers and wakes of all kinds from detailed consideration. Data for these flows need to be reviewed as well.

5.2. *Variable Density Flows*

A deficiency in the variable density data presented in the previous section is that the density difference between the jet and the coflowing air is not as large as one would like. Additional measurements in round jets of the type discussed above are needed in flows with increased initial density differences, and in the near-field region downstream of the jet exit where the density differences are greatest. For such measurements, care must be exercised in establishing well characterized initial conditions. The measurements should include means and higher moments of velocity, scalars, and important correlations.

Detailed measurements in planar jets and planar mixing layers would provide useful test cases for model development and evaluation. As mentioned in the introductory comments, both planar jets and planar mixing layers maintain a density difference

farther downstream than do axisymmetric jets. Thus, they would provide a more rigorous test of variable density models. Experimental work is needed, however, to establish the possible importance of large-scale structures in these flows before the suitability of currently available modeling approaches can be evaluated.

REFERENCES

1. ABRAMOVICH, G. N., *The Theory of Turbulent Jets*, M.I.T. Press (1963).
2. AIHARA, Y., KOYAMA, H. and MORISHITA, E., Effects of an air stream on turbulent diffusion of a helium jet from a small nozzle, *Physics Fluids* **17**, 665–673 (1974).
3. ALBERTSON, M. L., DAI, Y. B., JENSEN, R. A. and ROUSE, H., Diffusion of submerged jets, *Trans. Am. Soc. Chem. Engr.*, **115**, 639–697 (1950).
4. ANDERSON, P., LARUE, J. C. and LIBBY, P. A., Preferential entrainment in a two-dimensional turbulent jet in a moving stream, *Physics Fluids* **22**, 1857–1861 (1979).
5. Antonia, R. A. and BILGER, R. W., The heated round jet in a coflowing stream *AIAA J.* **14**, 1541–1547 (1976).
6. ANTONIA, R. A. and BILGER, R. W., An experimental investigation of an axisymmetric jet in a coflowing air stream, *J. Fluid Mech.* **61**, 805–822 (1973).
7. ANTONIA, R. A. and BROWNE, L. W. B., The destruction of temperature fluctuations in a turbulent plane jet, *J. Fluid Mech.* **134**, 67–83 (1983).
8. ANTONIA, R. A., BROWNE, L. W. B., CHAMBERS, A. J. and RAJAGOPALAN, S., Budget of the temperature variance in a turbulent plane jet, *Int. J. Heat Mass Transfer* **26**, 41–48 (1983a).
9. ANTONIA, R. A., BROWNE, L. W. B., RAJAGOPALAN, S. and CHAMBERS, A. J., On the organized motion of a turbulent plane jet, *J. Fluid Mech.* **134**, 49–66 (1983b).
10. ANTONIA, R. A., PRABHU, A. and STEPHENSON, S. E., Conditionally sampled measurements in a heated turbulent jet, *J. Fluid Mech.* **72**, 455–480 (1975).
11. ANTONIA, R. A., RAJAGOPALAN, S. and FULACHIER, L., Comparison of temperature and velocity spectra in a slightly heated turbulent plane jet, *AIAA J.* **22**, 311–313 (1984).
12. BASHIR, J. and UBEROI, M. S., Experiments on turbulent structure and heat transfer in a two-dimensional jet, *Physics Fluids*, **18**, 405–410 (1975).
13. BATT, R. G., Turbulent mixing of passive and chemically reacting species in a low-speed shear layer, *J. Fluid Mech.* **82**, part 1, 53–95 (1977).
14. BECKER, H. A., HOTTEL, H. C. and WILLIAMS, G. C., The nozzle-fluid concentration field of the round, turbulent, free jet, *J. Fluid Mech.* **30**, 285–303 (1976).
15. BILGER, R. W., ANTONIA, R. A. and SREEVIVASAN, K. R., Determination of intermittency from the probability function of a passive scalar, *Physics Fluids* **19**, 1471–1474 (1976).
16. BILGER, R. W., Turbulent flows with nonpremixed reactants, *Turbulent Reacting Flows*, P. A. Libby and F. A. Williams (Eds.), pp. 65–113, Springer-Verlag, New York (1980).
17. BILGER, R. W. and DIBBLE, R. W., Differential molecular diffusion effects in turbulent mixing, *Combust. Sci. Technol.* **28**, 161–169 (1982).
18. BIRCH, A. D., BROWN, D. R., DODSON, M. G. and THOMAS, J. R., The turbulent concentration field of a methane jet, *J. Fluid Mech.* **88**, 431–449 (1978).
19. BRADSHAW, P., Effect of external disturbances on the spreading rate of a plane turbulent jet, *J. Fluid Mech.* **80**, 795–797 (1977).
20. BRADSHAW, P., The effect of initial conditions on the development of a free shear layer, *J. Fluid Mech.* **26**, 225–336 (1966).
21. BROWN, G. L. and ROSHKO, A., On density effects and large structure in turbulent mixing layers, *J. Fluid Mech.* **64**, part 4, 775–816 (1974).
22. Browne, L. W. B. and ANTONIA, R. A., Measurements of turbulent Prandtl number in a plane jet, *Trans. Am. Soc. Mech. Engrs C: J. Heat Transfer* **105**, 663–665 (1983).
23. BROWNE, L. W. B., ANTONIA, R. A., RAJAGOPALAN, S. and CHAMBERS, A. J., Interaction region of a two-dimensional turbulent plane jet in still air, *Structure of Complex Turbulent Shear Flows* R. Dumas and L. Fulachier (Ed.), pp. 189–196 (1983).
24. BROWNE, L. W. B., ANTONIA, R. A. and CHAMBERS, A. J., The interaction region of a turbulent plane jet, *J. Fluid Mech.* **149**, 355–373 (1984).
25. CATALANO, G. D., MORTON, J. B. and HUMPHRIS, R. R., Experimental investigation of an axisymmetric jet in a coflowing airstream, *AIAA J.* **14**, 1157–1158 (1976).
26. CHEVRAY, R. and TUTU, N. K., Intermittency and preferential transport of heat in a round jet, *J. Fluid Mech.* **88**, 133–160 (1978).
27. CHIGIER, N. A. and STROKIN, V., Mixing processes in a free turbulent diffusion flame, *Combust. Sci. Technol.* **9**, 111–118 (1974).
28. CORRSIN, S. and UBEROI, M. S., Further experiments on the flow and heat transfer in a heated turbulent jet, *NACA Rep., 998* (1950).
29. CORRSIN, S., Investigation of flow in an axially symmetric heated jet of air, *NACA Wartime Rep. 94* (1946).
30. DAVIES, A. E., KEFFER, J. F. and BAINES, D. W., Spread of a heated plane turbulent jet, *Physics Fluids* **18**, 770–775 (1975).
31. DIBBLE, R. W. and HOLLENBACH, R. E., Laser Rayleigh thermometry in turbulent flames, *Eighteenth Symposium (International) on Combustion*, The Combustion Institute, Pittsburgh, pp. 477–485 (1981).
32. DIBBLE, R. W., KOLLMANN, W. and SCHEFER, R. W., Conserved scalar fluxes measured in a turbulent nonpremixed flame by combined laser doppler velocimetry and laser raman scattering, *Combust. Flame* **55**, 307–321 (1984).
33. DIBBLE, R. W., KOLLMANN, W. and SCHEFER, R. W., Scalar dissipation in turbulent reacting flows: measurements and numerical model predictions, *Twentieth Symposium (International) on Combustion*, The Combustion Institute, Pittsburgh (1985a).
34. DIBBLE, R. W., HARTMANN, V., SCHEFER, R. W. and KOLLMANN, W., Conditional sampling of velocity and scalars in turbulent flames using simultaneous LDV-Raman scattering, accepted for publication, *J. exp. Fluids* (1985b).
35. DIBBLE, R. W., SCHEFER, R. W., FARSHCHI, M. and KOLLMANN, W., Second-order closure for turbulent diffusion flows, *Fifth Symposium on Turbulent Shear Flows*, Cornell University (1985c).
36. DRAKE, M. C., LAPP, M., PENNEY, C. M., WARSHAW, S. and GERHOLD, B. W., Measurements of temperature and concentration fluctuations in turbulent diffusion flames using pulsed Raman Spectroscopy, *Eighteenth Symposium (International) on Combustion*, The Combustion Institute, pp. 1521–1531 (1981).
37. DRAKE, M. C., BILGER, R. W. and STARNER, S. H., Raman measurements and conserved scalar modeling in turbulent flames, *Nineteenth Symposium (International) on Combustion*, The Combustion Institute, pp. 459–467 (1983).
38. Driscoll, J. F., Schefer, R. W., and DIBBLE R. W., Mass fluxes measured in a turulent nonpremixed flame, *Nineteenth Symposium (International) on Combustion*, The Combustion Institute, pp. 477–485 (1983).
39. DURST, F., MELLING, A. and WHITELAW, J. A., *Principles and Practice of Laser-Doppler Anemometry*, Academic

Press, London (1976).
40. Dyer, T. M., Rayleigh scattering measurements of time-resolved concentration in a turbulent propane jet, *AIAA J.* **17**, 912–914 (1979).
41. Effelsberg, E. and Peters, N., A composite model for the conserved scalar PDF, *Combust. Flame* **50**, 351–360 (1983).
42. Everitt, K. W. and Robins, A. G., The development and structure of turbulent plane jets, *J. Fluid Mech.* **88**, 563–583 (1978).
43. Farshchi, M. and Kollmann, W., Reynolds stress closure for turbulent flows. Paper presented at *ASME-AIChE Conference*, Seattle (1984).
44. Fischer, H. B., List, E. J., Koh, R. C., Imberger, J. and Brooks, N. H., *Mixing in Inland and Coastal Waters*, Academic Press (1979).
45. Fiedler, H. E., Transport of Heat Across A Plane Turbulent Mixing Layer, *Turbulent Diffusion in Environmental Pollution* (Frenkiel and Munn Ed.), pp. 93–109, Academic Press (1974).
46. Fiedler, H. E. *et al.*, *Lecture Notes in Physics* Vol. **76**, p. 58, Springer (1977).
47. Gutmark, E. and Wygnanski, I., The planar turbulent jet, *J. Fluid Mech.* **73**, 465–495 (1976).
48. Hanjalic, K. and Launder, B. E., *J. Fluid Mech.* **52**, 609 (1972).
49. Heskestad, G., Hot-wire measurements in a plane turbulent jet. *Trans. Am. Soc. Mech. Engrs E: J. Appl. Mech.* **32**, 721–734 (1965).
50. Hill, W. G., Jenkins, R. C. and Gilbert, B. L., Effects of the initial boundary-layer state on turbulent jet mixing, *AIAA J.* **14**, 1513–1514 (1976).
51. Hinze, J. O. and van der Hegge Zijnen, B. G., Transfer of heat and matter in the turbulent mixing zone of an axially symmetrical jet *Appl. Sci. Res.* **A1**, 435–461 (1949).
52. Hinze, J. O., *Turbulence*, 2nd Edn McGraw-Hill (1975).
53. Jenkins, P. E. and Goldschmidt, V. W., Mean temperature and velocity in a plane turbulent jet, *Am. Soc. Mech. Engrs: J. Fluids Engng* **95**, 581–584 (1973).
54. Keagy, W. R. and Weller, A. E., A study of freely expanding inhomogeneous jets, *Proc. Heat Transf. Fluid Mech. Inst.* **1–3**, 89–98 (1950).
55. Keller, J. O., An experimental study of combustion and the effects of large heat release on a two-dimensional turbulent mixing layer, PhD Dissertation, University of California, Berkeley, CA (1982).
56. Kiser, K. M., Material and momentum transport in axisymmetric turbulent jets of water, *A.I.Ch.E. J.* **9**, 386–390 (1963).
57. Krothapalli, A., Baganoff, D. and Karamcheti, K., On the mixing of a rectangular jet, *J. Fluid Mech.* **107**, 201–220 (1981).
58. Johnston, S. C., Dibble, R. W., Schefer, R. W., Ashurst, W. T. and Kollman, W., Laser measurements and stochastic simulations of turbulent reacting flows, *AIAA J.* **24**, 918–937 (1986).
59. Jones, W. P., Models for turbulent flows with variable density and combustion, *Prediction Methods for Turbulent flows*, W. Kollmann (Ed.), Hemisphere Publ. (1982).
60. LaRue, J. C. and Libby, P. A., Measurements in the turbulent boundary layer with slot injection of helium, *Physics Fluids* **20**, 192–202 (1977).
61. List, E. J., Turbulent jets and plumes, *A. Rev. Fluid Mech.* **14**, pp. 189–212 (1982).
62. Lockwood, F. C. and Moneib, H. A., Fluctuating temperature measurements in a heated round free jet, *Combust. Sci. Technol.* **22**, 63–81 (1980).
63. Long, M. B., Chu, B. T. and Chang, R. K., Instantaneous two-dimensional gas concentration measurements by light scattering, *AIAA Jl* **19**, 1151–1156 (1981).
64. Moss, J. B., Simultaneous measurements of concentration and velocity in an open premixed turbulent flame, *Combust. Sci. Technol.* **22**, 119–129 (1980).
65. Pitts, W. M., Personal communication (Aug. 1985).
66. Pitts, W. M. and Kashiwagi, T., The application of laser-induced Rayleigh light scattering to the study of turbulent mixing, *J. Fluid Mech.* **141**, 391–429 (1984).
67. Rajaratnam, N., *Turbulent Jets*, Elsevier (1976).
68. Razdan, M. K. and Stevens, J. G., CO/air turbulent diffusion flame: measurements and modeling, *Combust. Flame* **59**, 289 (1985).
69. Rebollo, M. R., Analytical and experimental investigation of a turbulent mixing layer of different gases in a pressure gradient. PhD thesis. California Institute of Technology, Pasadena, CA (1973).
70. Rhodes, R. P., Harsha, P. T., Peters, C. E., *Acta astronaut.* **1**, 443 (1974).
71. Samaraweera, D. S. A., Turbulent heat transport in two- and three-dimensional temperature fields, PhD Thesis, University of London (1978).
72. Santoro, R. J., Semerjian, H. G., Emhmerman, P. J. and Goulard, R., Optical tomography for flow field diagnositics, *Int. J. Heat. Mass Transfer* **24**, 1139–1150 (1981).
73. Schefer, R. W. and Dibble, R. W., Mixture fraction measurements in a turbulent nonpremixed propane jet, submitted for publication, (1985a).
74. Schefer, R. W., Hartmann, V. and Dibble, R. W., Conditional sampling of velocity in a turbulent nonpremixed propane jet, submitted for publication (1985b).
75. Schefer, R. W. and Dibble, R. W., Simultaneous measurements of velocity and density in a turbulent nonpremixed flame, *AIAA J.* **23**, 1070–1078 (1985c).
76. Schefer, R. W., Johnston, S. C., Dibble, R. W., Gouldin, F. C. and Kollmann, W., Nonreacting turbulent mixing flows: a literature survey and data base, *Sandia Rep. SAND86-8217*, Sandia National Laboratories, Livermore, CA (1986).
77. Shaughnessy, E. J. and Morton, J. B., Laser light-scattering measurements of particle concentration in a turbulent jet, *J. Fluid Mech.* **80**, 129–148 (1977).
78. Sreenivasan, K. R., Antonia, R. A. and Stephenson, S. E., Conditional measurements in a heated axisymmetric mixing layer, *T.N.-F.M.*, Vol. 5, Dept. Mech. Engineering, University of Newcastle (1977).
79. Thring, M. W. and Newby, M. P., Combustion length of enclosed turbulent jet flames. *Fourth Symposium (International) on Combustion*, pp. 789–796, The Combustion Institute (1952).
80. Townsend, A. A., *The Structure of Turbulent Shear Flow*, 2nd Edn, Cambridge University Press (1976).
81. Tritton, D. J., *Physical Fluid Dynamics*, Van Nostrand Reinhold Company (1977).
82. Vankataramani, K. S., Tutu, N. K. and Chevray, R., Probability distributions in a round free jet, *Physics Fluids* **18**, 1413–1420 (1975).
83. Warshaw, S., Lapp, M., Penney, C. M. and Drake, M. D., Temperature–velocity correlation measurements for turbulent diffusion flames from vibrational Raman-scattering diagnostics, *Laser Probes for Combustion Chemistry*, (D. R. Crosley Ed.), Pap. 19, *Am. Chem. Soc. Symp. Ser.* **134**, 239–246 (1980).
84. Wilson, R. A. M. and Danckwerts, P. V., Studies in turbulent mixing-II, *Chem. Engng. Sci.* **19**, 885–895 (1964).
85. Wygnanski, I. and Fielder, H., Some measurements in the self-preserving Jet, *J. Fluid Mech.* **38**, 577–612 (1969).
86. van der Hegge Zijnen, B. G., Measurements of the distribution of heat and matter in a plane turbulent jet of air, *Appl. Sci. Res.* **A7**, 277–292 (1958a).
87. van der Hegge Zijnen, B. G., Measurements of the velocity distribution in a plane turbulent jet of air, *Appl. Sci. Res.* **A7**, 256–276 (1958b).
88. Yanagi, T. and Mimura, Y., Velocity–temperature correlation in premixed flame, *Eighteenth Symposium*

(*International*) *on Combustion*, The Combustion Institute, pp. 1031–1039 (1981).

89. KONRAD, J. H., An experimental investigation of mixing in two-dimensional shear flows with application to diffusion-limited chemical reactions. PhD Dissertation, California Institute of Technology, Pasadena, CA (1976).

APPENDIX A—INITIAL CONDITIONS

The importance of well-characterized inlet conditions on the development of the downstream flow is well established. In addition, parabolic computational models used in predicting shear flows require inlet conditions to initiate calculations in the downstream direction. For these reasons, care was taken to measure the inlet velocity and mixture fraction profiles in the propane jet presented in Section 4. These results are shown below in Figs A.1–A.3.

Radial profiles of the mean and fluctuating axial velocities were measured in the coflowing air stream at the test section inlet ($x/D=0$) using hot-wire anemometry, and are shown in Figs A.1(a) and A.1(b). The growth of a thin boundary layer with a thickness of approximately 0.3 jet diameters is apparent along the outer edge of the jet tube (corresponding to $y/D=1.0$). At increasing radial distances the mean and fluctuating velocity rapidly approach free stream values of 9.2 m/sec and 0.4 %, respectively.

Scattered laser light from the jet tube required that Rayleigh scattering measurements of propane mixture fraction be made downstream of the jet exit where scattered light was sufficiently reduced. Shown in Fig. A.2 are the mean and fluctuating propane mixture fraction at an axial distance of 4 dia downstream of the jet exit. The mean mixture fraction values of unity (corresponding to pure propane) indicate the existance of a potential core which extends approximately 0.2 dia from the centerline. At increased radial distances the mean mixture fraction decreases rapidly and mixture fraction fluctuations increase as mixing occurs between propane issuing from the jet and the surrounding coflowing air.

The corresponding axial and radial velocities (measured using two-color laser velocimetry) are shown in Fig. A.3. The mean axial velocity, presented as excess velocity, is shown in Fig. A.3(a). Results are shown for the case of LV seed added to the coflowing

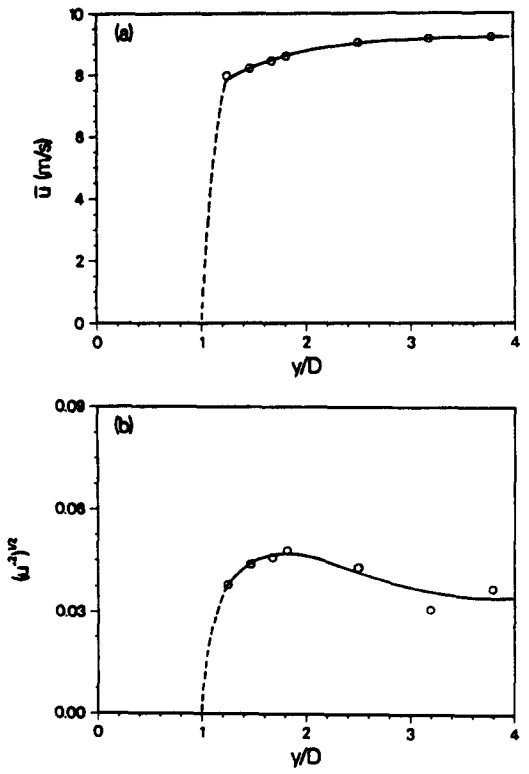

FIG. A.1. Inlet profiles of mean and fluctuating axial velocity. Bulk jet velocity = 53 m/sec; coflowing air velocity = 9.2 m/sec. (a) Mean axial velocity; (b) axial velocity fluctuations.

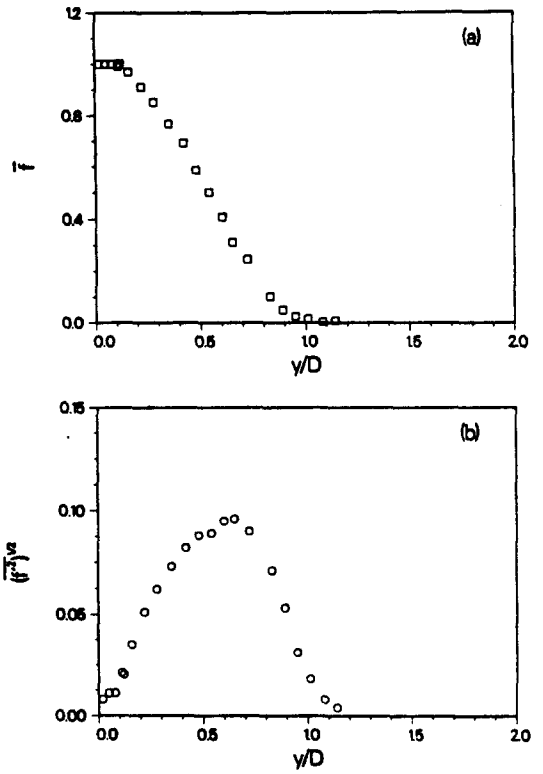

FIG. A.2. Radial profiles for a turbulent nonreacting propane jet at an axial location of $x/D=4$. Bulk jet velocity = 53 m/sec; coflowing air velocity = 9.2 m/sec. (a) Mean mixture fraction; (b) mixture fraction fluctuations.

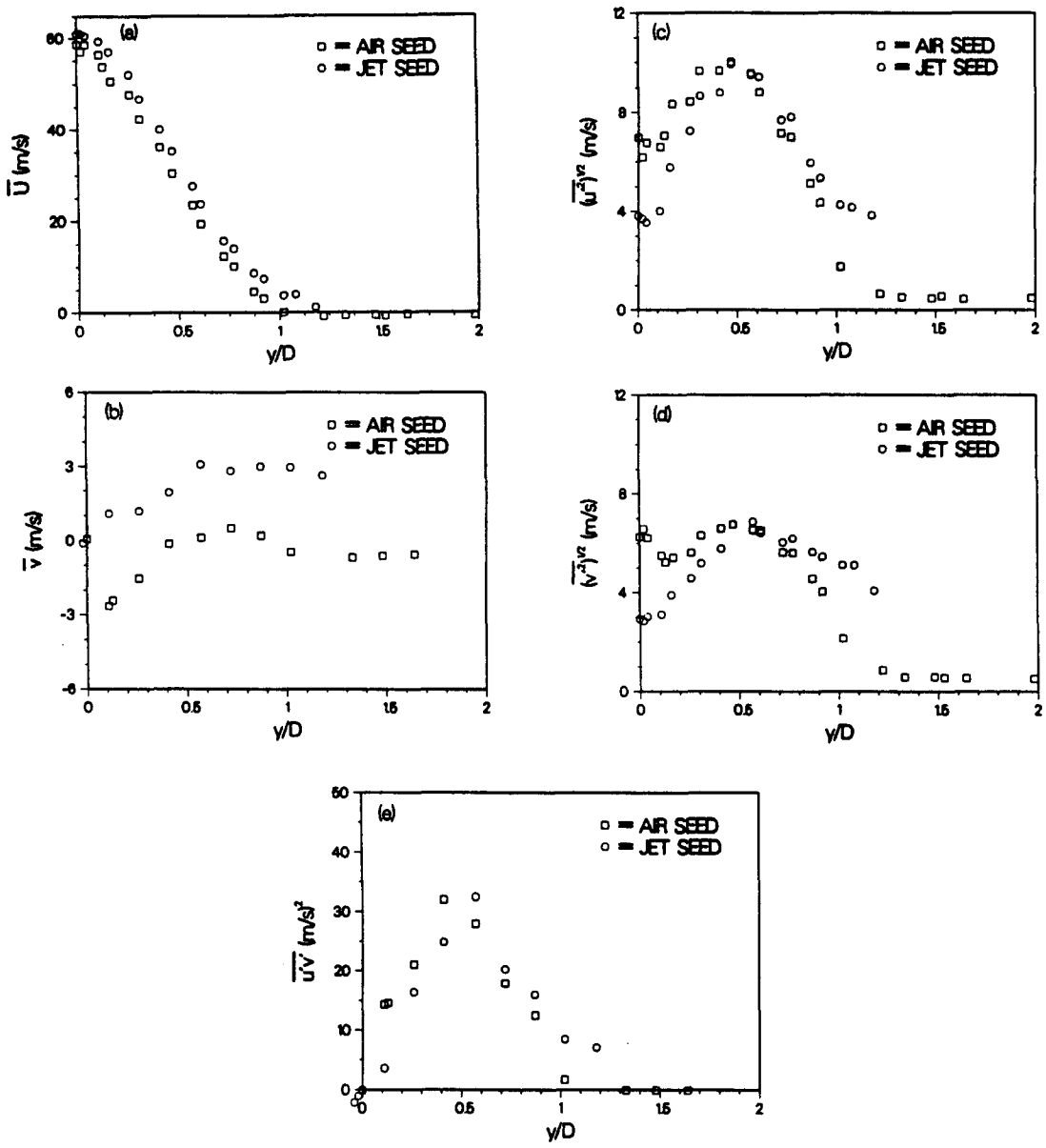

FIG. A.3. Radial velocity profiles for a turbulent nonreacting propane jet at an axial location of $x/D=4$. Bulk jet velocity = 53 m/sec; coflowing air velocity = 9.2 m/sec. □, LV seed added to coflowing air; ⊙, LV seed added to jet. (a) Mean axial velocity; (b) mean radial velocity; (c) axial velocity fluctuations; (d) radial velocity fluctuations; (e) axial and radial velocity correlation.

air only and to the jet fluid only. The maximum value of axial velocity at the centerline ($u_{j,\max}=69$ m/sec) is consistent with full-developed pipe-flow theory ($u_{cl}/u_{j\,\text{bulk}}=1.28$). The radial velocity profiles, Fig. A.3(b), indicate rapid entrainment coflowing air (negative values of v_{air}) and rapid outward expansion of fluid originating from the jet. Maximum fluctuations in both axial and radial velocities occur in the mixing region between the high velocity central jet and the lower velocity coflowing air.